January 2020

A Preliminary Study Of Leo To Geo Transfers For Inclination Changes Using Libration Point Orbits

John Shepard

A PRELIMINARY STUDY OF LEO TO GEO TRANSFERS FOR INCLINATION CHANGES USING LIBRATION POINT ORBITS

by

John Philip Shepard
Applied Associates of Science, Community College of the Air Force, 2012
Applied Associates of Science, Community College of the Air Force, 2019
Bachelor of Science, Chadron State College, 2012

A Thesis
Submitted to the Graduate Faculty

of the

University of North Dakota

in partial fulfillment of the requirements

for the degree of

Master of Science

Grand Forks, North Dakota

May
2020

This thesis , submitted by John Shepard in partial fulfillment of the requirement for the Degree of Master of Science in Space Studies from the University of North Dakota, has been read by the Faculty Advisory Committee under whom the work has been done and is hereby approved.

DocuSigned by:
Ronald Fevig
Dr. Ronald Fevig

DocuSigned by:
Mike Gaffey
Dr. Michael Gaffey

DocuSigned by:
John Collings
Dr. John Collings

Name of Committee Member 3

Name of Committee Member 4

Name of Committee Member 5

This thesis is being submitted by the appointed advisory committee as having met all of the requirements of the school of Graduate Studies at the University of North Dakota and is hereby approved.

DocuSigned by:
Chris Nelson
Chris Nelson
Dean of the School of Graduate Studies

4/29/2020
Date

PERMISSION

Title A Preliminary Study of LEO to GEO Transfers for Inclination Changes Using Libration Point Orbits

Department Space Studies

Degree Master of Science

In presenting this thesis in partial fulfillment of the requirements for a graduate degree from the University of North Dakota, I agree that the library of this University shall make it freely available for inspection. I further agree that permission for extensive copying for scholarly purposes may be granted by the professor who supervised my thesis work or, in his absence, by the Chairperson of the department or the dean of the School of Graduate Studies. It is understood that any copying or publication or other use of this thesis or part thereof for financial gain shall not be allowed without my written permission. It is also understood that due recognition shall be given to me and to the University of North Dakota in any scholarly use which may be made of any material in my thesis.

John P. Shepard
May 7th, 2020

TABLE OF CONTENTS

LIST OF TABLES

LIST OF FIGURES

ACKNOWLEDGEMENTS

The knowledge imparted by this work comes not only from the work that I have done, but from the understanding and help of others. For this reason, there are many people that I would like to thank for their contributions.

The first person that I would like to acknowledge and thank is Professor Ronald Fevig, having provided a strong foundation for my understanding of orbital mechanics. Professor Fevig was not only my professor for my orbital mechanic courses but had also provided me with the original research article that acted as the inspiration of the work conducted. It was my privilege to have been his student and conduct research with his guidance.

Another individual that I would like to thank for his contributions is Sam Carp. Sam was a fellow co-worker at Lockheed Martian from whom I have had many conversations with discussing different mathematical inquires. Having discussed the different mathematical concepts related to the research conducted many hurdles had been overcome.

In general others that I feel the need to be thanked is the scientific community. The work produced by all the different scientists and researchers that have been referenced from this research for providing a detailed understanding, ideas to further explore, and methods to advance their work. All the referenced scientists and researchers have acted as my inspiration and guidance for all the work that I have conducted.

ABSTRACT

The required change in velocity for a satellite to change inclination has prompted studies of efficient orbital transfers. Modeling the motion of a spacecraft by including the gravitational forces associated with the Sun, Earth, and Moon has historically proven effective in obtaining new scientific knowledge. In modeling the motion of satellites, the circular restricted three body problem (CR3BP) demonstrates the interactions from two primary bodies and a satellite. The dynamics created about the equilibrium points within the CR3BP can be used to construct low-energy transfers. The invariant manifolds of the libration point orbits (LPO) can be used to create an orbit using a weak stable boundary (WSB) to approach a coplanar Lagrange point. Following the use of two distinct libration point orbits a satellite can adjust for a return at a greater difference of inclination compared to a one impulse maneuver. On approach to the second Lagrange point, the satellite follows a horizontal Lyapunov orbit to use another maneuver placing the satellite in a vertical Lyapunov orbit. Following the vertical Lyapunov orbit the weak unstable boundary is used for a return toward Earth at a different inclination. Given the trajectory created, a 90-degree inclination change has been developed. The maneuver cost is compared to a Hohmann transfer and bi-elliptic transfer for a decrease in fuel as well as an increase in the time of flight. An analysis of the periodic orbital transfer created in this research is performed, as well as other orbits from associated research articles suggest that a significant amount of velocity savings can be achieved. Continuing with the use of such constructed trajectories, a brief investigation on to financial and environmental impacts are also reviewed. The result of this study demonstrates the utility of periodic orbital transfers and their importance in mission design for plane change maneuvers.

1. INTRODUCTION

Traditionally orbital transfers, such as a Hohmann transfer or patched-conic transfer, need high fuel consumptions for large velocity maneuvers. Optimization of orbits are designed to consume the least amount of fuel, for the least amount of velocity possible. With optimizing fuel usage, the trade-off is between time and velocity. Different studies that model the trade-offs between different methods can provide options in mission design. An investigation into the NASA Genesis mission and the rescue of AsiaSat-3/HGS-1 aids in the understanding of periodic orbit trajectories.

In August 2001 the NASA Genesis sample return mission was designed to collect isotopes from solar winds (Williams, 2002). The trajectory designed for the mission was one in which the spacecraft experienced a low energy injection toward a Halo orbit around the first Lagrange point. After completing several revolutions around the first Lagrange point the spacecraft proceeded with a Halo orbit around the second Lagrange point. The Genesis satellite trajectory demonstrates the successful use of periodic orbits in mission design and implementation. Furthermore, AsiaSat-3/HGS-1 in 1998 underwent an Apollo-style free-return trajectory to adjust inclination of 40 degrees (Ocampo, 2005). Edward Belbruno had also proposed a low-energy transfer that would have adjusted the inclination by 50 degrees. Although the ballistic capture method developed by Edward Belbruno was not used, his trajectory design lead to the use of the moon to rescue the satellite. The orbital maneuver of AsiaSat-3/HGS-1 allowed for the satellite to be repurposed as PAS 22 and continued to operate to the date of July 2002.

A periodic orbit trajectory like the one used by NASA's Genesis mission, the proposed maneuver for the rescue of AsiaSat-3/HGS-1, and designs created by further studies are advantageous for mission planning and satellite rescue missions. The CR3BP can be used to recreate the Genesis mission and the AsiaSat-3/HGS-1 transfer. CR3BP further enables the analysis of periodic orbit trajectories for mission use and can provide a general understanding of motion around the Lagrange points. Davis, Anderson, & Born (2011) proposed a trajectory design using periodic orbit transfers to change inclination and continued analysis with maneuvers around the LPO for a subset of inclinations. Expanding on the use of periodic orbit transfers to change inclination with an additional maneuver at the LPO, a transfer involving both horizontal and vertical Lyapunov orbits is investigated. The results allow for contingency planning involving changes with inclination and flexibility for mission design.

1.1 Inclination Change

Inclination changes require large amounts of velocity change and are most often avoided to conserve fuel. A graph calculating the velocities needed for an inclination change with all other orbital parameters kept constant can provide a visualization of the challenge of plane change maneuvers. Equation 1.1 is used to calculate inclination change and the graph from figure 1-1 provides a visual representation of the cost of velocity change as inclination changes. Given an initial orbit at LEO (6556 km) and a final orbit at LEO the change in velocity required for a 90-degree plane change would approximately be about 11.02 km/s. Similarly, given an initial orbit at LEO and a final orbit at GEO (42,164 km) the change in velocity required for a 90-degree plane change would approximately be about 4.34 km/s.

$$\Delta v = 2v * \sin\left(\frac{\Delta i}{2}\right) \tag{1.1}$$

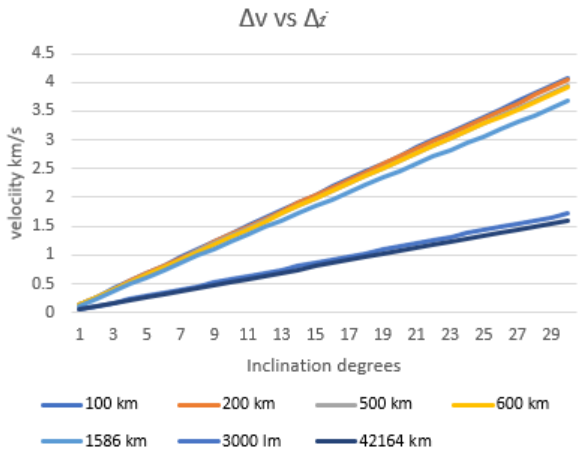

Figure 1-1 Change of Inclination vs. Change of Velocity

As a result of the velocities required for a plane change maneuver a common approach is for the launch vehicle to inject a spacecraft into a transfer optimal for the designed mission orbit. A consequence of using the launch vehicle to assist in the plane change maneuver is that the transfer trajectories are typically like that of the launch site. When considering the bi-elliptical transfer which is typically more economical compared to the Hohmann transfer, the bi-elliptical method is only more effective when the ratio of the initial orbital radius over the final orbital radius is greater than 15.58. When considering the bi-elliptical transfer the intermediate transfer is typically limited due to miscalculations caused by gravitational forces from other objects like the Moon or the Sun.

With the amount of velocity required for a change in inclination other methods for decreasing the amount of velocity required for a transfer are desirable.

1.2 The Circular Restricted Three-Body Problem

The motion of n-body masses in three-dimensional space only being acted upon by gravitational forces can be described by Newton's universal law of gravitational motion. One subset of the n-body problem, n =2, is known as the two-body problem, which describes the motion of one mass about another. The two-body problem of motion has been proven to have a closed form analytical solution. However, when introducing an additional third body to the problem of motion, the general three-body problem has no closed form analytical solution.

The complexities of the three-body problem are due to having nine different spatial coordinate components, a set of three for each object each with a different set for velocity. Given the different potential movements within the three-body problem there are 18 degrees of freedom. From the general equation of the three-body problem a set of 10 independent algebraic integrals can be derived. The equations being three for classical conservation of linear momentum for position and velocity, position and energy, and three for angular momentum. In 1912 Sundman found a complete solution for the three-body problem given in terms of a power series expression. However, his method converges very slowly and cannot be used for any practical application (Musielak, E., & Quarles, 2015). Given the nature of the three-body problem, deriving the acceleration with various position and velocity vectors through numerical analysis does provide a method of determining the orbit of a desired object.

To reduce the complexities of the general three-body problem a set of assumptions can be used to simplify the problem. The CR3BP makes two assumptions to form a simplified model. First, the primary and secondary bodies move in circular motion about the center of mass which lies between both primary bodies. Second, the third body being the satellite is assumed to have infinitesimal mass compared to both primary bodies. In the CR3BP the third body is described relative to a rotating reference frame determined by the motion of both primaries. However, even with simplifying assumptions, the CR3BP is still not solvable in a closed form. Given the CR3BP, equations of motion can be derived to describe the motion of the object of interest with an initial set of position and velocity vectors. Within the model, approximate analytical solutions are available for motion around the equilibrium points. Using numerical solutions for the equilibrium

points, motion about the equilibrium points and about the system can provide information about motion of the object of interest. The solutions derived from the model can be further explored thereby leading to a multitude of discoveries demonstrating new types of orbital trajectories for a variety of different missions.

1.3 Mission Scenario

In this section an attempt is made to provide an example potential mission use for the orbital maneuver designed in this research. This section does not provide applicational use but rather focuses on what this maneuver would entail if used in a mission. The benefit of the orbit maneuver being described in this research is with the amount of fuel needed for a thrust to achieve a large inclination change. Factors not taken into consideration in this section, but later discussed include the space environment, communications issues, and other factors beyond the direct use of the maneuver. In this section a satellite named Satellite A is used as the example spacecraft that is completing the maneuver within a fictitious scenario to demonstrate usability in real conditions as a simplified example.

In this scenario Satellite A has a mission that requires operations at LEO that would follow an inclination of 0 degrees with a mass of 4600 kg. To keep economic costs for the satellite down the cheapest available launch is chosen. In 2013 the published price for a such an endeavor was $56.5 million through SpaceX (Belfiore, 2013). The cost example provided was considered the cheapest known example. SpaceX has three typical operating launch facilities, those three being Cape Canaveral Air Force Base, Vandenberg Air Force Base, and Kennedy Space Center. Satellite A's mission design is to orbit about the equator making Kennedy Space Center and Cape Canaveral Air Force Base both viable options for launch location. Having multiple choices for launch locations could provide some flexibility with schedule. With projects that involve the use of satellites and launch dates for a specific launch site, it would not be uncommon for launch windows to be extended well into the future. Depending on how far into the future a launch is scheduled, planning time for development can become impacted. If a launch window is unavailable for an extended period, maintaining personnel could be a cost factor and drive design and development schedules beyond reasonability. If options are available for a launch site, time constraints could be less of an impact. However, launch windows and schedule impacts are difficult to quantify as development time scales are not published. If the given launch inclination for LEO is relativity low (less than 57 degrees) then either Cape Canaveral or Kennedy Space Center would be

preferred. Satellite A in this scenario is set to launch on a Falcon 9 Rocket at Kennedy Space Center, Florida. The latitude and longitude place the site near the equator and the Atlantic Ocean. The location provides an advance in speed due to the Earth's rotation. After the mission duration time is complete several options are available for Satellite A. One option that can be explored is re-purposing Satellite A provided it has the necessary payload instruments and capacity for the bus to maintain the new desired orbit.

Satellite A after having conducted a complete mission is now being re-purposed for GEO with a new inclination of 22 degrees. As noted from section 1.1 inclination change maneuvers are typically avoided due to the high cost of fuel. In this scenario to start with an inclination of 0 degrees and move to an inclination of 22 degrees the cost would be approximately 1.17 km/s in addition to the change from LEO to GEO of about 3.94 km/s for an approximate total of 5.114 km/s. As a cost estimate LEO near the equator starts off with about 1.5 km/s with about $10000 for a pound of material getting from launch to orbit. To maintain an orbit at LEO a constant velocity of approximately 7.797 km/s is required and at GEO an approximate velocity of about 3.07 km/s is required, which would mean that any unnecessary thrusts could shorten the lifespan of a satellite.

Satellite A, now in LEO with an inclination of 0 degrees can either take a classic maneuver with the cost of 5.114 km/s Δv or undergo a fuel-efficient maneuver. The fuel-efficient maneuver described in this research is that of a satellite using invariant manifolds and LPOs. The use of periodic orbits has shown that a plane change maneuver can be achieved without the costs of undergoing such a maneuver. In section 3.2 a periodic transfer of one LPO is examined. Using the method described in section 3.2 the maneuver was originally designed to determine end state inclination for a given set of initial conditions. Given a point along the orbit of Satellite A with a potential thrust of 4.415 to 4.45 km/s allows for varying time of flight results that end the maneuver in GEO. Given the previously mentioned maneuver the required thrust would be 4.415 km/s with a time of flight of approximately 388 days. The savings compared to a traditional plane change maneuver for percent difference is less than 15% when comparing results calculated at GEO. As the difference of inclination continues to increase, the percent difference continues to go in favor of the fuel-efficient maneuver. As the inclination difference continues to increase from the initial orbit to the final orbit the fuel savings continue to increase up to a maximum difference of 71.6 degrees.

Based on the previous scenario a change in the desired end state inclination to 90 degrees is now presented with the same launch location and initial inclination of 0 degrees. The change of end state inclination now requires the satellite to perform a 90-degree plane change maneuver resulting in a polar orbit. Based on the calculations from section 1.1 a required approximate velocity of 4.35 km/s for the inclination is necessary in addition to the 3.94 km/s needed for transfer to GEO for the desired end state. Using the maneuver just mentioned it is not possible based on the original research where the maximum change of inclination the maneuver can provide is approximately 71.6 degrees of difference. To further increase the potential for change of inclination an additional maneuver is made at the LPO to follow a different LPO for a return to Earth. In this research the results demonstrate that Satellite A would conduct an initial thrust of about 3.2 km/s near Earth, at the LPO another thrust of about 1.56 km/s, and finally a thrust of about 0.2 km/s circularizing the orbit about the Earth. The total thrust for the maneuver is approximately 5.076 km/s which would provide a percent difference of approximately 48% compared to a traditional plane change. Although such difference may not directly yield savings they could be the difference between a mission being possible or not. This maneuver being a multi-thrust maneuver does create the potential for added risk and the need for correction should Satellite A veer off path. From the contingency study for the ISEE-3 satellite, the mission used created a set of contingency thrusts to correct for additional perturbations or other factors. With the development of the maneuver, created contingency thrusts would also be created if used for a real mission. Figure 1-2 and 1-3 provide a trace of the trajectory with potential additional thrust points to ensure success.

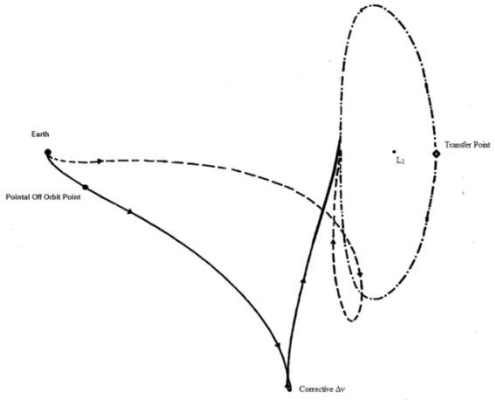

Figure 1-2 Contingency Maneuver for Lyapunov Orbit (2-Dimensional View)

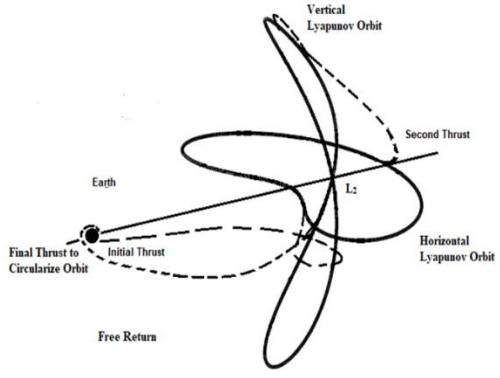

Figure 1-3 Trajectory of full Orbital Maneuver (3-Dimensional View)

Figure 1-3 was created prior to being generated within the model and subject to change in appearance. As Satellite A returns from the maneuver a final thrust will place Satellite A in the final polar orbit. Contingency maneuvers are calculated based on the current position and velocity and determining the difference as needed for an additional thrust providing orbital correction. The beginning and end results can be realized in a classic two-body model after having gone under a maneuver with the three-body model. Also, due to the three-body model not being complete with all the potential forces acting on Satellite A additional corrections to thrust would need to be taken to account for such perturbations. The designed orbital maneuver adds more to the time of flight and slightly increases the required amount of thrust to further increase the maximum amount of inclination change achievable. The example provided is one of many that could be loosely fitted for the maneuver created. Additional usage and savings could also apply to retrograde orbits. More common uses typically include rescue and salvage or missions that take advantage of the trajectory being implemented. As different orbital techniques are created for various situations more options exist to assist orbital analysts and guidance navigation and control engineers.

1.4 Previous Contributors

When studying orbital motion Newton's second law and his universal law of gravitational motion is a typical starting point. In 1687, Sir Isaac Newton published his mathematical finding in the Principia, which contained the dynamical analysis for the three-body problem. Continuing Newton's work, in 1767 Euler had proposed a special form of the general three-body problem where three bodies of finite mass were placed along a straight line suitable for initial conditions. The third body within the system is assumed to be infinitesimal, thereby introducing the "restricted three-body problem" (Musielak, E., & Quarles, 2015). The proposed setup would have the line of both primary bodies rotate about the center of mass leading to periodic motion of all three bodies. The Lagrange solution to the restricted three-body problem proved two corresponding orientated triangular regions of stability. Overall, there are five identified equilibrium solutions known as the Lagrange points. Poincaré's developed several qualitative methods to study periodic orbits, while demonstrating non-integrability of the three-body problem. His work on the existence of periodic solutions led to the beginning of modern dynamical systems theory (Musielak, E., & Quarles, 2015).

1.4.1 Libration Point Orbits and Manifolds

Continuing the contributions of Poincaré's work on the existence of periodic orbits within the three-body problem, further advancements have demonstrated a wide family of orbits. Among the contributions for studying periodic orbits, characterization using Lyapunov exponents describe trajectories in phase space converging on to stable and unstable manifolds (Musielak, E., & Quarles, 2015). Given the restricted three body model, the work of Farquhar and Kamel computed a family of Halo orbits permanently formed from the perspective of Earth about the Lagrange points (Breakwell, Brown, & V., 1979). The work of Breakwell and Brown in 1979 concluded numerically that orbits near the Lagrange points grow larger and have shorter periods as they approach the second primary body (Breakwell, Brown, & V., 1979). In 1972, Farquhar and Kamel used the Lindstedt-Poincaré method and computerized algebraic manipulation to form analytical solutions for quasi-periodic orbits. Their research was focused on use of a communications relay satellite that would take advantage of the collinear libration point orbits. As a result of their research they confirmed the existence of large Halo orbits for both the L_1 and L_2 Lagrange points with any mass parameter μ: $0 < \mu \leq 0.5$ (Farquhar & Kamel, 1972). Howell's research continued from Farquhar and Kamel's with the existence of Halo orbits near all three collinear libration points of varying size differences. In her research most orbits decreased in period as they approach the nearest mass, with stable orbits roughly halfway between libration points (Howell, 1983). As the behavior of Lissajous orbits continued to become well-defined, further research focused on a wide range of topics to further describe such dynamic motion and its potential applications.

With the dynamical motion created by the CR3PB and motion about the colinear Lagrange points, the use of manifolds and heteroclinic connections have become a major topic of discussion. In the research of Gómez and Masdemont a transfer between L_1 and L_2 with a heteroclinic orbit with no maneuver is demonstrated. The result of the research was a methodology to compute various orbits of joining libration point orbits (Gomez & Masdemont, 2000). With the continued use of modeling, Hénon's research extends the number of periodic solutions to include seven new families of periodic orbits. Previous limitations were due to computer limitations in 1996 which were overcome by 2002. Overall, there exist an infinite number of families of periodic orbits and for those numerically computed each presented show instability (Henon, 2002). With heteroclinic connections mapped out within a system continued research from Gómez and Masdemont with the addition of Lo, Marsden, Koon, and Ross a framework of connections can be constructed to

act as a transport mechanism. Their research constructed numerous ways of using stable and unstable manifolds to and from different libration point orbits requiring no maneuvering (Gomez, et al., 2004). Further analysis of the behavior of trajectories into periodic orbits by Nakamiya, Scheeres, Yamakawa, and Yoshikawa demonstrate behavior about the Hill's region. Through their numerical results the manifolds from periapsis to Lyapunov and Halo orbits can intersect the surface of any planet in the solar system given changes with the Jacobi integral (Nakamiya, Scheeres, Yamakawa, & Yoshikawa, 2008). The dynamics about libration point orbits have shown great utility moving from one primary body to another or about a system. They also can demonstrate a great usefulness in fuel efficient transfers to increase inclination.

In 2003, Villac and Scheeres studied three-body forces to create large inclination changes based on the geometries of the CR3BP. Previous analysis of plane change maneuvers had been constructed from the two-body problem. One example provided by Villac and Scheeres was that of the J_2 perturbations, which refers to third-body forces acting on a satellite provide a change in orbital parameters as a change of distance between the two primary bodies and their gravitational forces (Villac & Scheeres, 2003). Their research provided analysis on highly eccentric transfers acted upon by the secondary primary body and how such forces would create a plane change. Their research demonstrated a 25% fuel savings compared to a one-impulse maneuver greater than 60 degrees. Villac and Scheeres furthered their research by finding an analytical estimated limit of optimality. One-impulse maneuver plane changes are less expensive for inclination changes greater than 45 degrees compared to traditional methods (Villac & Scheeres, 2009). In 2010, Davis, Anderson, Scheeres, and Born developed a technique known as the bounding sphere to understand different gravitational effects caused by the second primary body (Davis, Anderson, Scheeres, & Born, 2010). The idea behind the bounded sphere is to develop an optimized path for a plane change maneuver for a desired inclination. Their research continued with constructing optimal transfers between unstable periodic orbits of different energies. With a satellite using a different final periodic orbit from the initial periodic orbit primer vector theory could be used to better determine the most optimal path compared to their bounded sphere method (Davis, Anderson, Scheeres, & Born, 2011). The bounded sphere is a region of different manifolds intersection paths to determine an optimal path. The primer vector theory as used in their research adjusts an initial and final coastal arc and a transition for the most optimal path, implementing a two-impulse maneuver. Davis, Anderson, and Born continued their research with an orbital

maneuver to demonstrate a maneuver from LEO to GEO using invariant manifolds to provide a plane change without a plane change maneuver (Davis, Anderson, & Born, 2011). Throughout all the research conducted, the overall result was that with the use of invariant manifolds and libration point orbits 40 – 70% fuel savings can be achieved compared to a Hohmann transfer.

1.4.2 Application in Mission Design

A NASA technical note in 1971 purposed the use of a Halo orbit for a relay satellite for lunar communications (Farquhar, 1971). The communications satellite proposed would perform an orbital maneuver to take advantage of a trajectory that would lead directly into a Halo orbit. Unfortunately, this method was not selected. Later, in 1996 Barden, Howell and Lo generated trajectories for the Suess-Urey mission with the three-body problem using stable and unstable manifolds, which differed from traditional trajectory design being rooted in the two-body problem and conics (Barden, Howell, & Lo, 1996). The Suess-Urey mission was to collect solar wind particles for the duration of two years, other similar missions that would take advantage of periodic orbits prior to Barden, Howell and Lo's analysis were ISEE-3, WIND, SOHO, and ACE. As advancements in technology continued to develop, the use of computers for analysis also helped further the development of periodic orbits in mission design.

With applicational use to missions such as Genesis and low energy Earth to Moon transfers Koon, Lo, Marsden, and Ross developed heteroclinic connections between libration point orbits using modeling and simulation. Heteroclinic orbits describe the path in phase space in which two different libration point orbits can be joined together. The discovery of heteroclinic connections provide a fast channel of transport between interior and exterior Hill's regions that can be exploited by spacecraft to explore vast regions of space around a planetary body (Koon, Lo, Marsden, & Ross, 1999). In 2001, Paffenroth and Dichmann used the software tool AUTO to model families of periodic orbits (Paffenroth, Doedel, & Dichmann, 2001). The AUTO2000 software is an open source program that computes bifurcation diagrams with a wide range of applicational use beyond the CR3BP. Gómez and Masdemont showed that the invariant manifold structures of the collinear libration points have different types of motion inside the manifold and outside the manifold (Gomez, et al., 2001). Their work was focused around the potential for mission use of a Petit Grand Tour of the Jovian moon system with a numerical algorithm that can be used for any three-body system. In 2004, Chow, Gralla, and Kasdin constructed a LEO constellation design using the L_1

Lagrange point to deploy multiple satellite while implementing a plane change. Their research displayed the use of Lissajous orbits about the L_1 Lagrange point with a minimal change in velocity for each satellite. The mission design that was developed however did not take into consideration cost related issues due to radiation and communication gaps. Overall, the cost savings for using a Lissajous orbit from LEO is approximately 38% (Nakamiya, Scheeres, Yamakawa, & Yoshikawa, 2008). In 2008, a study conducted by Sucarrat demonstrated the use of libration point orbits and transfer trajectories from LEO to GEO. With the Earth acting as the second primary body the dynamics of the manifold act as an assist with a low-cost velocity change that approaches the equilibrium points (Sucarrat & Soler, 2009). The work presented in this research continues to further the use of plane change maneuvers with the use of the L_2 Lagrange point with a trajectory from LEO to GEO with a result of having a different inclination.

1.5 Current Work

For application use of efficient fuel transfers for plane change maneuvers, the initial design begins with the CR3BP for the Sun-Earth/Moon system. A first-order linear approximation for a small amplitude Halo orbit near the L_2 Lagrange point is used to obtain a Lyapunov vertical and horizontal orbit. In addition to the family of orbits obtained a one impulse maneuver is created from LEO to demonstrate a plane change maneuver. The orbital design takes advantage of invariant manifolds providing a change of inclination. Furthermore, the use of a horizontal and vertical Lyapunov orbit relate to an additional maneuver to demonstrate a fuel-efficient method for a 90-degree plane change. A brief review of retrograde orbits is also studied with the constructed method. Measurements of optimality are briefly reviewed with bounding spheres and primer vector theory. Finally, fuel efficiency is compared with traditional inclination transfer methods and results with previous research.

The libration point orbits are conducive to plane change maneuvers as the geometries of the system create large inclination changes. With an initial impulse a satellite will follow a weak stable boundary out to a libration point orbit and return to the initial primary body following a weak unstable boundary, while having undergone a plane change. In previous research a variety of different Halo orbits were chosen for various resulting inclination changes with a single impulse. This research will use a two impulse maneuver to further increase the change of inclination. To decrease the scope of this research the use of Lyapunov horizontal and vertical orbits are used to

demonstrate large inclinations changes and retrograde changes. For the two impulse maneuver patch points are selected and increase time of flight is incurred. Fuel efficiency and time of flight are viewed as the primary factors of consideration of trajectory design. The solutions developed are not only compared to other transfer methods but also other factors that can impact the mission use. Factors reviewed include cost savings with fuel, launch locations and launch schedules. Negative impactors taken into consideration include communication gaps and radiation impacts. Orbits are modeled with a python script modified from a trans-lunar injection script (Baines, Hew, & Toyama). Additional modeling is created with MATLAB provided by Orbital Mechanics for Engineering students (Curtis, 2020). Finally, all the results from the trajectories formed will be compared to different overall mission costs to determine overall effectiveness.

1.6 Overview

In chapter 2, a discussion for the model chosen is provided along with derivation of the equations. The CR3BP differential equations are formulated along with the Jacobi constant. A method of computation for the collinear equilibrium points within the system is included. First-order analytical approximations are summarized for Lyapunov orbits about the first and second collinear equilibrium points and the state transition matrix is defined. Methods of correcting periodic orbits for variations along the path are described and invariant manifold theory is introduced.

In chapter 3, a reconstruction of the trans-lunar trajectory and results are used to test a python model with the research results of (Baines, Hew, & Toyama). Changes within the model are in the form of initial conditions along with an expansion into three dimensions for the CR3BP. Many different orbits from the Lyapunov family are represented in the vicinity of the L_2 equilibrium point. A recreation of a single impulse maneuver using a Lyapunov orbit is demonstrated to compare with the results of Davis et al. (2011). A brief review on transfer methods to connect two impulse maneuvers with a bounding sphere and primer vector theory are also described. Orbits with characteristics that support a two impulse maneuver are derived to provide large inclination changes. Criteria for evaluation include fuel efficiency and time of flight for the developed trajectory. A brief trajectory design of retrograde orbits is reviewed to determine capability and cost savings.

In chapter 4, the advantages of the maneuver constructed from the previous chapter is analyzed for overall efficiency. Additionally, a brief review of rescue and salvage missions is conducted to demonstrate the current use for low energy transfers. To further develop the constructed orbits for potential mission use, a review of environmental conditions is also conducted. Negative impacts to using the trajectory designed such as communication gaps and impacts of radiation are discussed. Finally, other economic and mission benefits are analyzed to determine the overall feasibility.

Finally, in chapter 5 the conclusion of the research provides a summary and result with overall efficiency savings, time of flight and mission effectiveness. A discussion of future work is provided for continued advancements in the research that has been presented.

2. BACKGROUND

Traditional methods of orbital maneuvers are constructed with two body conics. However, the two-body method does not describe the full motion within a system as an object is being perturbed by multiple bodies. A conics model does not provide any notion or modeling capability for near equilibrium points. In a system describing the motion of three bodies one being infinitesimal in mass compared to the other two bodies a set of differential equations can be used to describe the motion taken by the object of interest. Methods of modeling n – bodies (where n is greater than 2) are more complex compared to a two-body problem or conic approach in that no closed form solution exists. Despite the CR3BP not having a closed form, numerical integration yields unexpected solutions for a variety of periodic orbits in the vicinity of the primary bodies without orbiting either one with an infinite variety of orbital trajectories. The motion of a satellite within the CR3BP can be modeled from the differential equations formulated. The method of determining position and velocity along a trajectory path within the conducted research is numerically computed with a Runge-Kutta numerical method. The equilibrium points in this system are easily computed. The Jacobi constant relates position to velocity at any given point as a conserved quantity for the system and can be used to derive numerous solutions. A linear approximation is derived from an understanding of the Lagrange points and corrected for a nonlinear system. The state transition matrix is introduced with a method for future variations along a given path. Finally, a brief introduction into invariant manifold theory is provided.

2.1 The Circular Restricted Three-Body Problem

The general three body problem is formed by creating a model based on the notion that there are only three bodies, all three bodies are treated as a point mass, and the only interactive force within the system is caused by gravity. The position of a first body (denoted as P_3 with a mass of m_3) relative to two other bodies (denoted as P_1 with mass m_1 and P_2 with mass m_2 respectively) is depicted in Figure 2-1 in the inertial reference frame of motion in a free body diagram. To describe the motion in which P_3 is governed within the system Newton's Law of Gravitational Motion provides the differential equation,

$$m_3 \frac{d^2\vec{r}_3}{dt^2} = -\frac{Gm_3m_1}{\|\vec{r}_{13}\|^3}\vec{r}_{13} - \frac{Gm_3m_2}{\|\vec{r}_{23}\|^3}\vec{r}_{23} \tag{2.1}$$

where G is the universal gravitational constant $6.674\text{x}10^{-20}$ $km^3\,kg^{-1}\,s^{-2}$. From equation (2.1), $\vec{r}_{13}$ and $\vec{r}_{23}$ are the relative positions of P_3 with respect to P_1 and P_2.

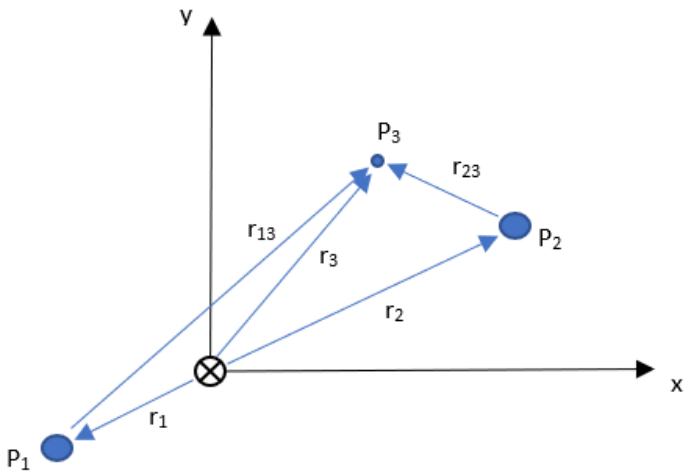

Figure 2-1 Three-Body Problem Inertial Reference Frame

The CR3BP is considered restricted in that one body is smaller compared to the other two. The mass is restricted such that $m_1 > m_2 >> m_3$. This implies that m_3 is infinitesimal and cannot impact the motion of m_1 or m_2. For the model being conducted this assumption is acceptable in that a satellite is not going to have a meaningful impact on the Sun or the Earth/Moon as a combined mass. A second restriction onto the CR3BP is that the orbits of the two primary bodies are circular about the center of mass or barycenter. To determine if the Sun-Earth/Moon model is a valid setup it is important to check the circularity of the orbit. Earth's eccentricity (e) about the sun is 0.0162, thus assuming e = 0 is relatively realistic. A final check of the assumptions made is to compare the masses and mass ratio value of m_1 and m_2 to ensure that the mass of the first and second primary bodies are such that $m_1 > m_2$ and that the mass ratio follows μ: $0 < \mu \leq 0.5$. Using a system where the first primary mass is the Sun and the second primary mass is the Earth/Moon the mass ratio for the system is $\mu = 3.04 \times 10^{-6}$. With two primary bodies orbiting around a barycenter Figure 2-1 can be redefined such that P_1 and P_2 are fixed along an axis with a rotating reference frame as depicted in Figure 2-2 free body diagram.

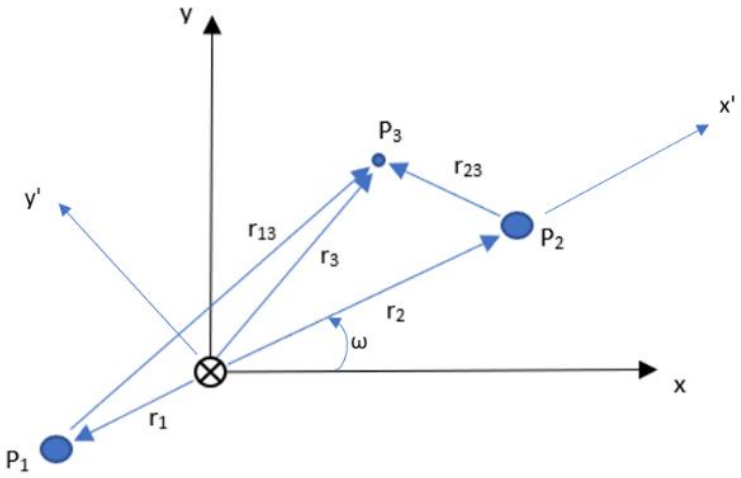

Figure 2-2 Restricted Three-Body Problem Rotating Reference Frame

Equation 2.1 can be generalized by introducing characteristic quantities of length and time. The characteristic length l is the sum of the vectors r_1 and r_2 such that

$$l^* = \|\bar{r}_1\| + \|\bar{r}_2\| \tag{2.2}$$

The characteristic time t is computed as

$$t^* = \sqrt{\frac{l^{*3}}{GM_{total}}} \tag{2.3}$$

With the motion of P_2 about P_1 being assumed to be circular, the characteristic length remains constant. Using equations (2.2) and (2.3) with the mass ratio,

$$\mu = \frac{m_2}{m_1+m_2} \tag{2.4}$$

equation (2.1) becomes

$$\frac{d^2\vec{r}_3}{d\tau^2} = -\frac{1-\mu}{\|\vec{r}_{13}\|^3}\vec{r}_{13} - \frac{\mu}{\|\vec{r}_{23}\|^3}\vec{r}_{23} \tag{2.5}$$

where

$$\vec{r}_3 = \frac{\vec{r}_3}{l^*} = x\hat{x} + y\hat{y} + z\hat{z} \tag{2.6}$$

$$\vec{r}_{13} = \frac{\vec{r}_{13}}{l^*} = (x + \mu)\hat{x} + y\hat{y} + z\hat{z} \tag{2.7}$$

$$\vec{r}_{23} = \frac{\vec{r}_{23}}{l^*} = (x - (1 + \mu))\hat{x} + y\hat{y} + z\hat{z} \tag{2.8}$$

and the non-dimensional time is represented as,

$$\tau = \frac{t}{t^*} \tag{2.9}$$

Equation (2.5) can be expanded kinematically. The motion of P_3 can be described in relation to the barycenter of the system in the rotating reference frame. The rotating reference frame must be taken into consideration as derivatives are taken. Using the kinematic transport theorem, the rotating frame can be expressed as

$$I\frac{dp^{\omega}}{dt} = I\frac{dp}{dt} + \omega \times p \tag{2.10}$$

Using the transport theorem for a second time the kinematics of motion for the rotating reference frame become

$$\ddot{\vec{p}} = (\ddot{x} - 2y - x) + (\ddot{y} + 2\dot{x} - y) + \ddot{z}\dot{z} \tag{2.11}$$

The time derivatives within equation (2.11) are represented differentially with respect to τ. Given the expressions (2.6) – (2.11) the vector equation from (2.5) can be rewritten in scalar form as

$$\ddot{x} - 2\dot{y} - x = -\frac{(1-\mu)(x+\mu)}{\|\vec{r}_{13}\|^3} - \frac{\mu(x-(1-\mu))}{\|\vec{r}_{23}\|^3} \tag{2.12}$$

$$\ddot{y} - 2\dot{x} - y = -\frac{(1-\mu)y}{\|\vec{r}_{13}\|^3} - \frac{\mu y}{\|\vec{r}_{23}\|^3} \tag{2.13}$$

$$\ddot{z} = -\frac{(1-\mu)z}{\|\vec{r}_{13}\|^3} - \frac{\mu z}{\|\vec{r}_{23}\|^3} \tag{2.14}$$

Equations (2.12)-(2.14) describes the motion of the third body in the rotating frame within the CR3BP. These equations are non-linear due to the denominator on the right-hand side of the expressed equations. Another observation is that the x and y axis are coupled and cannot be separated or solved independently from each other. The z-axis is uncoupled meaning that if only planar motion is provided the resulting trajectory will remain planar. The planar circular restricted three body problem (PCR3BP) only considers the x and y axis as a simplification to the CR3BP by setting z axis position and velocity equal to zero. The PCR3BP is common throughout literature and often referenced as the CR3BP. Also, given that the only force within the model is caused by gravity and that gravity is a conservative force, it can be written as the gradient of a potential, Ω.

The gradient of a potential can be expressed as

$$\vec{F} = -\nabla\Omega \tag{2.15}$$

Given the defined rotating reference frame from the CR3BP the pseudo-potential Ω^* can be expressed as

$$\Omega_* = \frac{1-\mu}{\|\vec{r}_{13}\|^3} + \frac{\mu}{\|\vec{r}_{23}\|^3} + \frac{x^2+y^2}{2} \tag{2.16}$$

With the pseudo-potential the equations of motion for the CR3BP can be expressed as

$$\ddot{x} = 2\dot{y} + \Omega_{x*} \tag{2.17}$$

$$\ddot{y} = 2\dot{x} + \Omega_{y*} \tag{2.18}$$

$$\ddot{z} = \Omega_{z*} \tag{2.19}$$

2.2 Equilibrium Points

Within the CR3BP the only force within the system is gravity from each primary body. The point of which the forces of gravity are equal for both bodies create equilibrium points. From the motion of the second primary body orbiting the first primary body five equilibrium points are in constant position to both main bodies. The equilibrium points are defined as a point in which all time derivatives of position are zero in the rotating reference frame. The system equilibrium points are also called the Lagrange points or libration points. The Lagrange points are determined from equations (2.16)-(2.19). Within the equations of motion setting all acceleration and velocity to zero the following relationships yield the constant equilibrium solutions as

$$0 = x - \frac{(1-\mu)(x+\mu)}{\|\vec{r}_{13}\|^3} - \frac{\mu(x-(1-\mu))}{\|\vec{r}_{23}\|^3} = \Omega_{x*} \tag{2.20}$$

$$0 = y - \frac{(1-\mu)y}{\|\vec{r}_{13}\|^3} - \frac{\mu y}{\|\vec{r}_{23}\|^3} = \Omega_{y*} \tag{2.21}$$

$$0 = -\frac{(1-\mu)z}{\|\vec{r}_{13}\|^3} - \frac{\mu z}{\|\vec{r}_{23}\|^3} = \Omega_{z*} \tag{2.22}$$

Given the scope of the research conducted the focus of determining Lagrange points is centered around the collinear Lagrange points. The three equilibrium points, i.e. L_1, L_2, and L_3, are computed by defining y = 0 and z = 0 in equations (2.20)-(2.22). The form of the resulting equation is

$$0 = x - \frac{(1-\mu)(x+\mu)}{(x+\mu)^3} - \frac{\mu(x-(1-\mu))}{(x-1+\mu)^3} \tag{2.23}$$

and provides the positions for the L_1, L_2, and L_3 equilibrium points along the x-axis. Table 2-1 and figure 2-2 summarize the values for the collinear Lagrange points.

Table 2-1 Locating the Collinear Lagrange Points μ = 3.04x10-6

Lagrange Point	Location
L_1	0.9899897
L_2	1.0100741
L_3	-1.0000043

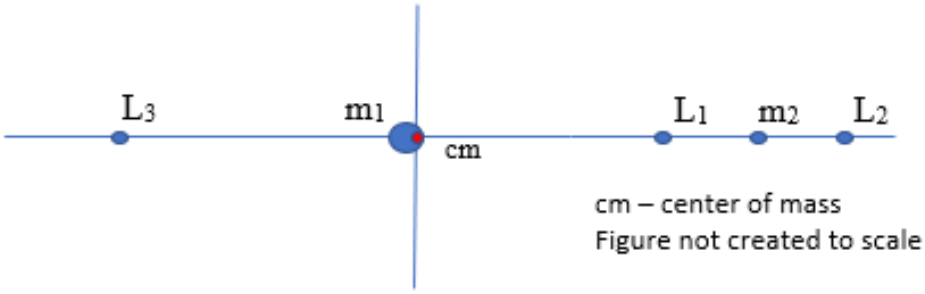

Figure 2-3 Collinear Equilibrium Points in the CR3BP

2.3 Numerical Computation Runge-Kutta Method

In the 20th century German mathematicians Carl Runge and Martin Kutta formulated the Runge-Kutta method. These iterative methods of numerical analysis are commonly used in computational physics. These methods are closely related to the Taylor series expansion without differentiation. Of the numerous Runge-Kutta methods and techniques, for this given body of research the Runge-Kutta 4th order is selected to provide numerical solutions. The 4th order method is used to solve ordinary differential equations (ODE). The general formula for the Runge-Kutta 4th order method is

$$k_1 = dt \cdot g[t_i, f_i] \tag{2.24}$$

$$k_2 = dt \cdot g[t_i + \frac{dt}{2}, f_i + \frac{k_1}{2}] \tag{2.25}$$

$$k_3 = dt \cdot g[t_i + \frac{dt}{2}, f_i + \frac{k_2}{2}] \tag{2.26}$$

$$k_4 = dt \cdot g[t_i + dt, f_i + k_3] \tag{2.27}$$

$$f_i = f_i + \frac{k_1}{6} + \frac{k_2}{3} + \frac{k_3}{3} + \frac{k_4}{6} \tag{2.28}$$

This approach only solves the first order ODEs within the system. However, this method completes four evaluations for every step on the right-hand side of the equation of the ODEs. From the above method k_1 is a whole step whereas k_2 and k_3 are half steps that are evaluated by the midpoint with k_4 trailing from the final point. The Runge-Kutta method of numerical computation is also used in programs such as STK and other orbital simulators.

When using methods of numerical analysis, it is critical to test the accuracy of the method for the given system and to optimize the size of the integration. One technique to test accuracy for a

method is to loop through several step sizes and compare the numerical results to an analytical solution. With graphing, the numerical results can be observed using trajectories created over several step sizes allowing for a visual check to determine changes in a path for a particles motion. A backwards compatibility test is conducted by randomly selecting initial conditions at some point in time and integrating backwards to see how the trajectory of a particle is affected. The ending conditions created from integrating backwards are then used as the initial conditions and integrated forward in time. Both paths of integration can be compared by observing how they change with respect to different step sizes of time.

2.4 Constructing Libration Point Orbits

The dynamics of the three-body problem allow for the introduction of libration point orbits. With the CR3BP being a simplified version of the three-body problem libration point orbits are still capable of being demonstrated within the model. With the ability to demonstrate libration point orbits a wide variety of orbital trajectories can be developed and tested for efficiency. The use of the Jacobi constant for different trajectories relates the object of interest's position and velocity to unique solutions and forbidden regions. Given a set of initial conditions different families of libration point orbits can be created. For the scope of the research conducted a method of creating horizontal and vertical Lyapunov orbits is constructed.

2.4.1 Jacobi Constant and Forbidden Regions

With the CR3BP the Jacobi constant is the only known conserved quantity. As conserved quantity the Jacobi constant can act as a numerical value for the system and trajectory taken. From equation (2.12)-(2.14) and (2.16) when multiplied each by their perspective velocities and added together the result formulates the following equation

$$\dot{x}\ddot{x} + \dot{y}\ddot{y} + \dot{z}\ddot{z} = \Omega_{x*}\dot{x} + \Omega_{y*}\dot{y} + \Omega_{z*}\dot{z} \tag{2.29}$$

When expanding the right-hand side of the equation

$$\dot{x}\ddot{x} + \dot{y}\ddot{y} + \dot{z}\ddot{z} = \frac{\delta\Omega_*}{\delta x}\frac{dx}{d\tau} + \frac{\delta\Omega_*}{\delta y}\frac{dy}{d\tau} + \frac{\delta\Omega_*}{\delta z}\frac{dz}{d\tau} \tag{2.30}$$

both sides can be integrated by the non-dimensional time. The result of integrating both sides of the equation provide the following equations

$$\frac{1}{2}(\dot{x}^2 + \dot{y}^2 + \dot{z}^2) = \Omega_* - C \tag{2.31}$$

$$C = 2\Omega_* - V^3 \tag{2.32}$$

In equation (2.32) C is the Jacobi constant and V is the magnitude of the velocity. Mapping the Jacobi constant to Sun-Earth/Moon model figure 2-4 outlines different regions in which a third object can be present for a given velocity.

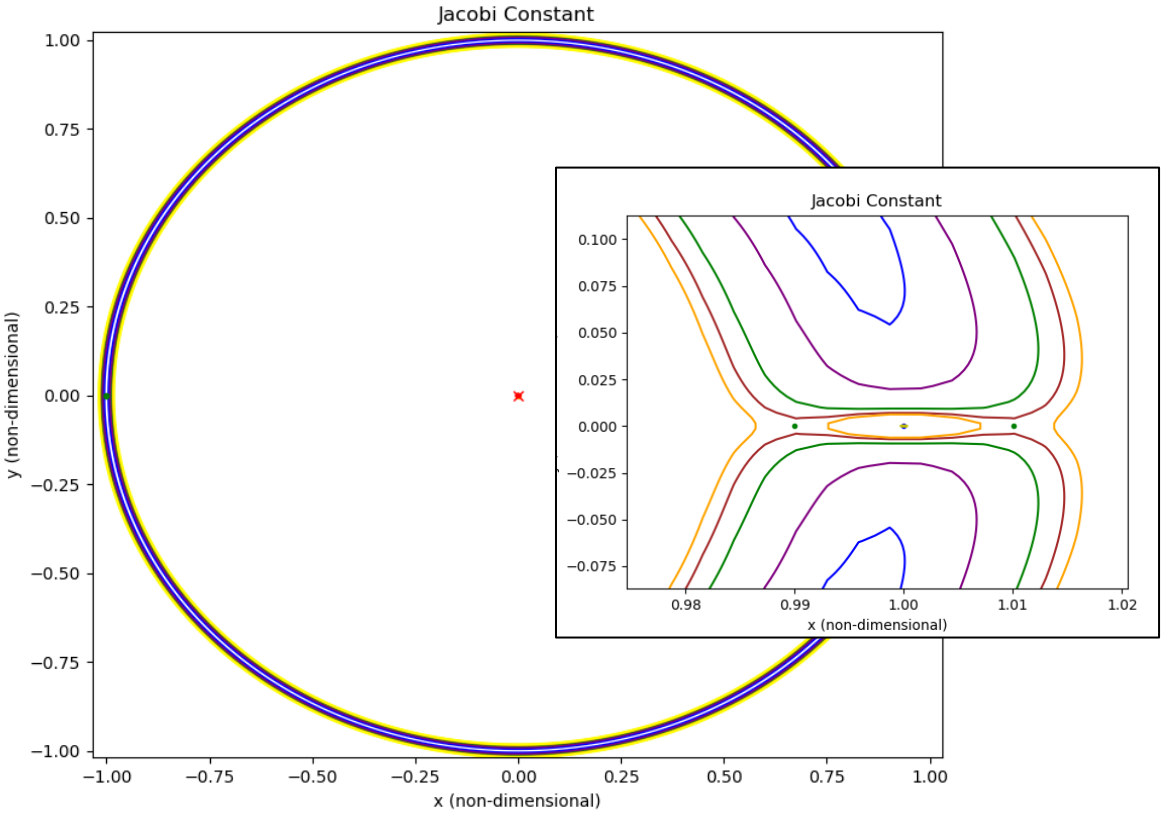

Figure 2-4 Jacobi Contour Sun-Earth/Moon (x – y View)

From figure 2-4 for a given value of the Jacobi constant the curves of zero velocity are represented by the different color outlined shapes. These boundaries cannot be crossed by a secondary mass moving within the allowable region that is only moving under the influence of gravity from both primary bodies. As the Jacobi constant decreases the region between the two primary bodies increase. This area is known as the Hill's region. As the Hill's region grows the secondary mass can now move between or transfer in orbit from one primary to another. When adjusting the Jacobi constant, the L_1 point opens first followed by the L_2 and finally the L_3. At different states of lower Jacobi constant values there are still forbidden regions around the L_4 and L_5 regions before the forbidden region is completely gone as the Jacobi constant decreases. When

creating orbits that take advantage of the equilibrium points the Jacobi constant can also provide a limit for size of the libration point orbit.

2.4.2 Linear Approximation for Lyapunov Orbits

A first-order linear analytical approximation of motion for the collinear libration point orbits are derived with respect to the equilibrium points. From the equations of motion (2.16) and (2.20)-(2.22) an initial step is to set a point some distance away from the equilibrium points. The initial setup for a point away from the equilibrium point is demonstrated with the following equations

$$\xi = x - x_{eq} \tag{2.33}$$

$$\eta = y - y_{eq} \tag{2.34}$$

$$\zeta = z - z_{eq} \tag{2.35}$$

The points ξ, η, and ζ are relative variations to the equilibrium points from the numerical values of x_{eq}, y_{eq}, and z_{eq}. To form linearized equations a first order Taylor series expansion is taken from equations (2.33)-(2.35) with the equations of motion to provide the following results

$$\ddot{\xi} - 2\dot{\eta} = \Omega_{xx}\xi + \Omega_{xy}\eta + \Omega_{xz}\zeta \tag{2.36}$$

$$\ddot{\eta} + 2\dot{\xi} = \Omega_{xy}\xi + \Omega_{yy}\eta + \Omega_{yz}\zeta \tag{2.37}$$

$$\ddot{\zeta} = \Omega_{xz}\xi + \Omega_{yz}\eta + \Omega_{zz}\zeta \tag{2.38}$$

The equation (2.16) describes the pseudo-potential Ω^* with all the following being the different second order partial derivatives

$$\Omega_{xx} = 1 - \frac{1-\mu}{\|\vec{r}_{13}\|^3} - \frac{\mu}{\|\vec{r}_{23}\|^3} + \frac{3(1-\mu)(x+\mu)^2}{\|\vec{r}_{13}\|^5} + \frac{3\mu(x-1+\mu)^2}{\|\vec{r}_{23}\|^5} \tag{2.39}$$

$$\Omega_{yy} = 1 - \frac{1-\mu}{\|\vec{r}_{13}\|^3} - \frac{\mu}{\|\vec{r}_{23}\|^3} + \frac{3(1-\mu)y^2}{\|\vec{r}_{13}\|^5} + \frac{3\mu y^2}{\|\vec{r}_{23}\|^5} \tag{2.40}$$

$$\Omega_{zz} = -\frac{1-\mu}{\|\vec{r}_{13}\|^3} - \frac{\mu}{\|\vec{r}_{23}\|^3} + \frac{3(1-\mu)z^2}{\|\vec{r}_{13}\|^5} + \frac{3\mu z^2}{\|\vec{r}_{23}\|^5} \tag{2.41}$$

$$\Omega_{xy} = \Omega_{yx} = \frac{3(1-\mu)(x+\mu)y}{\|\vec{r}_{13}\|^5} + \frac{3\mu(x-1+\mu)y}{\|\vec{r}_{23}\|^5} \tag{2.42}$$

$$\Omega_{xz} = \Omega_{xz} = \frac{3(1-\mu)(x+\mu)z}{\|\vec{r}_{13}\|^5} + \frac{3\mu(x-1+\mu)z}{\|\vec{r}_{23}\|^5} \tag{2.43}$$

$$\Omega_{yz} = \Omega_{zy} = \frac{3(1-\mu)yz}{\|\vec{r}_{13}\|^5} + \frac{3\mu yz}{\|\vec{r}_{23}\|^5} \tag{2.44}$$

With the focus of the analytical results being for collinear equilibrium points $z_{eq} = 0$ and $y_{eq} = 0$ making $\Omega_{xz} = \Omega_{yz} = \Omega_{xy} = 0$, $\Omega_{zz} < 0$, and $\Omega_{yy} < 0$. Therefore equations (2.36)-(2.38) simplify to

$$\ddot{\xi} - 2\dot{\eta} = \Omega_{xx}\xi \tag{2.45}$$

$$\ddot{\eta} + 2\dot{\xi} = \Omega_{yy}\eta \tag{2.46}$$

$$\ddot{\zeta} = \Omega_{zz}\zeta \tag{2.47}$$

Once again with the created equations of motion equations (2.45) and (2.46) are coupled and equation (2.47) is independent. The general solution for equation (2.47) is

$$\zeta = C_1 \cos(\tau v) + C_2 \sin(\tau v) \tag{2.48}$$

Where C_1 and C_2 are constants. Given that a linear system has been created equations (2.45)-(2.47) can be represented in matrix format

$$\dot{x} = A\vec{x} \tag{2.49}$$

With the matrix format from equation (2.49) and the z component being uncoupled

$$A = \begin{bmatrix} 0 & 0 & 1 & 0 \\ 0 & 0 & 0 & 1 \\ \Omega_{xx} & \Omega_{xy} & 0 & 2 \\ \Omega_{xy} & \Omega_{yy} & -2 & 0 \end{bmatrix} \tag{2.50}$$

The eigenvalues of the matrix of equation (2.50)

$$\lambda^4 + (4 - \Omega_{xx} - \Omega_{yy})\lambda^2 + (\Omega_{xx}\Omega_{yy} - \Omega_{xy}\Omega_{yx}) = 0 \tag{2.51}$$

Equation (2.51) expressed in a quadratic equation

$$\Lambda^2 + 2\beta_1\Lambda - \beta_2^2 = 0 \tag{2.52}$$

where

$$\beta_1 = 2 - \frac{\Omega_{xx}+\Omega_{yy}}{2} \tag{2.53}$$

$$\beta_2^2 = -\Omega_{xx}\Omega_{yy} + \Omega_{xy}\Omega_{yx} \tag{2.54}$$

$$\lambda_{1,2} = \pm\sqrt{\Lambda_1} \tag{2.55}$$

$$\lambda_{3,4} = \pm\sqrt{\Lambda_2} \tag{2.56}$$

The results of λ represent the eigenvalues for equations (2.45)-(2.47) and the general solution for ξ and η are

$$\xi = \sum_{i=1}^{4} A_i e^{\lambda_i \tau} \tag{2.57}$$

$$\eta = \sum_{i=1}^{4} B_i e^{\lambda_i \tau} \tag{2.58}$$

The values of A and B are dependent on each other as constants. Substituting equations (2.57) and (2.58) into equations (2.45) and (2.46) perspectivity providing the relationship of A and B to be

$$B_i = \frac{\lambda_i + \Omega_{xx}}{2\lambda_i} A_i \tag{2.59}$$

Equations (2.57) and (2.58) are with respect to τ and substituted into equation (2.59) while evaluated at an initial point $\tau = 0$, then

$$\xi_0 = \sum_{i=1}^{4} A_i \tag{2.60}$$

$$\dot{\xi}_0 = \sum_{i=1}^{4} A_i \lambda_i \tag{2.61}$$

$$\eta_0 = \sum_{i=1}^{4} \frac{\lambda_i - \Omega_{xx}}{2\lambda_i} A_i \tag{2.60}$$

$$\dot{\eta}_0 = \sum_{i=1}^{4} \frac{\lambda_i - \Omega_{xx}}{2\lambda_i} A_i \lambda_i \tag{2.61}$$

From equation (2.52) when evaluating the collinear equilibrium points where all points along the y-axis are equal to zero the results form equations (2.53) and (2.54). Simplifying the form of equation (2.52) the results provide one positive, negative, and two purely imaginary answers. This means that all the collinear equilibrium points are unstable saddle points. Therefore, if A_1 and A_2 correspond to the stable and unstable points then at a certain point $A_1 = A_2 = 0$, where ξ, η, and ζ can be expressed as

$$\xi = \xi_0 \cos(s\tau) + \frac{\eta_0}{\beta_3} \sin(s\tau) \tag{2.62}$$

$$\eta = \eta_0 \cos(s\tau) + \xi_0 \beta_3 \sin(s\tau) \tag{2.63}$$

$$\zeta = \zeta_0 \cos(v\tau) + \frac{\zeta_0}{v} \sin(s\tau) \tag{2.64}$$

From equations (2.62)-(2.64) s and β_3 are

$$s = \sqrt{\beta_1 + (\beta_1{}^2 + \beta_2{}^2)^{1/2}} \tag{2.65}$$

$$\beta_3 = \frac{s^2 - \Omega_{xx}}{2s} \tag{2.66}$$

The period of motion for the above equations is 2π over s. Also, s and v numerically are relativity close in value suggesting that the motion being modeled is quasi-periodic. The quasi-periodic motion in a dynamical system is an orbit that contains a finite number of rotations about a point. From equations (2.62)-(2.64) further simplification can be made for conditions of quasi-periodic orbits. Making the conditions specified by an amplitude A_ξ in the ξ and A_η in the η direction equations (2.62)-(2.64) become

$$\xi = -A_\xi \cos(s\tau + \varphi) \tag{2.67}$$

$$\eta = A_\xi \beta_3 \sin(s\tau + \varphi) \tag{2.68}$$

$$\zeta = A_\zeta \sin(v\tau + \psi) \tag{2.69}$$

With the motion of interest being horizontal Lyapunov orbits, equations (2.64) and (2.69) are not needed, however stated for completeness. When modeling equations (2.67) and (2.68) a libration point orbit can be created within a linear system. Figure 2-5 is the resulting motion when using equations (2.67) and (2.68). Measurements of amplitude pertain to the maximum distance from the equilibrium point with respect to a given axis to quantify the size of a libration point orbit.

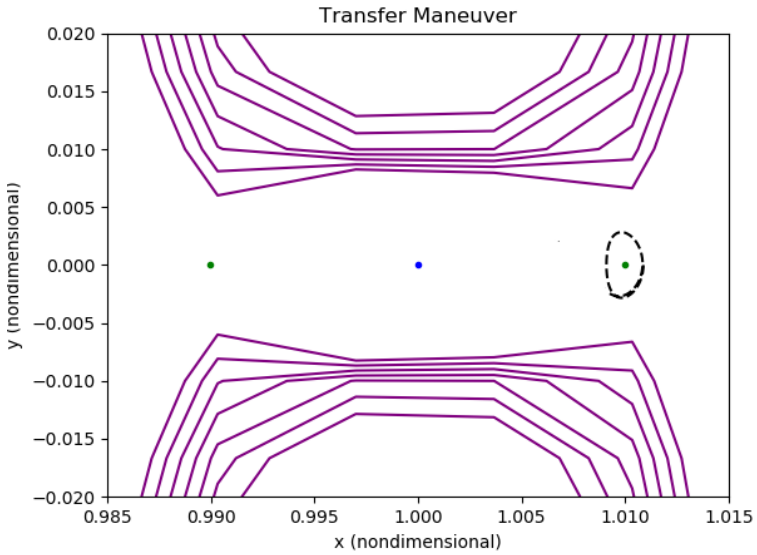

Figure 2-5 Linear Approximation for the L2 Horizontal Lyapunov Orbit

Figure 2-5 is a linear approximation imposed onto the system. Although the linear approximation is a decent starting point further adjustment is required to obtain a Lyapunov orbit within the CR3BP system.

2.4.3 Non-Linear Correction

Developing an analytical approximation provides insight to different aspects of the system. In figure 2-5 an analytical linear approximation for a Lyapunov orbit was created and imposed onto the CR3BP model. In the previous section the collinear equilibrium points were determined to be saddle points. Also, a first method of creating orbits using motion from the dynamics of the three or more bodies was created. However, the equations of motion (2.12)-(2.14) show that the model is non-linear. Figure 2-6 is the same linearized approximation generated within the non-linear system model. With the equations of motion different methods can be created for correcting the initial conditions which will provide the desired trajectory. To further develop the modeling of

orbits (Grebow, 2006) created an analytical correction process to adjust for the non-linearity within the model. Another approach to correcting for the non-linearities for the system is a shooting scheme.

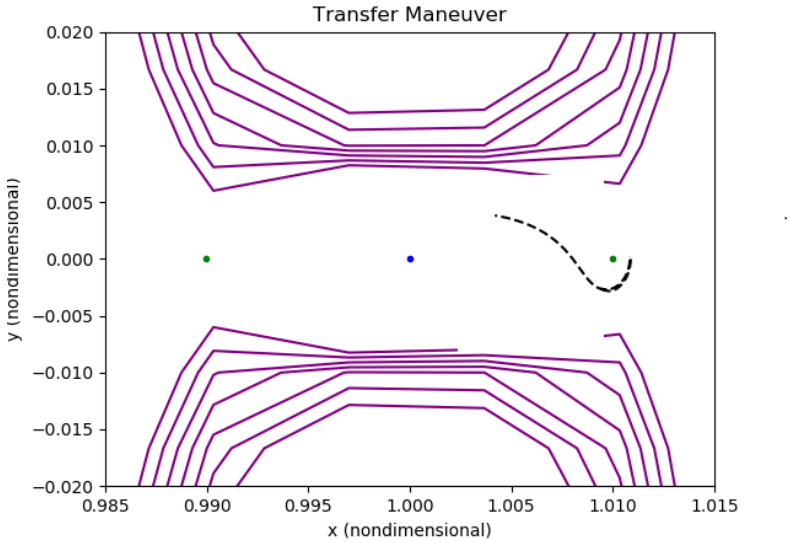

Figure 2-6 Linear Approximation Mapped with Non-linear System

A common task within dynamics in determining a trajectory is getting an object from point A to point B. Unfortunately, like most real dynamic problems like the CR3BP there is no closed form solution and it requires the use of numerical methods. In numerical analysis a shooting scheme is a method for solving the desired end state. Using the equation for Newton's Method generalized for multiple dimensions instead of a single variable and changing the division of vectors into multiplication of the inverse equation (2.70) is formed.

$$\boldsymbol{X}_{n+1} = \boldsymbol{X}_n - f'(\boldsymbol{X}_n)^{-1} f(\boldsymbol{X}_n) \tag{2.70}$$

where $f'(\boldsymbol{X}_n)$ is a matrix of partial derivatives of the function with respect to the variables defined by equation (2.71).

$$f' = \begin{bmatrix} \frac{\delta f_1(t_f)}{\delta x_1(0)} & \frac{\delta f_1(t_f)}{\delta x_2(0)} & \cdots & \frac{\delta f_1(t_f)}{\delta x_n(0)} \\ \frac{\delta f_2(t_f)}{\delta x_1(0)} & \frac{\delta f_2(t_f)}{\delta x_2(0)} & \cdots & \frac{\delta f_2(t_f)}{\delta x_n(0)} \\ \vdots & \vdots & \ddots & \vdots \\ \frac{\delta f_m(t_f)}{\delta x_1(0)} & \frac{\delta f_m(t_f)}{\delta x_2(0)} & \cdots & \frac{\delta f_m(t_f)}{\delta x_n(0)} \end{bmatrix} \tag{2.71}$$

When given an input of x_o with the point that is desired x_d if no correction is done the result will be x_f due to the nonlinearities in the model. The initial states can act as a function of $f(x_o) = x_f$ which will have some error with respect to x_d. To drive the difference from the calculated end point and the desired end point Newton's Method is used. With the described method a trajectory from point A to point B can be generated with the general form of Newton's Method. Initial conditions for the dynamics of the CR3BP are represented as

$$x = \left[x_0, y_0, z_0, v_{x_0}, v_{y_0}, v_{z_0}\right] \tag{2.72}$$

Given the above method and the initial condition an iterative approach is created to achieve the intended trajectory. Figure 2-7 shows a graphical representation of the iterative approach taken to form the Lyapunov orbit.

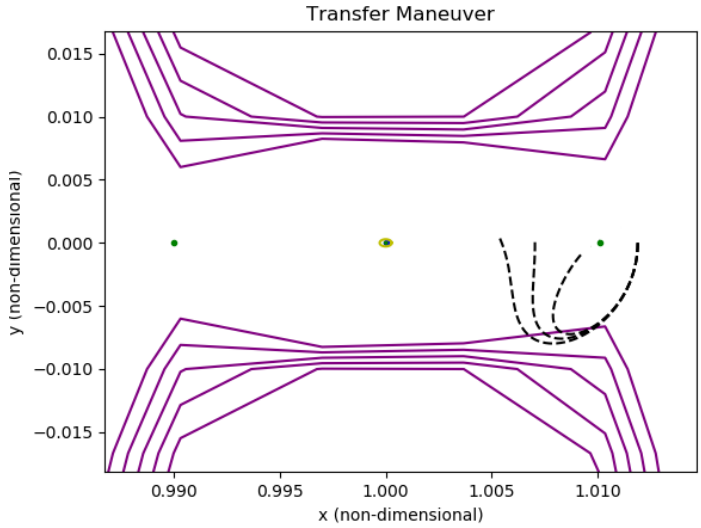

Figure 2-7 Iterative Non-linear Correction for the L2 Horizontal Lyapunov Orbit

After successfully creating a Lyapunov orbit about the L_2 equilibrium point the constructed method can be used to create an entire family of Lyapunov orbits. The demonstrated approach in this research is also used for creating vertical Lyapunov orbits as well. A natural extension of the work conducted would include Lissajous, Halo, Axial, and other orbits with the addition of motion within the z-axis from equation (2.50) state-transition matrix. In table 2-2 the family of Lyapunov orbits is provided with the initial conditions for a system in which $\mu = 3.04 \times 10^{-6}$ and all other parameters from equation (2.72) set to zero. From table 2-2 a graphical representation of the Lyapunov orbit family is created in figure 2-8.

Table 2-2 Initial Conditions for L2 Lyapunov Orbits

x	$\dot{y}$
1.010574	-0.003433
1.010874	-0.005674
1.011574	-0.011650
1.011874	-0.014585
1.012074	-0.016614
1.012274	-0.018600
1.012474	-0.020421
1.012674	-0.022004
1.012874	-0.023337
1.013074	-0.024454
1.013274	-0.025411
1.013474	-0.026240
1.013674	-0.026973
1.013874	-0.027632
1.014074	-0.028235
1.014274	-0.028793

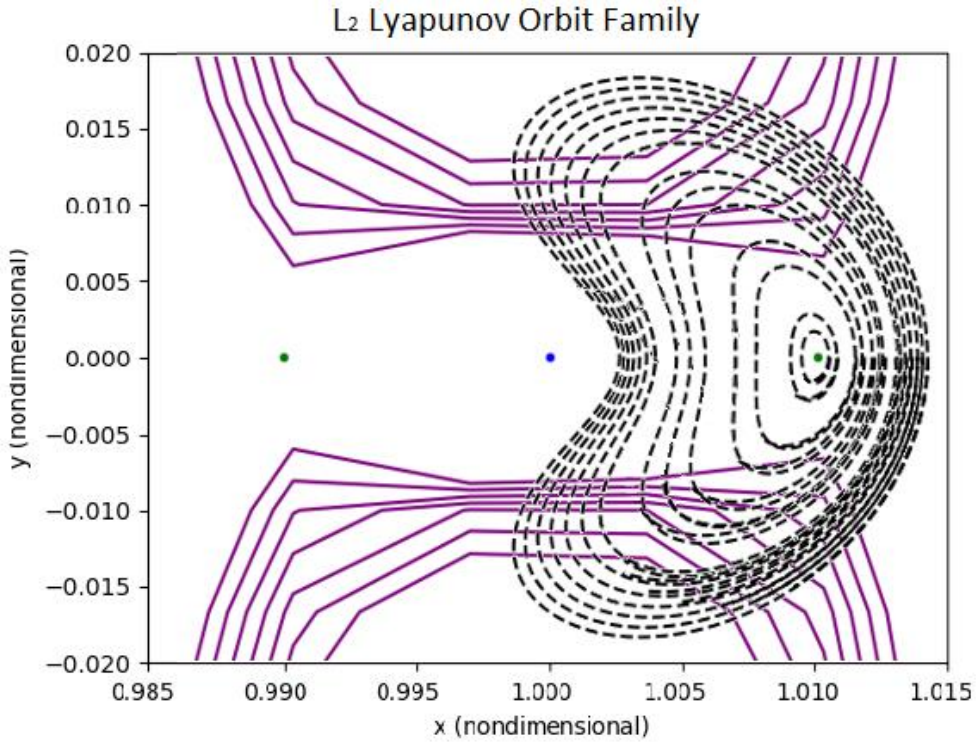

Figure 2-8 Linear Approximation for the L2 Horizontal Lyapunov Orbit

2.5 Brief introduction to Invariant Manifold Theory

In dynamical system theory models like the CR3BP, phase space is a space in which all possible states of a system are represented. Within a given subspace the center, stable, and unstable areas in phase space are useful in obtaining various trajectories. The phase space offers information about a model regarding the characteristics of flow. Viewing a model in phase space is often used for analyzing the original system in a simpler manner. However, there is no general way to construct such mapping. The invariant manifolds associated with unstable and stable subspaces for different periodic and quasi-periodic solutions are viewed in phase space for designing toward and away from various orbits.

For a periodic orbit any point along the path can be represented by one six-element state vector in the form of equation (2.72) along the path. Given a point along the path the state vector can be represented in matrix format like section 2.4.2 with analysis of the eigenvalues like equation (2.56). For a given eigen structure if a periodic orbit has both an unstable and stable mode than the eigenvalues can be used to develop linear approximations to an unstable W_u and stable W_s subspace. For a point in which W_u and W_s subspaces exist globally within the system unstable and stable manifold can be created. The notation from (Grebow, 2006), with the globally constructed manifold, $\hat{Y}_i^{W_u}$represents a six-dimensional vector that leads to the unstable mode of the periodic or quasi-periodic orbit. The vector representation can be decomposed into three-dimensional components for position $\vec{R}_i^{W_u}$ and velocity $\vec{V}_i^{W_u}$ as follows,

$$\hat{Y}_i^{W_u} = \begin{Bmatrix} \vec{R}_i^{W_u} \\ \vec{V}_i^{W_u} \end{Bmatrix} \tag{2.73}$$

The unstable direction for the constructed vector is represented as

$$\vec{X}_i^{W_u} = \frac{\hat{Y}_i^{W_u}}{\left|\vec{R}_i^{W_u}\right|} \tag{2.74}$$

A small perturbation or in the case of the research conducted an initial thrust in the unstable direction $\vec{X}_i^{W_u}$ a satellite will leave the local region heading toward the reference solution. The flow in the unstable direction is represented by,

$$\begin{Bmatrix} \delta\vec{R}_i^{W_u} \\ \delta\vec{V}_i^{W_u} \end{Bmatrix} = d \cdot \vec{X}_i^{W_u} \tag{2.75}$$

In equation (2.75) for the research conducted d is the ΔV provided by the satellite to start the desired orbital maneuver. Analytically, the stable manifold is constructed the same way as the unstable manifold only leading the satellite back to the originating region. The use of these time invariant manifolds is beneficial in that due to the dynamics of the system less force is required to initiate a maneuver compared to other methods. Figure 2-9 graphically represents different unstable trajectories to towards a libration point orbit.

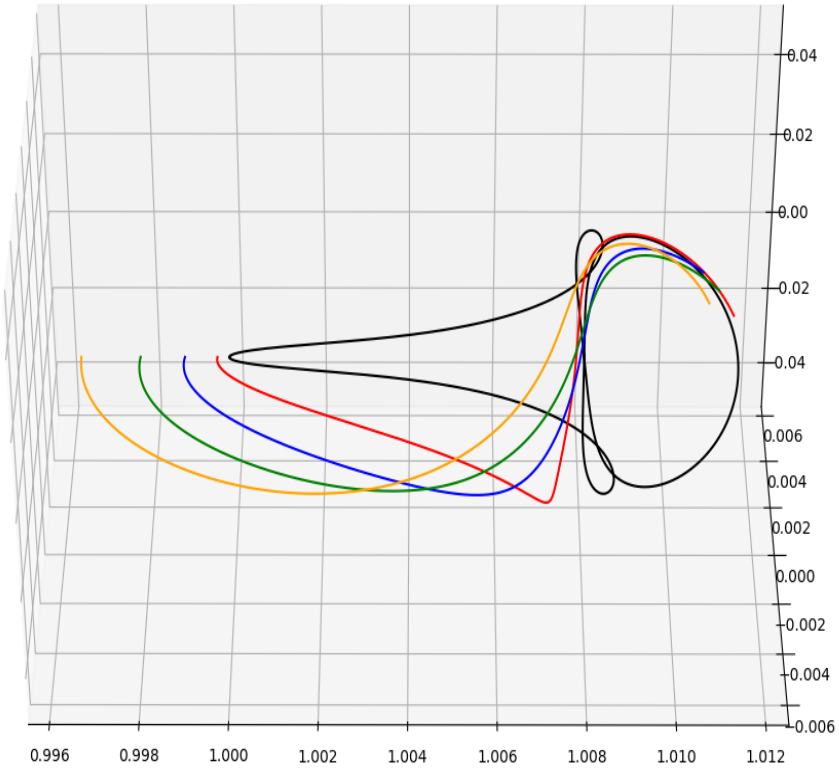

Figure 2-9 Unstable Trajectories Toward a Lyapunov Orbit

3. GENERATING LARGE INCLINATION ORBITAL MANEUVERS

To understand the body of research conducted by other authors different orbital trajectories have been collated together. The methods of capture dynamics and the use of the Moon was first introduced by Belbruno (2004) which acts as a starting point with a brief discussion of his research. Continuing the use of the moon to further develop the concepts of capture dynamics Baines et al. (2018) provides a full method of calculations with a python script for modeling. In understanding the model used, alterations to the equations of motion and initial conditions provide the necessary capability to develop trajectories that are explored in the research of Davis et al. (2011). As a natural extension of the work conducted an orbital maneuver is created with both horizontal and vertical Lyapunov orbits to create a large inclination change. With the use of different unstable and stable boundary trajectories an orbit ending in retrograde motion is briefly explored. Finally, a comparison of efficiency is conducted with a Hohman transfer maneuver.

3.1 Exploring Capture Dynamics and Chaotic Motion

With a brief overview of Belbruno's (2004) research a study of motion using manifolds and the general motion of the CR3BP is formed. In determining periodicity $\tau = \acute{\omega}/\omega$, where ω is the orbit about P_2 and $\acute{\omega}$ is the orbit about P_1, describes the motion by P_3 about the system. When τ is a positive number P_3 is in resonance for the value of τ and when τ is irrational the orbital motion is quasi-periodic. Figure 3-1 is a precessing elliptical motion of P_3 about both primary bodies. As τ varies on a set of irrational numbers a family of quasi-periodic orbits is formed.

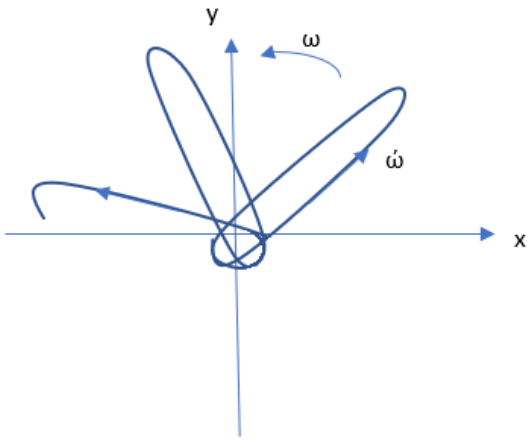

Figure 3-1 P_3 Precessing Motion

As mentioned in section 2.4.2 the collinear equilibrium points can be thought of geometrically as a saddle point. Due the geometry of the space around the saddle point there exists a local smooth stable and unstable manifold tangent to the equilibrium point. The notion of a local stable and unstable point is viewed as a case of the stable manifold theorem. With the existence of local manifolds, the notion of global manifolds is a natural extension of the local case. In section 2.5 a decomposition of the global manifold within the system is formed. The stable boundary is considered motion moving toward the primary body, while the unstable motion is considered motion moving away. The motion of P_3 at the point in space where unstable and stable coincide then move away from the primary body again in a cyclic motion is called a homoclinic loop. An example of a homoclinic loop is the trajectory from the NASA Genesis mission as the satellite crossed in and out of the different libration point orbits.

Continuing a brief study of Belbruno's research, W is defined with respect to the motion about the primary bodies P_1 or P_2. For the purpose of the research conducted W is an expression in a P_2 centered rotating motion. For W to be well defined the Jacobi constant C needs to be well known. The motion of W can be considered as a radial line from P_2 following the trajectory toward the L_2 equilibrium point. When considering the motion of W as described, the motion should satisfy the following requirements:

- The initial velocity vector describing the trajectory for P_3 is normal to the line of motion and points in a retrograde direction.
- The motion of P_3 is such that it has negative or zero Keplerian energy with respect to P_2.
- The eccentricity of P_3 being an ellipse is fixed along the line of motion, then varies along the line of motion.

In modeling the motion of P_3 the trajectory starts on an oscillating ellipse and is assumed to start at periapsis. The motion is considered stable when after leaving the line of motion P_3 makes a full cycle about P_2 without making a full cycle about P_1 and returns toward the originating point. Therefore, the motion of P_3 is unstable for motion away from P_2 and makes a cycle about P_1. Motion where P_3 is leaving along the line of motion corresponds to ballistic capture, whereas the motion of P_3 moving away from P_2 corresponds to ballistic escape. Given the system model for the CR3BP a numerical result demonstrates at a finite distance along the line of motion, lengths

shorter than the finite distance are stable and lengths greater than the finite distance are unstable. The finite point along the line of motion having an effect of stability means that W is a two-dimensional value based on position and velocity, which is known as the weak stability boundary. The set of W can be represented by the Jacobi constant and the trajectory along the line of motion. The research conducted by Baines et al. (2018) demonstrates the trajectory required for a ballistic capture by the Moon and is the foundation for the modeling created in the research conducted.

3.2 Test Case 1: The Original Model & Changes for Desired Maneuvers

The research by Baines et al. (2018) provides a C program and Python script to recreate the entirety of the work conducted. For the purpose of all the research conducted in current effort the Python script was chosen due to the ability to make rapid changes with quick execution. The compromise with using Python over C is with increase run time processing. Additionally, some of the logic used in the creation of the research conducted can be found with the MATLAB scripts provide by Curtis (2014). Before rewriting sections of code developed and using the model for the desired research, an important test is to recreate the research the code was intended to be used for. Just as the previous authors have provided their supporting code, in Appendix A the code used for the research conducted can be found. In the following section a comparison of results is conducted with an analysis of what the results mean for the model in general.

As an initial test of the Python script used the parameter for ΔV was set to zero and the height was changed with different variable distances about the surface of the earth. Although in the CR3BP the bodies are treated as point masses, a minimum distance from the central point can be created to ensure different orbital trajectories do not cross below a body's surface. Reviewing the results generated from the model the orbital period for a circular orbit can be found using equation (3.1) where Earth is the central body being orbited.

$$P_3 = 2\pi\sqrt{\frac{r_{23}^3}{1-\mu}} \tag{3.1}$$

As anticipated with the CR3BP, variations of the model, and as mentioned in the results of Baines et al. (2018) the trajectories of motion demonstrate that circular orbits are obtained from the completion of one cycle of the model. As the distance of P_3 increases from the nearest primary body less and less of a complete cycle can be formed. The results reveal that the P_3 exhibits changes in velocity due to perturbing forces from the second primary body. In figure 3-2 the influence of

the Moon increases with the increase in height. On the left side of the figure are images created compared to the images on the right from the research of Baines et al. (2018). The two images on the left are of P_3 at LEO and GEO (6556 km and 42164 km). The heights of LEO and GEO above the Earth's surface were chosen to later compare with the work of Davis et al. (2011). One important note with the images is that to make LEO and GEO visible the scale for the different images were adjusted. The differences in orbital period of P_3 about the system can be compared to Kepler's 3rd law. A key result from using the script is that a 0.633% error with position and velocity is found over time.

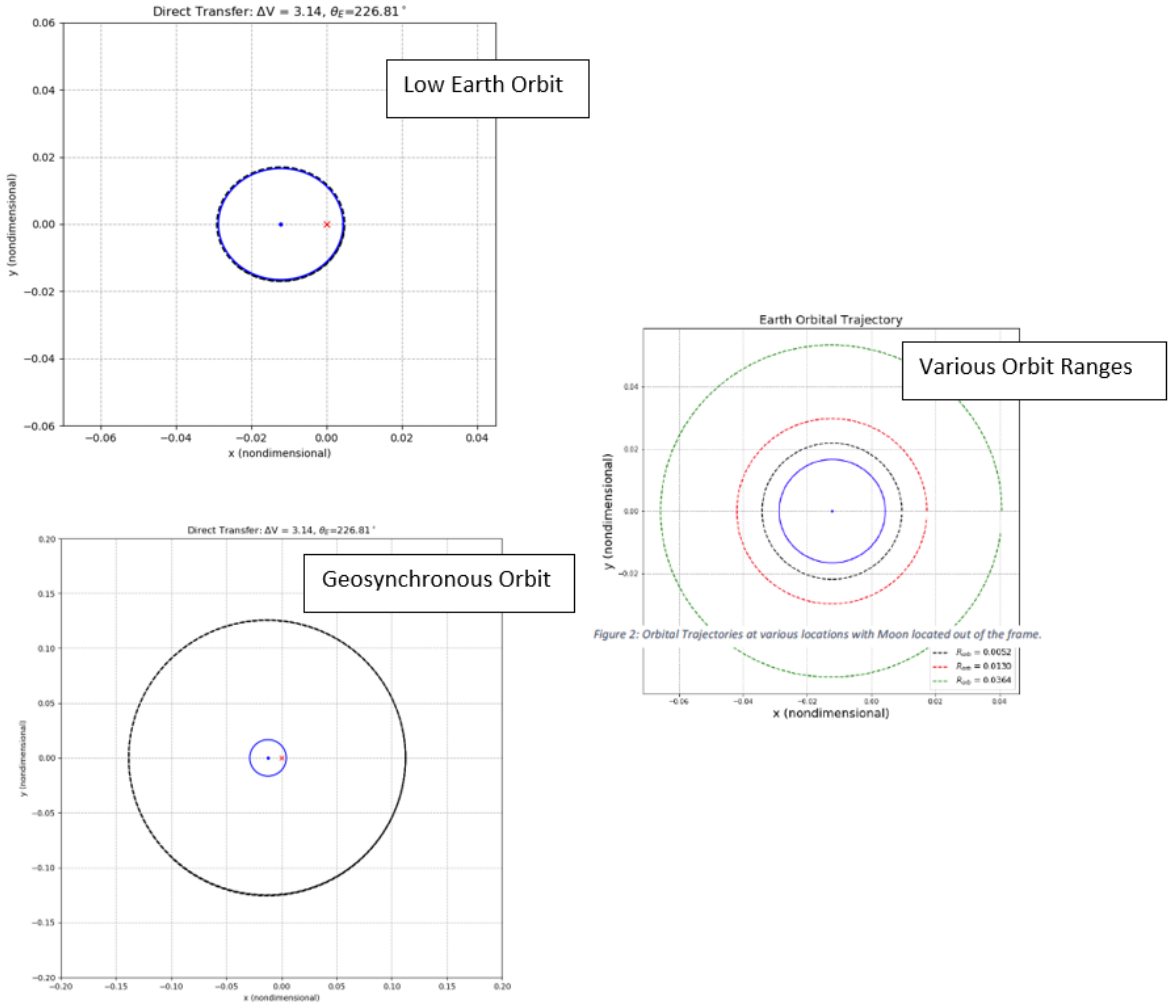

Figure 3-2 P_3 Orbital Period Comparison. Adapted from "The Restricted Three Body Problem Trans-Lunar Injection" by Baines, T., Hew, Y. J., & Toyama, S. (n.d.). Page 8, figure 2: Orbital Trajectories at various locations with Moon located out of the frame.

Next, testing various conditions of the step size taken with the numerical analysis will provide what level of accuracy is required to achieve the expected results. Through various testing observations of how the path changes demonstrate the effects of different step sizes to assist in determining the optimal numerical value. When N = 1000000 with an i5 6-core 64-bit processor and 8 Gig of RAM memory errors will occur, creating errors that prevent calculations to complete. With figure 3-3 on the left N = 100000 and to the right N varies demonstrating the different intervals of N with error within integration calculation. The right side of figure 3-3 is to compare the results of Baines et al. (2018). The left side of figure 3-3 demonstrates that with the hardware limitation the research conducted can be competed with N set to 100000.

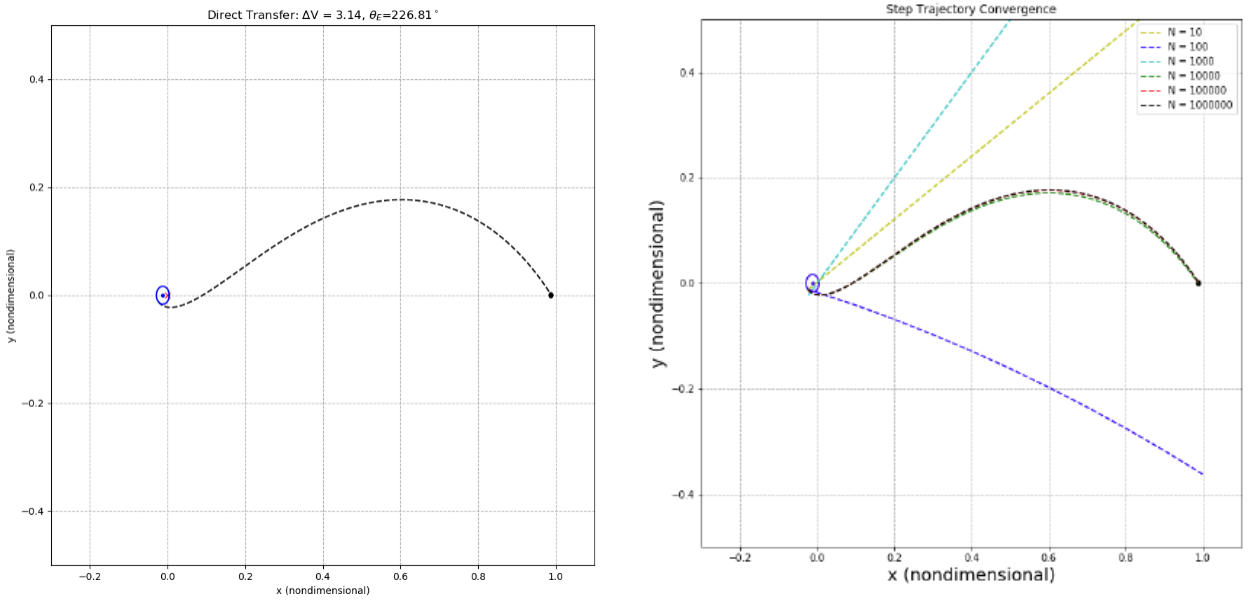

Figure 3-3 Trajectory Differences with N Slices Comparison. “The Restricted Three Body Problem Trans-Lunar Injection” by Baines, T., Hew, Y. J., & Toyama, S. (n.d.). Page 7, figure 1: The plot shows the trajectory of the given z at various time steps. You can see as N increase our values begin to coverage to their true values. You can see that values N > 10000 nearly overlap one another which suggest the optimal time step. The dot and circle correspond to the Earth and it’s “radius” while the black dot is the moon and it’s “radius”.

As a final review and test of the Python script used, various initial conditions of the trans-lunar injection transfer are tested by Baines et al. (2018) and created by No, Tae Soo, et al. (2012) are used as a final metric for comparison of results. From equation (2.72) any change will create different overall outcomes each diverging from each other.

In the case of the PCR3BP the three initial conditions that need to be considered are the ejection velocity (ΔV), the radius from the point mass (height above the Earth's surface), and the angle in in which the trajectory was initiated. Using the PCR3BP greatly simplifies the dynamics and allows for a greater focus on the x-y plane. In section 3.2.2 more details on the differences between the PCR3BP and the CR3BP are provided. As an initial demonstration the difference in trajectories of $\pm 0.01\%$ and $\pm 5\%$ with figure 3-4 change of ejection velocity. The results on the left are generated and compared to the results of the right generated from Baines et al. (2018). From the model any decrease with ejection velocity would result in the secondary body falling back toward the originating primary body.

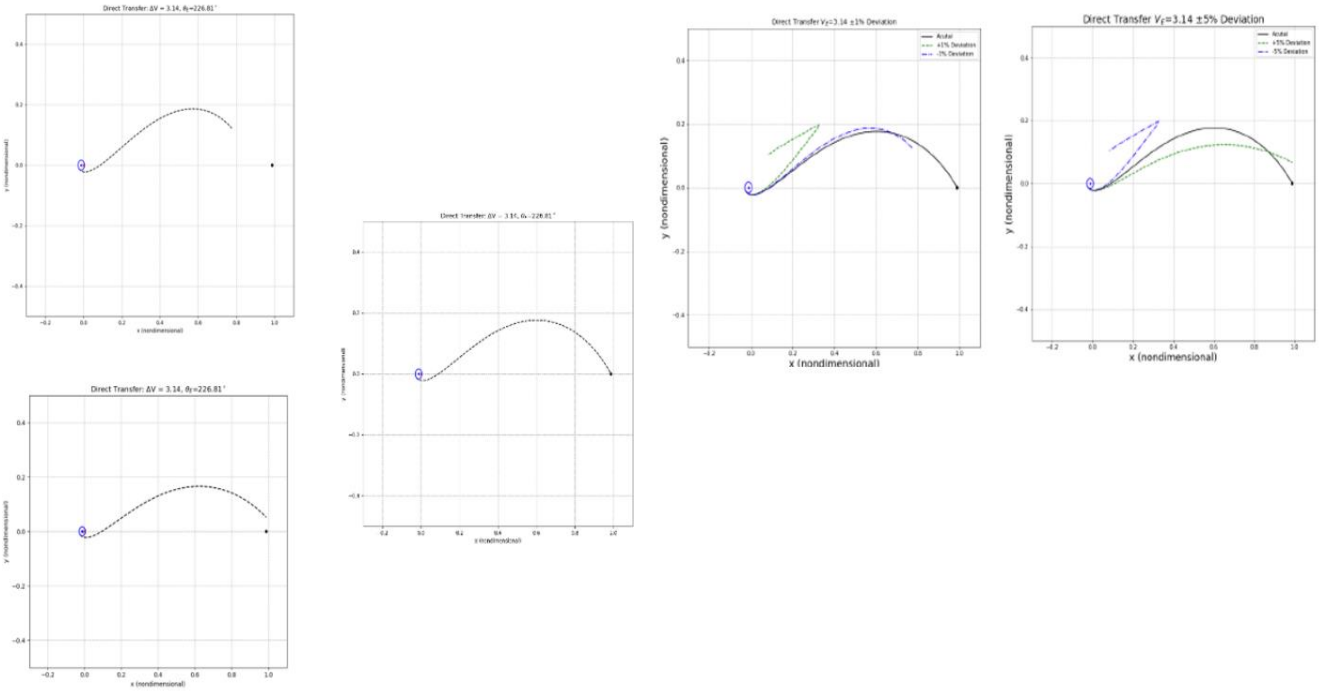

Figure 3-4 Transfer Trajectories Change with Various Ejection Velocities. "The Restricted Three Body Problem Trans-Lunar Injection" by Baines, T., Hew, Y. J., & Toyama, S. (n.d.). Page 10, figure 4: shows the 1% change in ejection velocity, figure 5: show the 10% in ejection velocity.

Furthermore, the model also demonstrates that when P_3 has too much of an ejection velocity the trajectory is unaffected by either primary bodies and becomes unbounded. The trajectory of the unbounded secondary mass spirals out. The added ejection velocity was a 5% increase to required velocity for a ballistic lunar capture. It is important to note that the Python script is modeling motion with the rotating reference frame giving the spiral appearance. Figure 3-5 shows a spiraling out unbounded secondary mass. Figure 3-5 is like figure 3-4, both being a comparison of generated work on the left and that of other research conducted with the Python script on the right.

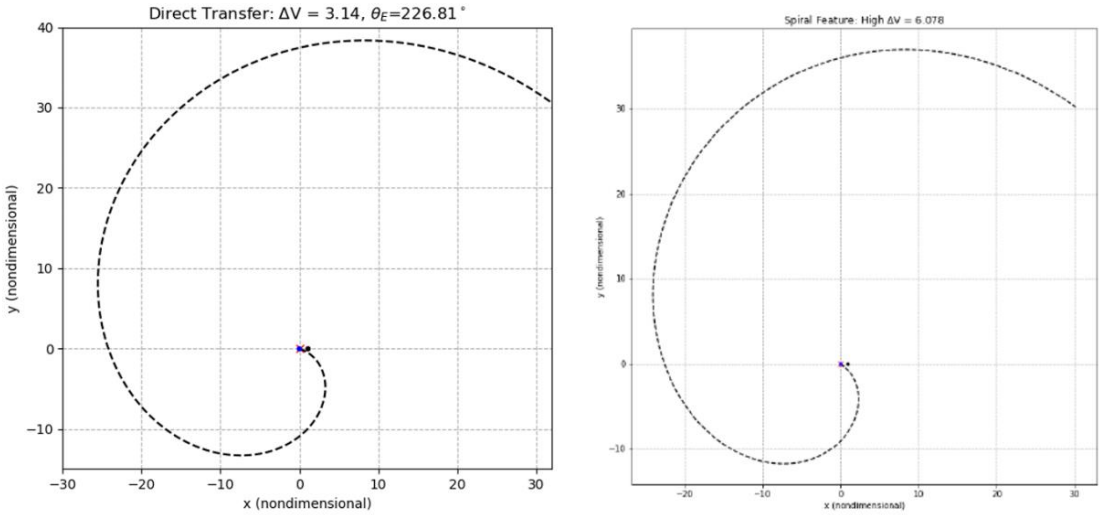

Figure 3-5 Transfer Trajectories with Ejection Velocities. "The Restricted Three Body Problem Trans-Lunar Injection" by Baines, T., Hew, Y. J., & Toyama, S. (n.d.). Page 10, figure 6: Spiral Feature that occurs when the velocity is to great and because unbound from the system. Spiral feature is due the rotating frame of reference.

Using the CR3BP equations of motion with numerical analysis a list of the sets for equation (2.72) is formed. The full list of position and velocity over time describes the trajectory an object takes based on the gravitational influence of the primary bodies. The Python script is written in such way to store the full list of position and velocity vectors to provide graphical results. Another set of graphs that can be created is the change of velocity over time. In figure 3-6 graphical results of position vs time and velocity vs time graphical results provide further insight into the dynamics of the system model. From figure 3-6 there is a greater change in the x-axis compared to the y-axis

because of the initial change in velocity's proximity to the Earth as a point mass. Due to the object of interest being near the point mass representing Earth more velocity is required in the x-axis than on the y-axis. Over time differences in the x-y axis become more apparent. From figure 3-6 the velocity in the y-axis for the object of interest moves with increased velocity away from Earth until the velocity becomes zero. The object of interest continues to decrease in velocity because of the Moon's gravitational attraction. One important note with the model is that when approaching a point mass a sharp increase in position and velocity occurs with a surface impact. The velocity vs time graphs also provide an initial point where the object of interest is in a stable orbit or unstable orbit. The zero-crossing point for velocity vs time can provide an initial region for the weak stability boundary for a given set of initial conditions. Although much can be derived from the velocity vs time graphs, only the position graphs are used for the rest of the research conducted.

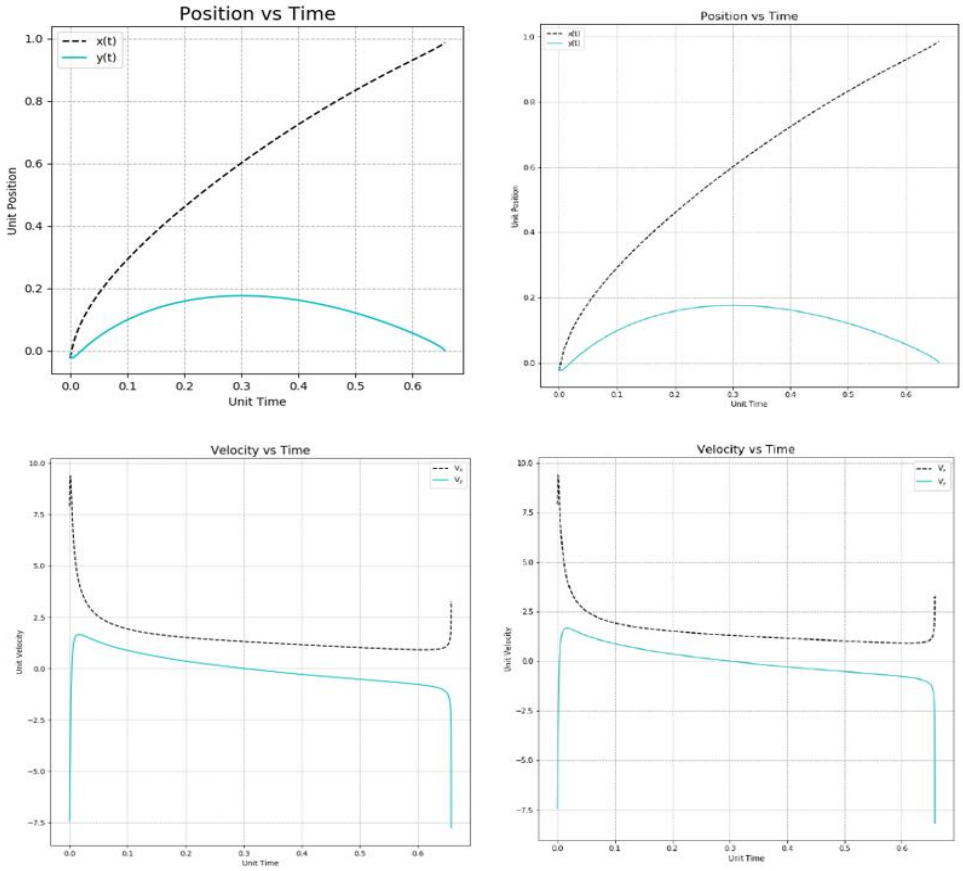

Figure 3-6 Position vs Time and Velocity vs Time. "The Restricted Three Body Problem Trans-Lunar Injection" by Baines, T., Hew, Y. J., & Toyama, S. (n.d.). Page 11, figure 8: position x and y as a function of time of the direct transfer trajectory. Figure 9: Dimensionless time and velocity plot for Direct Transfer Lunar Injection.

3.2.1 Adjusting the Equations of Motion and Numerical Method

In section 3.2 the results demonstrated a successful recreation of the data for the Python scripts original implementation. Before modifying the script, it is important to understand the different components that the script is constructed from. From section 2.1 the PCR3BP is commonly referenced as the CR3BP. Using the PCR3BP is useful when only considering the motion in the x-y plane. With the z-axis being uncoupled from the x-y plane there is no impact to solutions derived from the PCR3BP and they can be treated as a special case of the CR3BP in which position and velocity equal zero in the z-axis. If the assumption is to always have the z-axis provide no input into the system, then the equation in the z-axis is often not part of the model. For the constructed model the equations of motion are represented as a function. With the addition of the equation of motion in the z-axis the PCR3BP becomes the CR3BP

$$a = \dot{v}_z \tag{3.1}$$

$$v_z = -(1-\mu)\frac{z}{\sqrt{(x+\mu)^2+y^2+z^2}^3} - \mu\frac{z}{\sqrt{(x-1+\mu)^2+y^2+z^2}^3} \tag{3.2}$$

With the addition of the z-axis equation of motion further additions to implement the change in motion will need to include a change with calculations within the numerical analysis and initial conditions.

With the numerical analysis portion of the model, the Runge Kutta 4th order method of calculations for any given axis are the same. Logically it would make sense that the method of calculation does not impact the result rather only the equations of motions determine the outcome. From equation (2.24) - (2.28) the formula for the Runge Kutta method is described and the resulting impact onto the model is present in Appendix A. Finally, the last change to the model that is required to implement motion in three dimensions is the change with initial conditions. However, based on the overall review of section 3.2 it is important to not just select a random point in space rather a point in which motion can be examined with a known outcome. No, Tae Soo, et al. (2012) examine a circular orbit around the first primary body within the PCR3BP. In understanding the initial conditions, a new set of initial conditions can be derived to ensure that the changes to the model are correct.

3.2.2 Earth-Moon Design Transfers

With a continued understanding of dynamical systems and optimized trajectories the research conducted by No, Tae Soo, et al. (2012) examines two different types of orbits for efficiency. The nature of their research was to determine an efficient orbit to the Moon for both fuel and time. The two trajectories studied are a spiral and direct departure from various low Earth orbits. The direct departure trajectory is that of figure 3-3 and the spiral departure is not constructed in this research. The spiral departure is created with more of a continuous velocity change with evaluating the altitude gradually. The gradual change in altitude is accomplished with alterations to the equations of motion with an added parameter. To avoid unnecessary changes to the model the spiral departure was not generated. The result of the research demonstrated that it is advantageous to use both an impulse maneuver and continuous thrust to decrease the time of flight and save on fuel usage. A ballistic capture method would ultimately save on fuel usage however the cost with time can result in tens of hundreds of days.

In the trajectory design implemented the object of interest was starting around P_1. However, for the modeling for the research conducted the object of interest's initial position is near P_2. Changing initial conductions from P_1 to P_2 requires changes to both position and velocity. For a circular orbit about P_1 the velocity can be defined as,

$$v_{P_1} = \sqrt{\frac{1-\mu}{r_{P_1}}} \tag{3.3}$$

Where r_{P_1} is the distance with respect to P_1. Position for an object about P_1 is offset by μ the mass ratio. For a circular orbit about P_2 the velocity can be defined as,

$$v_{P_1} = \sqrt{\frac{\mu}{r_{P_2}}} \tag{3.4}$$

Where r_{P_2} is the distance with respect to P_2. Position for an object about P_2 is offset by (μ - 1) with μ being the mass ratio again. The difference with position and velocity are caused by the design of the model where both primary bodies are moving about the barycenter. Because they are in a fixed position everything else within the model moves.

Another change from the model used from No, Tae Soo et al. (2012) and Baines et al. (2018) is that both research efforts used the PCR3BP for setup of initial conditions. In the original

implementation of the Python model the only two inputs into the system were angle of position and added velocity with respect to the second primary body. Restricting the inputs to angle of position and change in velocity is achievable because of the two-dimensional nature of the model. When adding a third dimension a different system for generating initial conditions is required to account for the added dimension. Of course, with either the PCR3BP or CR3BP initial conditions can be provided by explicitly defining each value from equation (2.72). However, such a method would require constant derivation. In the original model initial conditions are based on polar coordinates with respect from the first primary body. Given an angle (θ) and change in velocity (Δv) the inputs are changed by,

$$v = v_{P_1} + \Delta v \tag{3.5}$$

$$x = r\cos(\theta) - \mu \tag{3.6}$$

$$y = r\sin(\theta) \tag{3.7}$$

$$v_x = -1\, v\sin(\theta) + y \tag{3.8}$$

$$v_y = v\cos(\theta) - x \tag{3.9}$$

The result from the use of equations (3.5) – (3.9) provide initial conditions in the form of equation (2.72). The advantage of creating initial conditions in the manner presented is in providing a method to test expected and model created results. Figure 3-7 demonstrates that when given a height above P_1 with no Δv a circular orbit is achieved.

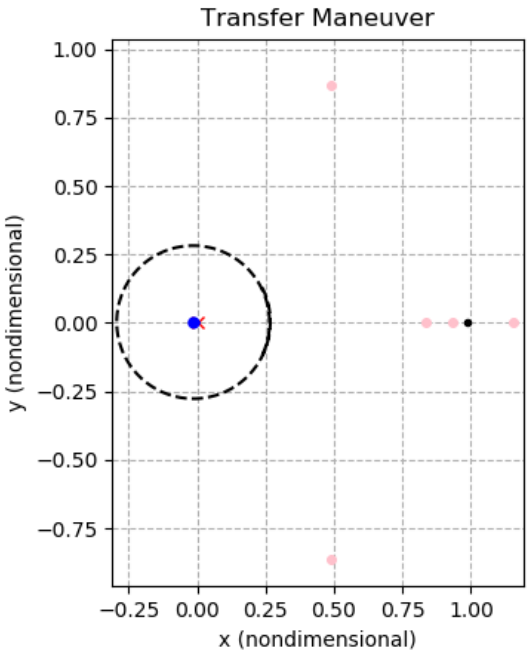

Figure 3-7 Test of Initial Conditions

With the original form of the model being in two dimensions using polar coordinates a natural extension for three dimensions would be to use spherical coordinates. Additional inputs for the model include angle with respect to the z-axis being ϕ. The added parameter and an orbit being centered around P_2 changes equations (3.5) – (3.9) as follows

$$v = v_{P_2} + \Delta v \tag{3.10}$$

$$x = r\cos(\theta)\cos(\phi) + 1 - \mu \tag{3.11}$$

$$y = r\sin(\theta)\cos(\phi) \tag{3.12}$$

$$y = r\sin(\phi) \tag{3.13}$$

$$v_x = -v\cos(\phi)\,\dot{\theta}\sin(\theta) + v\dot{\phi}\sin(\phi)\cos(\theta) \tag{3.14}$$

$$v_y = v\cos(\phi)\,\dot{\theta}\cos(\theta) + v\dot{\phi}\sin(\phi)\sin(\theta) + 1 - \mu \tag{3.15}$$

$$v_z = -v\dot{\phi}\cos(\phi) \tag{3.16}$$

The results from the use of equations (3.10) – (3.16) provide initial conditions in the form of equation (2.72) for the updated model. Figure 3-8 demonstrates that when given a height above P_2 with no Δv a circular orbit is achieved 3 dimensionally.

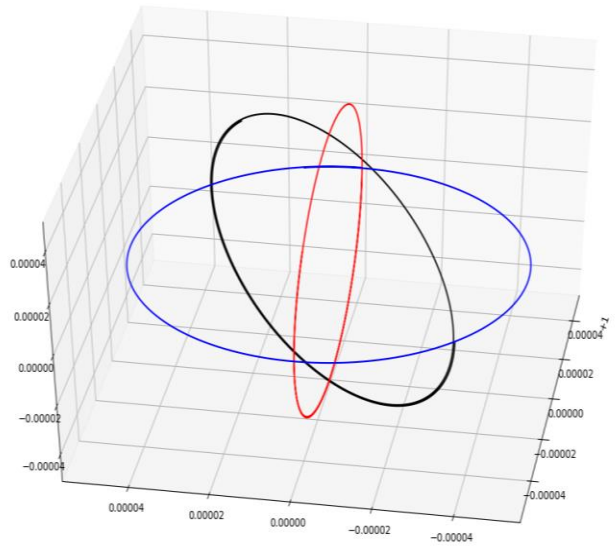

Figure 3-8 Three-Dimensional Adjustment for Initial Conditions

Figure 3-8 is a display of the xy-axis, xz-axis, and yz-axis mapped three-dimensionally. The center of all three spheres is the point mass of P_2 in the model. As the altitude increases perturbations from P_1 increase causing the final position not to meet with the initial position. With the three-dimensional initial conditions fully composed more complicated orbits can be demonstrated.

In section 2.5 a brief introduction to invariant manifolds equation (2.75) provides the initial starting point for analytically defining the weak stability boundary for the L_2 equilibrium point. Given a Jacobi constant and a restricted set of initial conditions for position a corresponding set of velocity conditions can be derived. With proximity to the second primary body an initial Δv is required and is denoted as d in equation (2.75). The derivation of the full set of initial conditions from equation (2.72) and Δv required is possible because the Jacobi constant is a conservative quantity in the CR3BP. The resulting conditions can then be compared to the trajectory of interest. In section 2.4.3, the table 2-2 and figure 2-8 demonstrate a set of values in the form of equation (2.72) showing a Lyapunov family. The set of formulated conditions for a given Lyapunov orbit with equation (2.32) from section 2.4.1 provides a Jacobi constant. With the set of initial and final conditions the shooting scheme is used to correct for slight variances to adjust for the approximation used. The same method of constructing a path from P_2 to the libration point can also be used to construct the return toward P_2 for a desired end orbit. In the research conducted the

desired initial state and end state are LEO and GEO perspectivity to measure differences in inclination.

In the next section inclination changes using Lissajous orbits are derived from the previously mentioned method described using Jacobi constants and amplitudes in the z-axis. For different libration point orbits the amplitude is the maximum and minimum separation from the libration point for a given axis. The amplitude can be used with the first order analytical approach from equations (2.67) – (2.69). With the z-axis uncoupled from the xy-axis the Lyapunov orbits formed in section 2.4.3 along with the approximation equation for the z-axis act as an initial set of Lissajous orbits prior to slight corrections from the nonlinearities of the system model. Due to the conditions being an approximation, corrections are required for a desired trajectory. When adjusting the LPO a continuous check of amplitude ensures an approximate result matching Lissajous orbits as mentioned in the research conducted by Davis et al. (2011). With a set of Lissajous orbits the use of invariant manifolds is constructed with a set of initial conditions at LEO with an added Δv. Without a set of initial conditions near Earth, several orbits can be created to satisfy the resultant trajectory from the work of Davis et al. (2011) due to not considering all the same variable and variances with Δv to follow the manifold. Their research outlines the use of Lissajous orbits to create large inclination changes and provides insight to the limitations of the proposed method in this research. Section 3.3 is not necessarily a recreation of the work for Davis et al. (2011), rather the focus of the section is to demonstrate the method used for creating a maneuver resulting with a plane change without the cost of a plane change.

3.3 Test Case 2: Orbital Transfers from LEO using Invariant Manifolds

The purpose of this study is to develop a large inclination change using two distinct libration point orbits. The research conducted by Davis et al. (2011) demonstrates the ability to create a large inclination using a single LPO. As a natural extension of their research the goal of this research is to use two LPOs to increase the change of inclination. The system model chosen for their research and this research is the Sun, Earth and Moon where the Earth and Moon are treated as a singular point mass. In section 2.1 a test of the system model demonstrated that the model conducted works within the confines of the CR3BP. The designed orbital maneuver is for the object of interest (a satellite) to initiate thrust in such a manner that inserts the satellite onto a stable manifold trajectory toward an L_2 LPO. The satellite would travel about the LPO to follow the

unstable manifold due to quasi-periodic motion. The unstable manifold would then be used to insert the satellite to the intended final orbit having caused a change with inclination. The gravitational dynamics involved from the described maneuver creates a plane change maneuver without the cost of such a transfer. The maneuver constructed is considered a low-energy efficient transfer that can be compared with the fuel cost of a Hohmann transfer. Section 3.4 further discusses the difference between an optimal transfer vs an efficient transfer with the maneuver that was created. As part of this study the benefits of the constructed maneuver as well as the consequences are explored.

Reconstructing similar orbits from the Davis et al. (2011) research, the approach from section 2.4.2 is taken starting with the creation of the LPO. From their research table 3-1 provides three different orbits that resemble the amplitude in the z-axis (A_z) with the corresponding Jacobi constant.

Table 3-1 Amplitude in the z-axis vs Jacobi Constant with $\mu = 3.04x10\text{-}6$

A_z (km)	Jacobi Constant
301	3.0008
613	3.0007
798	3.0006

Table results from table 3-1 can be compared with L_2 Halo orbits to approximate the LPO used in the described transfer. Using the same methodology that created the Lyapunov orbits, table 3-2 and figure 3-9 provide resultant Halo orbits for the Sun-Earth/Moon system. With the resultant orbits given the Jacobi constant is a conservative value a point along the Halo orbit can be used to cross compare a calculated Jacobi constant with table 3-1. Equation (2.32) provides how to calculate the Jacobi constant. The table and figure below are rough approximations of the Northern Halo orbits created in the work of Davis et al. (2011).

Table 3-2 Initial Conditions for L_2 Halo Orbit

x	z	$\dot{y}$
1.011724	0.00228	-0.014430
1.011874	0.00406	-0.018706
1.012474	0.00414	-0.023246

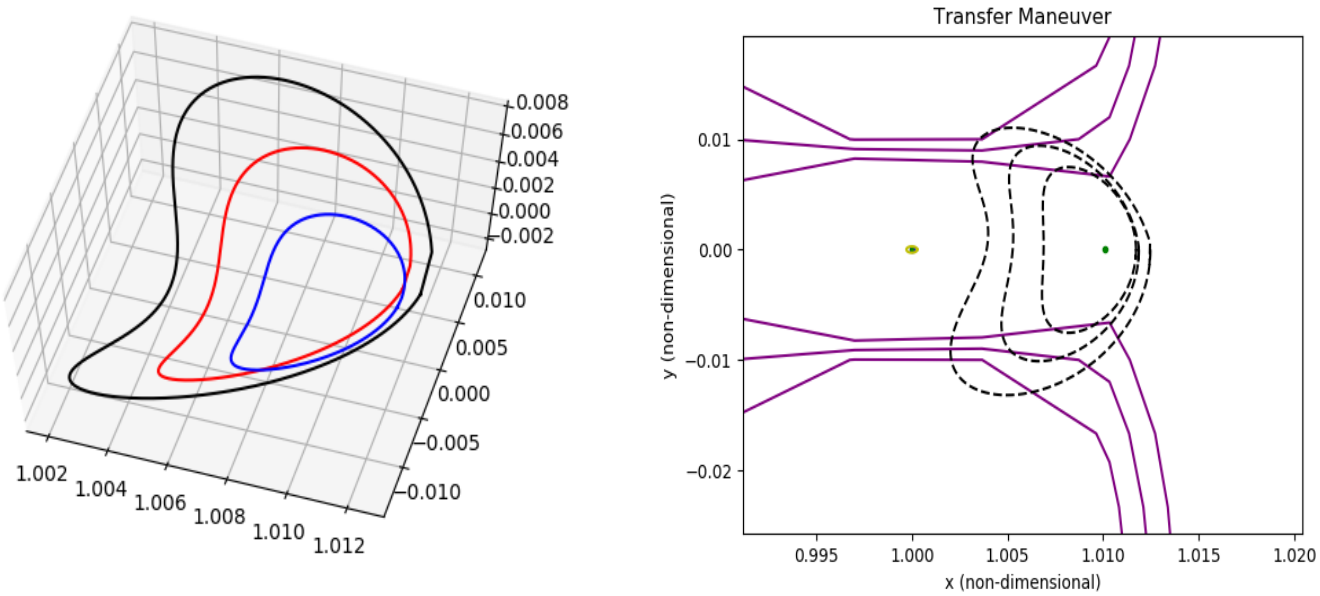

Figure 3-9 Set of L2 Halo Orbits

As additional check to ensure the orbits are comparable to previous research the z-axis amplitude with the values from table 3-1 are re-calculated. As mentioned in section 2.4.2 the measured amplitude can be taken by the maximum and minimum differences from the LPO and calculated with equation (3.17).

$$A_z = \frac{|Z_{max}| + |Z_{min}|}{2} \tag{3.17}$$

With the creation of the LPO the next step is to reconstruct the initial conditions that were used to create the desired orbital trajectory. Given an orbit starting at LEO and a known Jacobi constant a set of initial conditions can be constructed. Variances in the Δv can be caused by differences within the model, the constructed orbit, the path taken, initial conditions and more. However, the

greatest cause for different results is from the initial state vectors. Table 3-3 provides the thrust required to initiate the maneuver with relation to the Jacobi constant.

Table 3-3 Δv vs Jacobi Constant for Designed Transfer Orbit

Total Velocity (km/s)	Jacobi Constant
3.552	3.0008
4.147	3.0007
4.433	3.0006

An additional cost in velocity that is calculated for within this research is the cost of adjusting to maintain the final desired orbit. The additional cost results are provided in table 3-5 accounting for return to a circular GEO.

The information from table 3-2 provides an approximate trajectory for the designed LPO and with the additional information from table 3-3 a full maneuver is created. Figure 3-10 is the set of orbital maneuvers designed to achieve an inclination change with the use of invariant manifolds and LPOs. The figure 3-10 contains three different approximate trajectory paths to account for a wide spread of orbits created, without creating each orbit from the work of Davis et al. (2011). An analysis of the created orbits provides three main metrics of value such as time of flight, change of velocity, and inclination change. The defined metrics then allow for a comparison with other orbits to determine efficiency. Additionally, disadvantages and limitations can be examined with the desired orbital maneuver.

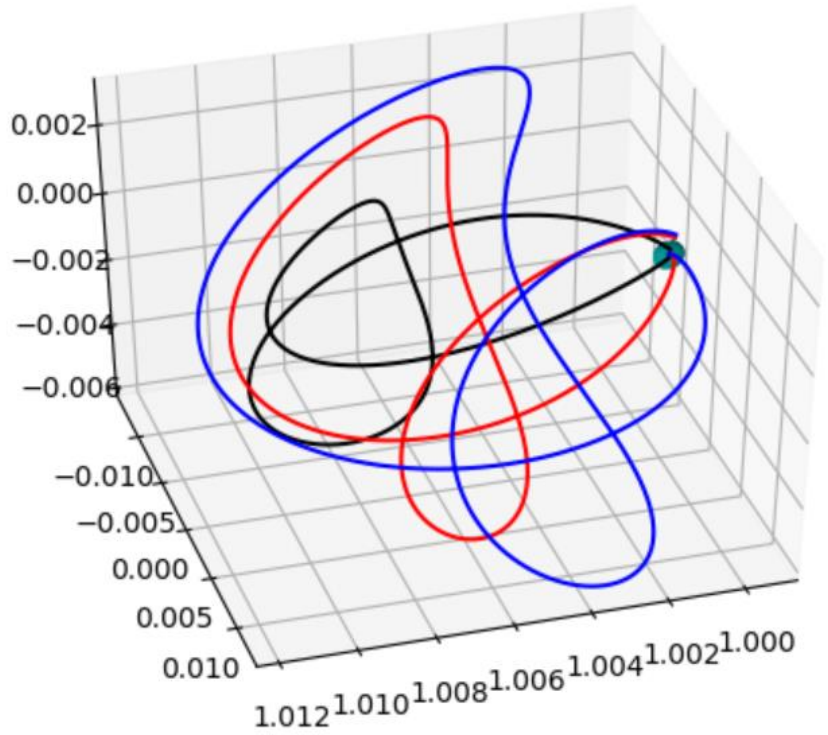

Figure 3-10 Three-Dimensional Adjustment for Initial Conditions

In creating the orbital trajectories for the maneuver, the metric that can be obtained directly from running the system model is time of flight. Using the equation (2.3) for the characteristic time to time conversion results provides time of flight which is given in table 3-4. Table 3-4 is a comparison for time of flight and the Jacobi constant. This method of finding time of flight does not attempt to optimize time for the given maneuver in any way such as differentially correcting the manifold trajectories. Rather, time of flight is the time given in the system model to integrate over, determining the different data points. Time of flight may have differed from the original research with initial conditions and other factors that might have been included in the original model. The model created in this research is only constructed from the equations of motion of the CR3BP with given accuracy as mentioned in 3.2.

Table 3-4 Time of Flight vs Jacobi Constant for Designed Transfer Orbit

Time of Flight (days)	Jacobi Constant
365	3.0008
387	3.0007
386	3.0006

The overall cost of velocity or Δv that is used for the orbital maneuver is the thrust to depart from LEO and the thrust to enter a final circularized orbit. The departing Δv from LEO is derived from the initial conditions for position and velocity to enter the invariant manifold. The thrust needed to enter a final circularized orbit is derived from the difference in velocity from the maneuver to the required velocity for a specific position. The specific position is determined to achieve an end state orbit. Similarly, with time of flight no optimization is conducted to determine a way to decrease for the ending Δv of the maneuver. Table 3-5 is the total cost of velocity in comparison to the Jacobi constant. The costs of velocity differ other research for many different reasons. A few reasons are that the model is sensitive to initial conditions, lacks accounting for perturbing forces, and any adjustments beyond the equations of motion for the CR3BP. The velocities in the table will get a spacecraft from LEO to account for the thrust needed to circularize at GEO.

Table 3-5 Δv vs Jacobi Constant for Designed Transfer Orbit.

Δv km/s	Jacobi Constant
4.15	3.0008
4.39	3.0007
4.58	3.0006

The final desired metric, inclination is different compared to time of flight and total Δv in that post model simulation further calculations are needed. In the CR3BP the primary and the secondary masses are on the same plane orbiting around the barycenter of the system. However, the angle in which the Earth is tilted is not zero degrees to the solar plane. Due to the Earth's tilt

changes in inclination from the model do not directly correspond to inclination from the perspective of Earth. To correct for the difference of Earth's tilt with respect to the orbital plane a coordinate transformation is required. Using the CR3BP with the Sun-Earth/Moon system for the designed maneuver the change in inclination (Δi) in table 3-6 is with respect to the orbital plane. Due to differences in the previous tables for time of flight and change in velocity propagation into change of inclination also causes results to differ from the original research. The main impact to the differences with inclination is a difference of inclination. Given the conditions are only approximations of similar orbital trajectories it is expected for the results to be different compared to the expected values.

Table 3-6 Δi vs Jacobi Constant for Designed Transfer Orbit

Change of Inclination (rounded)	Jacobi Constant
15	3.0008
24	3.0007
44	3.0006

Based on the values of this table although a maneuver from LEO to GEO with a plane change provides an advantage, this does not seem to hold from LEO to LEO orbits. Additionally, given the maneuvers the need to apply another thrust of velocity to circularize the orbit changes the inclination for a wider range of results that would require further exploration. At the point of circularizing the orbit it would not be difficult to achieve different results from table 3-6 with similar velocities from table 3-5. Although this method does not have a direct advantage compared to a plane change maneuver it is still worth investigating the use of multiple LPOs to determine if such change provides better results.

The CR3BP motion can also be considered in the ecliptic coordinate system. Given an initial position and final position transformation into the equatorial coordinate system provides how the maneuver increases inclination with Earth's tilt. With the results of table 3-6 the Δi is the same in both coordinate systems. However, for any mission design or comparison to other maneuvers equatorial coordinates is preferred.

$$\begin{bmatrix} x_{equatoriial} \\ y_{equatoriial} \\ z_{equatoriial} \end{bmatrix} = \begin{bmatrix} 1 & 0 & 0 \\ 0 & 0.9171 & 0.3987 \\ 0 & -0.3987 & 0.9171 \end{bmatrix} \cdot \begin{bmatrix} x_{ecliptic} \\ y_{ecliptic} \\ z_{ecliptic} \end{bmatrix} \quad (3.18)$$

With the position of the satellite in an equatorial orbit a final step to fully appreciate the changes to an orbit that would be described with the initial conditions and another orbit described to the final condition a final transformation from spherical coordinates to the six classical orbital elements is performed. The MATLAB script provided by (Curtis, 2014) provides the classical orbital elements (coe) when given the position vector and velocity vector. In addition, the vectors as inputs to the coe script, μ is the value between the Earth and a satellite. The script was used without modifications or changes from http://booksite.elservier.com/9780080977478/ with chapter 4.4 Orbital elements and state vectors by (Curtis, 2014) providing a full and detailed explanation of the transformation with an example. Table 3-7 encompasses the results containing the initial and final coe, Δi, Δv, and TOF.

For table 3-7 the classical orbital elements are represented of the final orbits. The initial orbits for all three are as follows:

a: 6556 km^2/s i: 38º, 48º, 68º Ω: 0º

e: 0.0 ω: 0º θ: 205º, 225º,265º

Table 3-7 Resulting Data from Orbital Maneuver

Classical Orbital Elements		Δi	Δv	TOF
a: 185	a: 42164	15°	415 km/s	365 years
i: 15º, 25º, 68º	i: 0	24°	4.39 km/s	387 years
Ω: 0, e: 0, ω: 0, θ: 0	Ω: 0, e: 0, ω: 0, θ: 0	44°	4.58 km/s	386 years

The resultant information from the table above differs from the research of Davis et al. (2011) which can be attributed to several factors. The orbital design ultimately ended up different with lower amounts of velocity and larger time of flight. Further research would need to be conducted to determine the extent of the differences that are beyond the scope of the desired research. Based

on the result obtained from Davis et al. (2011) the maximum A_z of 800,000 with a Δi of 71.6° provided a savings of 3.62 km/s and a cost of approximately 388 days. Limitations to this maneuver are further explored in section 3.5.3 Results and Comparison.

3.4 Optimality vs Efficiency

In section 3.3 and in this research conducted, both maneuvers are considered efficient orbits in that fuel is conserved in comparison to traditional methods. Efficient methods seek to improve transfers by decreasing a quantity of interest (e.g. fuel or time). This research is also considered a preliminary study as it is an initial investigation into the use of multiple LPOs within a maneuver, whereas an optimal method seeks to create the best solution for a given type of maneuver. The work of Koon et al. 2000, Gómez and Masdemont 2000, Gómez et al. 2004 created theoretical zero cost transfers using unstable manifolds that asymptotically approach a stable manifold on a second orbit. With the following sections a brief review is taken into two different methods, one that can increase efficiency and another to optimize specific connecting maneuvers. In section 3.4.1 the bounding spheres method is explored to create further efficiencies for a maneuver of different unstable manifold energies. While in section 3.4.2 the primer vector theory is applied to a transfer to determine the optimal trajectory for a given maneuver. As interest for different fuel-efficient methods continue to grow the use of invariant manifolds with LPOs will provide unique options for mission design.

3.4.1 Bounding Spheres

With the work of Davis et al. (2010), a technique to construct transfers between unstable periodic orbits with different energies was formed. Within the given technique using invariant manifolds, trajectories to depart one unstable periodic orbit is connected to another orbit. The research conducted is of interest because it connects the unstable boundary of one LPO to the stable boundary of another LPO. The methods produced act as a natural extension of the work of Davis et al. (2011), if the six different applied pairs of orbits were also constructed to determine inclination change. Using an impulse maneuver, a region of space is studied to determine a more efficient transfer. This region is known as a bounding sphere. The bounding sphere is centered on the second primary body within the system with a radius less than the sphere of influence. The region for the bounding sphere is set where the gravitational effects of the second primary body dominate to allow for a measure of angular momentum vectors between the point of unstable and stable manifolds. The location is adjustable within the sphere of influence for the second primary

body to limit the number of manifold trajectories. With further analysis varying locations for the bounding sphere can be selected. The constructed maneuver measures difference in Δv compared to the use with and without the derived techniques. As mentioned with this maneuver being a natural extension of the work of Davis et al. (2010) this can also be applied to the maneuver constructed in section 3.5.1 as well.

The CR3BP model contains an infinite number of trajectories with varying invariant manifolds and methods to determine individual manifolds to develop a low-cost transfer. The concept of the bounding sphere is like a planar Poincaré section map. Within the bounded sphere the unstable manifold of the first orbit and the stable manifold of the second orbit are integrated in time to show points of intersection. Appendix B contains a figure that further demonstrates the bounding sphere as referenced from Davis et al. (2010). Although the figure in Appendix B is demonstrated for a heteroclinic connection of the L_1 and L_2 Halo orbits the same concept can be applied to just the L_2 point of varying Halo orbits for departure and return. The cost to perform a maneuver within a manifold can be quite high. However, the bounding sphere technique uses a bridging trajectory where time is propagating forward to link two different orbits. The overall method could represent a substantial improvement compared a method of direct transfer. As a future study to the research conducted the bounding sphere can help to develop an orbit more efficient than the one composed in section 3.5.1. Additionally, once further studies of efficiency are explored another method to explore for optimizing a maneuver would be to employ the use of primer vector theory with connecting orbits.

3.4.2 Primer Vector Theory

In a different set of research conducted by Davis et al. (2011) a method was conducted to create optimal transfers between unstable periodic orbits with different energies. With a focus on the bridging trajectory connecting the unstable and stable boundary, primer vector theory is applied to determine the optimal maneuver. Primer vector theory was first developed by Lawden (1963) establishing the necessary conditions for an optimal maneuver. Howell and Hiday-Johnson (1994) developed a method to select departing and arriving Halo orbits connected with a Lissajous trajectory, this maneuver is employed with the use of primer vector theory. In the previous section the bounding sphere was used to determine a more efficient maneuver between two orbits of an LPO however the transfers method is not considered optimized. Continuing with research into

efficiency and optimization the primer vector theory is employed to further lower the cost of fuel to achieve an optimal maneuver. The method employed is constructed of a coastal arc along the initial orbital trajectory with a second coastal arc along the final orbital trajectory and the interior impulse. The conditions for an optimal impulse trajectory in terms of primer vectors are as follows:

- The primer vector is continuous with a continuous first derivative.
- The primer vector satisfies the following equation:

$$\ddot{p} = G_r p + G_v \dot{p} \tag{3.19}$$

  where G_r and G_v are the partial derivatives of g with respect to position and velocity. Section 2.4.2 provides details for the matrix setup and equations (2.39)-(2.44) are the equations for each partial derivative.

- The primer vector is a unit vector aligned to the optimal thrust direction for an impulse maneuver.
- The magnitude of the primer vector is equal to unity at the optimal impulse and has a value of less than unity at all other instances.
- At all interior impulses $\dot{p} = 0$, and derivatives of the primer vector with the primer are orthogonal to the energy of the maneuver.

Within a given trajectory of two coastal arcs and an impulse, the values of $\dot{p}_o$ and $\dot{p}_f$ are the initial and final points known as the terminals. The resulting values of the terminals determine different outcomes of adjustment to either coastal arc for optimization. Further studies with the maneuver created in section 3.5.1 will need to be conducted with the primer vector theory to create the lowest possible Δv for a transfer with a set number of maneuvers. Transfer costs could potentially decrease more with multiple loops with a drawback of increasing time of flight seven to eleven-fold depending on the maneuver implemented. When creating an optimal or efficient maneuver for mission design, limitations for time and fuel should be considered.

3.5 Orbital Construction

In section 3.2 the first case tested the CR3BP model under the research conditions it was developed for, followed by modifications for the intended use of this research. After having finished modifications, the second test case used the model to create maneuvers involving a single

LPO to measure inclination change in section 3.3. As a continuation of the research for inclination change with an LPO the proposed maneuver in section 3.5.1 seeks to use two different LPOs or transfers between unstable periodic orbits with different energies.

An understanding of the bifurcation associated with axial orbits yields knowledge about the geometry and intersection of invariant manifolds connected to both vertical and horizontal Lyapunov orbits. Bifurcation theory is the study of topological structures such as differential equations as exhibited in the CR3BP equations of motion. Bifurcation occurs when a small smooth change in the parameter values (e.g. position and velocity) of the system cause a topological change. The changing behavior in LPOs allow for the connection of other LPO's. In section 3.3 the use of Halo orbits and bifurcation with Lyapunov orbits demonstrated a large inclination change. In the following section the use of Axial orbits and bifurcation with vertical and horizontal Lyapunov orbits are designed to create a larger plane change using two LPOs. Using a horizontal Lyapunov orbit an Axial orbit is used to create a bridge connection to the vertical Lyapunov orbit. The use of one LPO's unstable boundary is connected to the stable boundary of another LPO.

3.5.1 Construction of Orbit

In constructing a maneuver of two different LPOs to take advantage of the different stable and unstable boundaries the method described patches the different orbits and maneuvers together. This research is constructed from the combination of all that material that has been covered from the previous sections. The goal of the constructed maneuver to achieve a 90^{o} plane change without the cost of a plane change maneuver. The maneuver is to also achieve a greater extent of inclinations beyond the limits of section 3.3. As a continuation of the material covered the maneuver created the same modeling being the Sun, Earth and Moon with the Earth and Moon treated as a singular point mass is used. The created maneuver will enable the use of mission designs for a satellite to initiate a thrust to follow the unstable manifold toward the L_2 Lyapunov LPO. The satellite will be traveling about the LPO to initiate an impulse maneuver. The impulse maneuver will take advantage of bifurcation from the horizontal Lyapunov orbit with an Axial orbit. The portion of the Axial orbit the satellite follows leads into a vertical Lyapunov orbit. The impulse maneuver following a portion of an Axial orbit acts as a bridge between the two different LPOs. After entering the vertical Lyapunov orbit the satellite will return to the second primary body with the invariant manifold traveling back along the stable boundary.1 The designed method

takes advantage of different aspects of the dynamic system model to achieve a savings in fuel usage with the known cost of increase time of flight.

In table 3-8 and 3-9 the conditions for a Lyapunov horizontal and vertical orbit are provided as the two distinct LPOs the satellite is intended to travel. Figure 3-11 and 3-12 provide the mapping of the family of orbits associated to the table from 3-8 and 3-9.

Table 3-8 Initial Conditions for L2 Horizontal Orbits

x	$\dot{y}$
1.010574	-0.003433
1.011574	-0.011650
1.012074	-0.016614
1.012474	-0.020421
1.012874	-0.023337
1.013274	-0.025411
1.013674	-0.026973
1.014074	-0.028235
1.014274	-0.028793

Table 3-9 Initial Conditions for L2 Horizontal Orbits

x	$\dot{y}$	$\dot{z}$
1.007635	-0.0106398	-0.03081
1.008035	-0.0106008	-0.02821
1.008435	-0.0105708	-0.02591
1.008835	-0.0106578	-0.02381
1.009235	-0.0107378	-0.02171
1.009635	-0.0111528	-0.02367

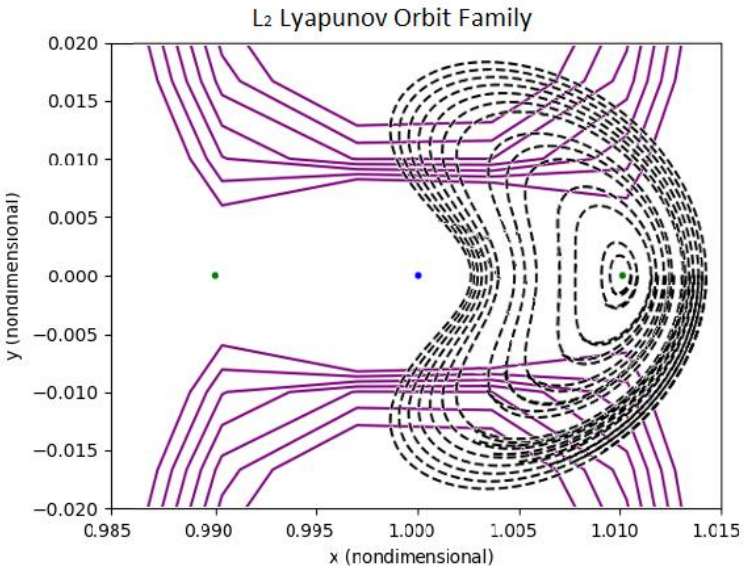

Figure 3-11 Set of L2 Horizontal Lyapunov Orbits

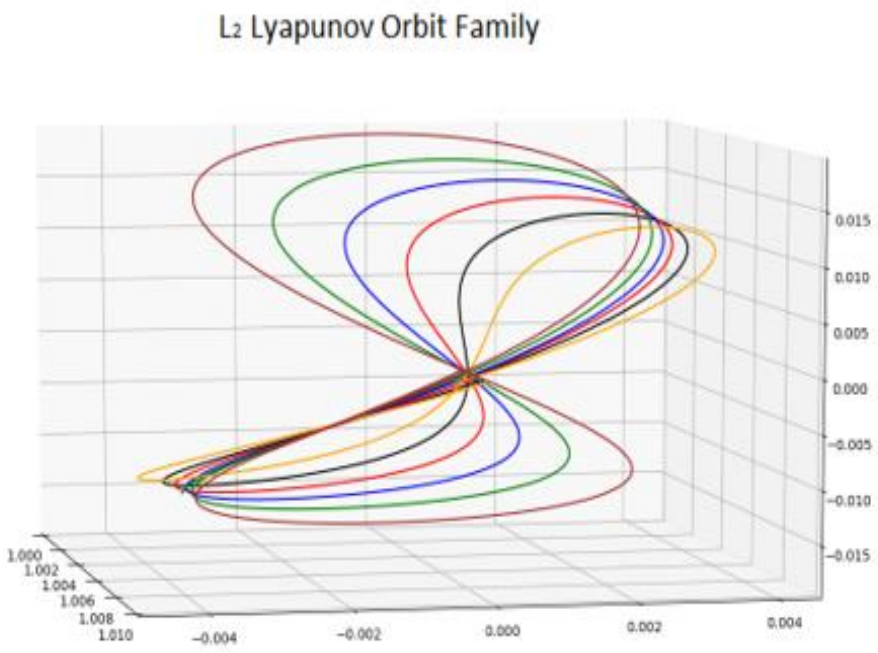

Figure 3-12 Set of L2 Vertical Lyapunov Orbits

With the initial and final LPO mapped in figure 3-11 and 3-12 the next step to construct the desired maneuver is forming a bridging impulse maneuver that allows for connecting the two LPOs. The family of Axial orbits have two distinct bifurcations with the Lyapunov horizontal and vertical families. The Axial orbits can be used as a way of changing from one Lyapunov type to another. The table 3.10 contains different initial positions that form the different Axial orbits that could be used for more complex maneuvers changing from different horizontal to vertical Lyapunov orbits.

Table 3-10 Initial Conditions for L2 Axial Orbits

x	$\dot{y}$	$\dot{z}$
1.007635	0.013963	0
1.007635	0.012664	0.00811
1.007635	0.008525	0.01600
1.007635	0.006873	0.01800
1.007635	-0.007457	0.02811
1.007635	-0.0106298	0.03081

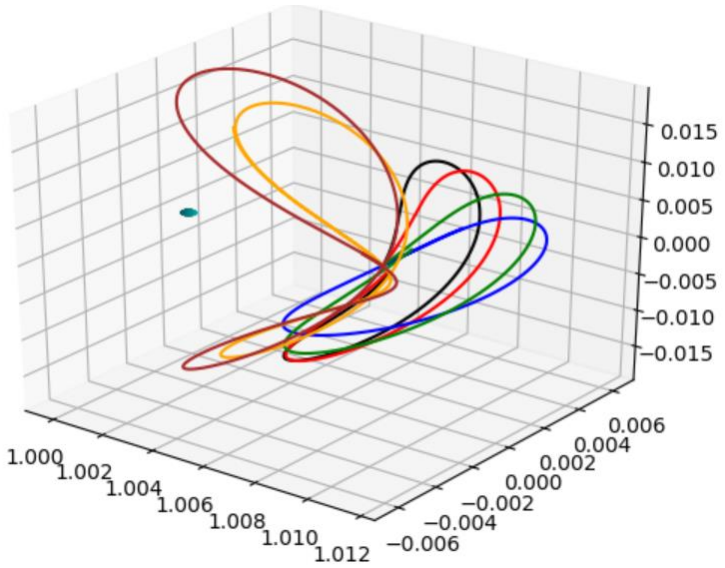

Figure 3-13 Set of Axial Orbits

The information from table 3-8, 3-9 and 3-10 provides the trajectory design for the maneuver set out to be created. For the purposes of this maneuver the horizontal Lyapunov orbit is chosen in connection to the vertical Lyapunov orbit to have at least one point in common. The common point between the two LPOs is used to transfer between the different LPOs with the change of velocity to change paths. Figure 3-14 is a combination of previous figures 3-10 and 3-11 to show the overall maneuver taken with the two different LPOs. The set of maneuvers designed is to achieve an inclination with the use of invariant manifolds and LPOs. Table 3-11 provides the amount of Δv is used for each of the different parts that make up the constructed maneuver. With the Jacobi

constant and Δv of the different maneuvers, selecting a point within the orbit enables the ability to derive the invariant manifold that is used to achieve the first LPO as part of the maneuver. Creating the invariant manifold further defines the maneuver with the ability to set out initial conditions. The initial conditions are designed with a starting point at LEO with a thrust to initiate the desired designed trajectory. Within the figure 3-14 three different trajectory paths are chosen to account for a spread of various orbits that could be created, like that which was done in section 3.3. With the given orbits, the cost of velocity that is calculated includes adjustments for maintaining the final desired orbit (i.e. thrust needed to return to a stable orbit). As in section 3.3 an analysis of the created orbits provides three main metrics of value such as time of flight, cost of velocity, and inclination change. The metrics then allow for a comparison with section 3.3 as well as other orbits to determine efficiency.

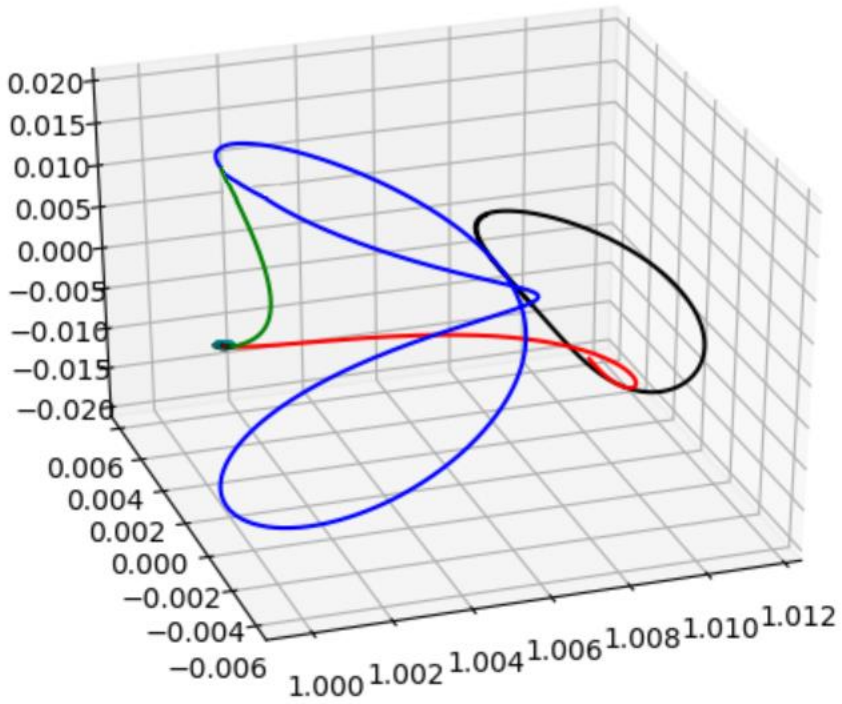

Figure 3-14 Multiple LPO Maneuver (With Multiple Impulse Points)

Table 3-11 Δv at different points along the maneuver from Figure 3-14

Δv km/s	Maneuver
3.222	Unstable Manifold
0.622	Vertical Lyapunov
0.030	Impulse from Vertical
1.202	Circularizing Orbit

The results have demonstrated a significant savings compared to a traditional transfer method in fuel efficiency. However, further research will need to be conducted as the final return to GEO is not using a manifold and only the initial thrust starting the maneuver is using the invariant manifold. The maneuver back to GEO is conducted with an impulse for a direct approach to the desired location. Given the direct approach taken, further savings in thrust can be realized with the use of the manifold on the return. It should also be noted that by adding the impulse maneuver at the vertical Lyapunov orbit a less efficient maneuver is presented. Also, when determining which vertical Lyapunov orbit just like the research conducted by Davis et al. (2011) it should be noted that only a subset of the vertical family can provide a cost savings for return to GEO whereas a selected vertical orbit beyond the subset can be more costly in return. The total from table 3-11 demonstrates for the selected vertical and horizontal Lyapunov orbit a Δv of approximately 5.076 km/s is used whereas the Hohmann transfer requires a total Δv of 8.29 km/s. The total Δv was determined by adding the different parts of the maneuver as seen with different colors in figure 3-14. The method of determining the total Δv was such because the maneuver was constructed of multiple impulse burns. When comparing the two different amounts to fuel used a 48% percent difference is realized. The fuel savings from Davis et al. (2011) was able to realize a 40% -70% difference and to realize the same level of savings with the method conducted both departing and returning manifolds would need to be used. During the calculations for velocity it was also discovered that the model has a 0.02 km/s second error from expected results.

Once again, time of flight is directly from running the system model from the created orbital trajectories. Given that this maneuver was patched together from two different LPOs the time from separated parts patched together provides the total time of flight. Using the equation (2.3) for the characteristic time conversion the results for time of flight are given with table 3-12. Table 3-12 is a comparison of time of flight and the Jacobi constant. Just as in the maneuver created in section 3.3 the created maneuver does not attempt to optimize the orbital trajectory. Further attempts to increase efficiency or optimize are left for future research such as differentially correcting the manifold trajectories or with potential studies as suggested in sections 3.4.1 and 3.4.2. The time of flight is solely determined by the system model as number points integrated over, determining the different data points. Using the same method of time of flight as in section 3.3 allows for a comparison based on the same measurements.

Table 3-12 Time of Flight for Designed Transfer Orbit

Time (unitless)	Time	Maneuver
6.5	377.82 days	Horizontal Lyapunov
5.5	319.69 days	Vertical Lyapunov
12	1.91 years	Total Maneuver

From table 3-12 following the full path of the LPOs may take more time than needed for the maneuver, rather than at the point of intersection between the LPO to us the manifolds for the maneuver. The suggested maneuver is by no means optimized to converse time, but rather demonstrates the savings in Δv.

Similarly, the overall cost of velocity or Δv that is used for the orbital maneuver is the thrust to depart from LEO and the thrust to enter a final circularized orbit. The departing Δv from LEO is derived from the initial conditions for position and velocity to enter the invariant manifold. The calculated results are altered based on corrections for the model to achieve the maneuver. The thrust needed to enter a final circularized orbit is derived in the same manner as in section 3.3. Position and velocity are selected by first approach from the stable manifold. Extending the time of flight for a second or third orbit also has the potential for decreasing Δv however that is saved for a future study. Similarly, with time of flight no optimization is conducted to determine a way

to decrease for the ending Δv of the maneuver. Time of flight and Δv are determined the same way as in section 3.3 to allow for a comparison between the two methods. Table 3-11 is the cost of velocity in comparison to the Jacobi constant. Finally, inclination is designed to be 90 degrees from the initial position.

In equation (3.18) the equation is used to take the initial conditions and ending points and transform them into coordinates centered with the Earth and Earth's tilt. Using the MATLAB script that was created by Curtis (2014), the information in table 3-11 is transformed into the information present in table 3-13. With all the information that has been gathered from this section table 3-13 is a coalited set of results providing initial and final coes for the three different orbits demonstrated in this research. Table 3-13 encompasses the results containing the initial and final coe, Δi, Δv, and TOF.

Table 3-13 Resulting Data from Orbital Maneuver .

Classical Orbital Elements		Δi	Δv	TOF
a: 6556	a: 42164	90°	5.076 km/s	1.91 years
i: -23.5	i: 66.5			
Ω: 0, e: 0, ω: 0, θ: 0	Ω: 0, e: 0, ω: 0, θ: 0			

The resultant information from the table above with use of two LPOs the Δi of 90° has a savings percent difference of 48% for a time of flight of approximately 1.91 years. Limitations to this maneuver are further explored in section 3.5.3 Results and Comparison.

3.5.2 Retrograde Motion & Rendezvous Missions Explored

In section 3.3 and 3.5.1 the CR3BP was noted to be in an ecliptic coordinate system with the rotation of model based on rotating around the barycenter of the system. This means that an inclination of zero, like the starting point of the maneuver conducted, is at an inclination of -23.5 degrees. The resulting maneuver then leads to an ending inclination of 66.5 degrees, a prograde orbit. Given that the model of motion is with respect to the barycenter of the system and not to the rotation of the second primary body, orbits of retrograde motion are possible. In this section a brief investigation is done on the capability of performing various inclination changes with little to no cost difference in thrust. The retrograde orbit of a satellite is defined as motion opposite to the spin

of the Earth. Understanding what this maneuver can provide for retrograde orbits is of interest due to cost inclination change involved.

With the maneuver conducted in section 3.5.1 the invariant manifold leads the satellite into the desired orbit. A slight change of impulse from section 3.5.1 on the stable boundary return will cause the satellite to have motion in the opposite direction with respect to the barycenter. That is the ending orbit created in section 3.5.1 can result in an orbit rotating with or opposite to that of the perspective of object on the surface of Earth. The maneuver started with an ecliptic inclination of zero degrees following a horizontal Lyapunov orbit. With the return to Earth being through a vertical Lyapunov orbit the result is a 90-degree shift in the ecliptic plane. When viewing the Earth in the equatorial plane this same inclination will now appear as an inclination of 66.5-degrees. The orbital maneuver created was accomplished with a horizontal and vertical Lyapunov orbit. However, that does not mean that the similar orbit can't be done with Halo orbits to provide different end state inclination changes as a satellite starts on one Halo orbit and transfers to another before the return to Earth.

The use of interchanging maneuvers between different LPOs has additional benefits for a wide variety of research. One topic of interest being rendezvous with temporarily captured near Earth asteroids could greatly benefit from the advantages of interchanging between different LPOs to better align with different asteroid paths. The research conducted by Breisford, Chyba, Haberkorn, and Patterson (2015) constructs the use of a Halo orbit as a station keeping location for the TCO 2006 RH_{120}. Limitations of TCO trajectories beyond 2006 RH_{120} when in the vicinity of a lagrange point can be overcome when using the lagrange point as a station keeping location and using LPO's to follow objects of interest. Their work conducted outlines a very specific type of mission whereas the suggestion here would be to use different LPOs to expand beyond the original mission after completion. The use of LPOs to change orbital trajectory are often used like in the example mission from section 1.3 Mission Scenario to provide additional purpose to assets that are already in space to provide further use.

From equation (1.1) calculation for an inclination change of 180° without any other parameter change, the change in velocity required is twice the velocity to maintain the current orbit. In comparison the maneuver from section 3.5.1 requires a velocity change of 7.679 km/s from LEO to GEO. This brief investigation of retrograde orbits would suggest that the use of invariant

manifolds could be used to significantly decrease the cost in velocity required for such maneuvers. Further investigation should be conducted for a wide range of different inclinations to determine the limitations of the created maneuver. Additionally, mission design for a retrograde orbit with the maneuver from section 3.5.1 would be subject to the conditions mentioned in section 4 that could limit applicational use.

3.5.3 Results and Comparison

In section 3.3 and in section 3.5.1 the velocities required for the mentioned maneuvers are impulse changes from LEO. Being an impulse change the velocities of both orbits start at a stable LEO velocity and end at GEO. As a comparison equations (3.20) and (3.21) are the numerical results for escape velocity and velocity at LEO.

$$v_{escape} = \sqrt{\frac{2GM}{r}} = \sqrt{\frac{(2*398600)}{(6378\ km+185\ km)}} = 11.02\ km/s \qquad (3.20)$$

$$v_{LEO} = \sqrt{\frac{GM}{r}} = \sqrt{\frac{398600}{(6378\ km+185\ km)}} = \qquad 7.79\ km/s \qquad (3.21)$$

The change in velocity from section 3.3 provides a maximum inclination change of 71.6° and change of velocity of 4.44 km/s with the research of Davis et al. (2011) stating that this method is a lower cost compared to a Hohmann transfer. The conducted maneuver has an inclination change limit that would require a Hohmann transfer or the use of a different impulse maneuver for larger inclination changes. The maneuver conducted would suggest that the use of different Halo orbits or as constructed the use of horizontal and vertical Lyapunov orbits can overcome such a limitation. As suggested by the work of Davis et al. (2011) the use of multiple LPOs does indeed yield further cost savings for large inclination changes.

The maneuver created in section 3.5.1 is designed to demonstrate a 90° inclination change with the use LPOs and invariant manifolds. A continuation of research into various orbits would need to be conducted to determine if an upper limit exists or if the use of any correct two inclinations can provide any desired inclination change with low thrust costs. If an upper limit of inclination exists for the maneuver created in section 3.5.1 a different method would be required for inclination changes beyond a such limit. Given the limited scope of the research conducted the inclination change demonstrated requires a change of velocity of 5.076 km/s. With the change of inclination and velocity a comparison is made with the Hohmann transfer method.

Using equation (1.1) the required velocity for an inclination change of 71.6° is approximately 1.82 km/s and for a 90° inclination a velocity of approximately 3.29 km/s. As a measure of how much a 90° inclination costs the velocity required is greater than the velocity need to escape Earth. That is if the inclination change was occurring at LEO a 90-degree change is twice the velocity needed to maintain orbital velocity whereas the velocity to escape Earth is 11.02 km/s. This method is based on two body conics only taking into consideration the primary body and the satellite. The Hohmann transfer method is also considered the most efficient for time with the cost in velocity. In addition to the efficiency of time because this maneuver occurs close to the primary body Earth satellites do not incur environmental conditions mentioned in section 4. Separate from the use of the Hohmann transfers another method often used is the bi-elliptical transfer method.

The bi-elliptic transfer method consists of two half elliptic orbits. The Hohmann transfer maneuver has an elliptic orbit between the desired initial and final orbits whereas the bi-elliptic orbit has an elliptic orbit that extends beyond the final orbit. With the bi-elliptical orbit, the further out the elliptic orbit the more potential savings in change of velocity. Just like the Hohmann transfer the bi-elliptic transfer is also based on two body problem conics and does not take into consideration perturbations from other bodies. As the distance from the primary body increases the more this method is prone to error. The advantage the bi-elliptical transfer has over the Hohmann transfer is that for r_f/r_i greater than 15.58 the transfer can save on fuel. In addition to fuel savings for a radius ratio greater than 15.58 if the intermediate maneuver point is at an extended distance than ratios between $11.94 < r_f/r_i < 15.58$ can also be more economical. With this study focused around the initial orbit being LEO and the final orbit being GEO the ratio of $r_2/r_1 \approx 6.42$, and therefore, a bi-elliptic transfer would not be advantageous. Figure 3-17 provides a visual depiction of the difference with efficiency between the two orbits.

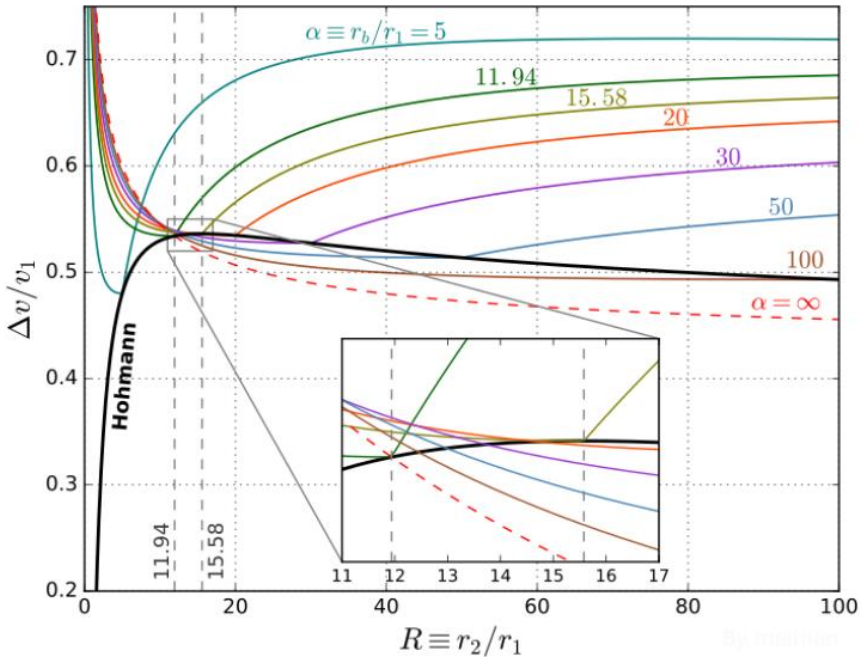

Figure 3-15 Traditional Transfer Methods. ”Bielliptic transfers comparison.svg” by Meithan Created 1 December 2016. Image take from https://commons.wikimedia.org/wiki/File:Bielliptic_transfers_comparison.svg

Given the results of the research conducted and the review of the Hohmann transfer and bi-elliptic transfer method, each maneuver has advantages and disadvantages for different amounts of inclination changes. The maneuver in section 3.3 had a minimum inclination change of approximately 7.8° and a maximum of approximately 71.6°. Transfers less than 7.8° are not feasible with a signal LPO and when introducing a second LPO further research would need to be conducted to determine the full change in velocity required. Given the research that has been conducted a preliminary analysis would suggest that small inclination changes would not be efficient with the maneuver conducted in section 3.5.1. For small inclination changes for an orbit at LEO the Hohmann transfer method is still the most efficient. For inclination changes that are between 7.8° and 71.6° the work conducted by Davis et al. (2011) is the most efficient for fuel. Finally, for an inclination change of 90° the constructed method in 3.5.1 using two LPOs is more efficient than a Hohmann transfer. A future investigation for testing efficiency would be to ensure that inclinations between 71.6° and 90° and for transfers greater than 90° is more efficient compared to a Hohmann transfer and potential limits with the constructed transfer. Although these transfers are more efficient in change in velocity both methods using LPOs do drastically increase time of flight to complete a transfer maneuver.

4. ENVIRONMENTAL CONDITIONS AND POTENTIAL APPLICATIONAL USE

It is the intent of the research conducted to create an impulse maneuver designed for large inclination changes as a cost savings technique beyond rescue or salvage. The impulse maneuver created in section 3.5.1 compares Δv and time of flight with respect to inclination change. In studies of efficiency and optimization of orbital maneuvers the general results are provided with Δv and time flight within the conclusion. Further analysis is left to mission design, should a maneuver be used. Past research with the focus of mission design is typically focused around a mission such as the NASA Genesis mission, Suess-Urey mission or others as examples from section 1.2.2. The reason a general mission design is often not covered is due to the changes in the specifics of different missions and parameters.

To understand different potential uses of the maneuver created, a more general mission design is reviewed instead of the use of a specific mission. This research seeks to review the general concepts of mission designs for the impulse maneuver created to understand the benefits and consequences. Looking at mission design will allow for greater understanding as to what these types of impulse maneuvers can provide. From the concluding research time of flight is only compared to time of the start of the maneuver to the end. However, another aspect of time measurement that could impact a mission is the time involved with scheduling a launch site, launch windows, and then a maneuver to achieve the desired position and velocity. It is common for mission designs of satellites to be launched from a site that would provide a similar inclination to the desired mission due to how expense inclination changes can be. Also, with the measurement of Δv a review is conducted to understand associated benefits as well.

The benefits of a given maneuver when talking about efficiency can potentially have greater application and use when considering differences at the beginning of planning. In addition to providing more options in planning, impulse maneuvers are also reviewed from an economical perspective to determine cost vs benefits. To limit the scope within this section the generalized orbits are restricted to those common for LEO mission types with a comparison to typical design. This section conducts a mission design review with the impulse maneuver to understand effects of inclination changes, and overall efficiency. A brief review of past usage with rescue and salvage missions will provide an understanding as to why these types of maneuvers have been typically restricted to such cases.

4.1 Rescue and Salvage Missions

The technique for ballistic capture was developed in 1987 using WSB transfers. Though the initial design of the transfer was for electric propulsion for the low quantities of thrust a secondary use was in the form of applications requiring fuel saving. The first use of ballistic capture into lunar orbit was in 1991 with the Japanese spacecraft Hiten. The spacecraft released a small orbiter named Hagoromo which had a transmitter failure preventing communications and control for orbital corrections. The Hiten Spacecraft mission objectives consisted of measurement of cosmic dust between the Earth and the Moon along with testing different maneuvering, insertion, and breaking techniques. The orbital maneuver consisted of ten lunar swing-by experiments and an areo-braking experiment with Earth's atmosphere. The impulse maneuver created saved about 25% in the Δv required for lunar capture and increased time of flight by about 90 days (Belbruno, Carrico, 2000). The maneuver was created in a similar fashion as from the maneuver created in this research in that first the designed orbit was generated followed by the impulse required to achieve the resultant maneuver. The modeling software for the Hiten Spacecraft maneuver used was STK/Astrogator to demonstrate the full realization of the maneuver with the desired outcome. The use of the maneuver was successful, and the mission was salvaged completing all mission objectives.

In section 1 of the Introduction the AsiaSat-3/HGS-1 is considered a rescue mission due to having to correct for a fourth stage thrust execution failure. The satellite's thrust failure resulted in an unstable orbit with an inclination of 51.6^{o} and an eccentricity of 0.73 instead of the intended geostationary orbit (Ocampo, 2005). AsiaSat-1 required an additional Δv of 2.42 km/s to correct for the mistake. To avoid complete loss of capability Asia Satellite Communications Ltd. sought non-standard transfer methods to best achieve a stable orbit. Edward Belbruno had devised an impulse maneuver using the WSB and capture dynamics with the moon to achieve an inclination of 12.5^{o}. Another maneuver created was a lunar flyby orbit to allow for an inclination adjustment on the free return. The lunar flyby orbit was chosen providing an inclination of 8^{o} and after many years in orbit 0^{o}. The impulse designed by Edward Belbruno was not selected due to TOF, continuous communication, and the ability in keeping guidance and control. AsiaSat-1 was known as a success with lasting a total 4 years in orbit. Even with the overall success of the mission the two different mission designs and reasons provided for selection demonstrate why one method would be more advantageous for operational use.

The first technique for lunar capture with WSB was created in 1987 with the first applicational use in 1991. This four-year turnaround time from creation to operational use was due to the need for rescue and salvage for a mission asset. With an increased number of satellites and modeling capabilities the creation of different maneuvers will allow for orbital designs that best fit different situations even if such techniques are considered non-standard. Non-standard techniques become a viable option when standard techniques are no longer possible, and risk is acceptable to avoid complete mission failure. The main advantage with the different methods that are derived from the three-body problem over two-body problem conics is with fuel savings. Many of the different methods mentioned have also shown that using gravitational forces over thrust increases TOF. In addition to increased TOF other disadvantages for such maneuvers consist of continuous communication and the ability to maintain guidance, navigation, and control. Separate from the disadvantages mentioned in both use cases additional concerns are reviewed in sections 4.2 and 4.3 for operations starting and ending in LEO. Despite the most common use of non-standard transfer methods with rescue and salvage there have been several satellite missions that have also used such maneuvers due to matching mission objectives.

In addition to rescue and salvage use other missions that have used a similarly designed orbit as section 3.5.1 is the NASA Genesis mission as described in section 1. The satellite's objective was to collect solar isotopes following multiple loops of an L_1 LPO in the Sun-Earth/Moon system continuing with a homoclinic loop to return to Earth. The trajectory selected best fits the unique mission design to achieve the intended objectives. In the case of the Genesis mission standard maneuvers or an orbit around a primary body would not have collected as much particles or dramatically increased cost to the mission. In the case of Genesis, the selected trajectory was used not for fuel savings or TOF but rather to increase the payload collection capabilities. A key uniqueness of the mission was that only a single deterministic maneuver was required to insert the spacecraft into the designed Lissajous and Halo orbits. The cost for the Genesis mission was about 264 million dollars and although no direct comparison can be made to another mission, the fuel savings would potentially contribute to a decrease in total cost or increase in mission life. The Genesis mission is often a commonly referred mission based on similarities with maneuver techniques using LPOs and the potential advantages that could be provided for different mission types. The mission was launched in February 2001 with a duration of over 15 years however a much earlier orbital mission example can be found with the ISEE-3.

In 1978 the NASA International Sun-Earth Explorer -3 (ISEE-3) was launched to measure solar wind from a Halo orbit about a L_1 LPO. The orbital design was set to maximize the payload collection capabilities just like the Genesis mission. The maneuver used was constructed in such a way to achieve mission success despite the poor engine performance with a variety of contingency planning possible throughout the trajectory. ISEE-3 was able to avoid a cold start thrust and lunar gravity assist by adjusting the maneuver to be completed with a three-impulse strategy. The first impulse maneuver would be to get the satellite to enter an LPO, the second burn would be to transfer the trajectory to a Halo orbit, with the final burn on the return. Within the contingency plans the added Δv is proportional to thrust needed to correct the trajectory. The original launch date for the satellite was July 23rd, which was changed to August 12th. This affected planning because the position of the moon changed as well. The difference in the moon's position changes the perturbations experienced by the satellite entering the LPO (Computer Sciences Corp., 1979). In section 3.5.1 the position of the Earth/Moon are treated as a point mass not accounting for perturbation changes from varying positions of the Moon within its orbit. The mission design of ISEE-3 would suggest similar contingency planning would be required for the maneuver created in section 3.5.1.

Although the original purpose of ballistic capture and the use of WSB transfers were developed for low thrust missions the fuel saving potential was almost immediately recognized. As an immediate implementation of these impulse maneuvers rescue and salvage missions have demonstrated an additional use. The Hiten Spacecraft mission modeling has led to wide variety of different maneuvers using WSB transfers and LPOs. However, some disadvantages that have been noted include increased TOF and communication issues depending on the mission. With missions that seek to use WSB transfers and LPOs like Genesis and ISEE-3 the use of traditional methods would create a disadvantage in achieving success. Additionally, with different orbital designs that have been created in a wide variety of research the use of contingency planning would still need to be created to ensure corrections due to perturbations from other forces. This preliminary use in mission planning would require contingencies like the once created for the ISEE-3 satellite. The corrections would help account for simplifications within the model and additional gravitational forces that would create error. Correcting for errors by creating contingency maneuvers would require specifics given a launch window and other parameters of a mission. Separate from

contingency maneuvers any use of the impulse maneuver created in section 3.5.1 would also need to account mission design changes.

4.2 Mission Design for Low Earth Orbit

This preliminary study being focused on LEOs requires satellite mission design to take into consideration factors such as environmental conditions, lifetime, and communication. The initial conditions for impulse maneuvers in section 3 started at an altitude of 185 kms and at such altitudes Earth's atmosphere affects satellites in two ways. Roughly below 600 km Earth's atmosphere affects satellites with drag and atomic oxygen. The effects of drag onto a satellite can shorten orbital lifetime and atomic oxygen can degrade surface areas. The amount of drag that is exerted can be altered with aerodynamics that are beyond the scope of this study. Additionally, the effects of drag can vary with atmospheric changes from solar activity and over time without correcting for such changes can create loss of altitude for satellites. Another effect that can negatively impact a satellite's orbit if not accounted for is atomic oxygen. Atomic oxygen is created in the upper atmosphere from radiation and charged particles from the splitting of O_2. The resulting oxidation combines with the metal components of the satellite causing rust which will degrade exposed materials like payload equipment. Issues with atomic oxygen can be mostly overcome with material structure which further increases complexities with aerodynamics beyond the scope of this research. From the two atmospheric conditions mentioned a slight adjustment would need to be accounted for with Δv or the ability to apply corrections to create and maintain a given orbit.

Within the upper layers of Earth's atmosphere and beyond other environmental conditions that become problematic are conditions such as out-gassing, cold welding, and heat transfer. The conditions of out-gassing are caused from material usage that could contain pockets of trapped air and burst when exposed to the vacuum of space. Out-gassing however is not typically a problem with solutions including careful selection of material, molecular coating, and heat testing. Another problem with the vacuum of space is cold welding caused by mechanical parts that have little separation between them. Depending on mechanical design and mission needs some moving parts are unavoidable and carefully selecting material can help, however cold welding may not be completely avoidable. With the vacuum environment of space, the primary method of heat transfer is radiation. Radiation acts as a dispersion of heat for energy loss during transfer from one component to another. Heat transfer is not typically an issue for orbital maneuvers however when

spacecraft failures occur impacted systems can limit what corrective maneuvers are possible. Other forms of radiation separate from Earth's influence and internal to the satellite can create potential issues as well as impacting fuel usage that may not be described with the model used in section 3.

4.2.1 Environmental Conditions

In addition to the radiation previously mentioned additional concerns include the effects of radiation from charged particles. As a spacecraft or satellite gets further into space a dangerous aspect of the environment is in the form of charged particles. Charged particles within the region of interest can expect radiation from solar winds and flares, and cosmic rays as the satellite extends beyond the magnetic shielding from Earth. The charged particles regardless of their origin negatively impact a satellite through charging, sputtering, single-event upsets, and total dose effect. Each of the negative impacts affect a satellite in different ways that need to be accounted for in mission planning and development.

The first negative effect caused by charged particles mentioned is charging, a condition when different components of the satellite store different amounts of electric charge. The charge is built up when impacted or traveling through concentrated areas of charged particles. As a charge builds up within different components at different rates an electrical discharge occurs, potentially damaging electronic systems. The stronger the electric field the more frequent discharges with larger pulses for potential damage. The electrical discharge may not necessarily occur immediately and may be considered unpredictable as to when during flight damage happens. To minimize the damage from charging mission often avoid maneuvers during solar activity. With any given point in the impulse maneuver subject to damage from this form of charged particles the ability to correct along the trajectory becomes vital for success.

Second, sputtering is caused by the intense speed in which the particles are traveling as they impact the surface of the satellite. The collision of charged particles will recoil in a variety of different directions after binding with a satellite's surface causing those atoms to be ejected. The average number of atoms ejected from satellite or spacecraft is known as the "sputtering yield" which can impact orientation of thrust and instrumentation (Plumes, Boyd, Falkf, 2001). Over the duration of a mission sputtering can create extensive surface damage impacting different component's performance and functionality. In the event of a large concentrated quantity of charged particles, a satellite would alter course to avoid damage making this form of damage

primarily from the accumulation over time. Similar course corrective maneuvers are employed as the primary method to avoid this type of environmental hazard.

Another negative effect caused by charged particles is a phenomenon known as a single-event upset. Single-event upsets are caused by charged particles impacting hardware creating bits within the software to change. The changing state within the software can created incorrect messaging between different components causing unintended changes to system operations. This form of radiation damage can be decreased with error correcting coding methods and physical protection against radiation damage. The physical hardware for satellites can be carefully selected for radiation protect and shielding can be added. Different forms of radiation protection for hardware components vary with radiation hardening techniques to radiation tolerant hardware. The impact this form of radiation could potentially have a satellite misinterpret a trajectory as correct, create thrust in a wrong direction, or even prevent response from Earth to make corrections.

Finally, the impact of charged particles onto a satellite over time can create an effect known as total dose. A total dose is caused by long term exposure to radiation to computer hardware components. The damage that is created by a total dose effect is different compared to the single-event upsets in that physical hardware is damaged instead of software. As different hardware components are exposed over time degradation to devices can create device failure. Carefully choosing what material hardware is made of can decrease the risk. Within the development stage of missions, different systems are tested for a variety of conditions. Depending on the amount of radiation exposure, performance curves can help to provide a level of expectation of a satellite's capability. Due to this effect being caused from long term expose to radiation this would potentially limit the duration of a mission and a satellite's usefulness. The effects of a total dose with an impulse maneuver are beyond the scope of this research, however, performing a maneuver under these conditions would be considered risky depending on the failed system or decrease in performance.

In understanding a few of the different space environment hazards the brief review conducted provides some important factors to consider with mission planning. The tracking of space weather is important to avoid extreme radiation damage caused by solar flares or other events. Like the mission design from ISEE-3 the development of contingency maneuvers for trajectory corrections need to be planned. Finally, when developing a mission for the space environment at increasing

distances from Earth more damage is likely to occur. Careful selection of materials can help decrease the potential damage from radiation for deep space impulse maneuvers.

4.3 Overall Efficiency

In section 4.2 the brief study presents a few of the different environmental hazards of what could be expected at the L_2 LPO. The impulse maneuver created is compared with equation 1.1 method of transfer for efficiency. The radiation hazards from section 4.2 are more of a concern with the impulse maneuver created compared to a satellite that might be better protected being close enough to Earth. The hazards from the space environment along with the benefits of fuel savings and flexibility in launch window are used to compare the two different types of maneuvers. However regardless of the approach taken solar weather and timing would still need to be taken under consideration to avoid hazardous conditions. Given the stated differences between maneuvers that stay at LEO and an orbit that would travel into deep space a comparison of economics, costs, and mission design is briefly covered to assist with determining efficiency.

This research seeks to use different analogues missions to determine the economic costs of a traditional LEO satellite maneuver compared to an impulse maneuver as described in this research. For traditional LEO satellites, planning and costs are typically associated to launch site which will prevent the need for a large inclination change. Due to the planning involved having a direct cost analysis will not be possible. However, an assumption of this research will be that the launch sites are specifically chosen for minimal inclination maneuvering. Additionally, the cost for different launch sites and insurance are not publicly provided. With the different missions that are used for comparing the different type of fuel used and thrust efficiency are also not accessible for comparison. General information about specific engines with different types of fuel can be computed. However varying costs would be difficult to compare back to the total costs of missions. The main determination within this study will be based on the overall cost or estimated cost from mission class type of previous analogous missions, and how long different missions have lasted.

Another aspect to consider for efficiency are differences with mission planning. A spacecraft can be broken into two main parts, these parts being the bus and the payload. Typically, the payload is specific to the intent of the mission being achieved and not desirable to change for differences of maneuvers. Additionally, there could be a case in which material or mission design from the payload would support deep space maneuvers regardless of the design of the bus. However, the

planning and development of a bus can change to achieve the needed trajectory. This study will consider differences in material, risks, and possible contingencies. The overall efficiency will then be based on both economic costs and mission planning.

4.3.1 Economic Efficiency

Two analogous missions chosen to use a comparison with the type of impulse maneuver created within the research are ISEE-3 and the NASA Genesis mission. ISEE-3 mission was to conduct a survey of the Earth's magnetosphere and the study of two comets. The satellite was launched in 1978 and lost in 2014. As an explorer class mission, the cost are limited to $200 million and in 2014 the satellite was repurposed with new flight hardware with funds raised of $159.5 thousand. The NASA Genesis mission was a sample return mission for solar wind particles designed specifically for the trajectory of LPOs. The mission was launched in 2001 and the return capsule landed in 2004 successfully. The satellite cost was $264 million with a 1 to 3-year mission. With both missions described each had a payload design specifically designed to take advantage of the orbital motion about an LPO. During the mentioned missions, communication disruptions were an inherent risk as the satellites traveled further away from Earth with different objects blocking transmissions. Within the total cost of the missions the cost of fuel is determined based on the needs of the mission. With traditional research into impulse maneuvers like in section 3.5.1 fuel cost saving can lead directly into overall cost savings or allocation of resources in other aspects of the a given project.

To avoid the specifics of the different missions connected to different types of LEO satellite missions the following satellites were selected; Aura and Sentinel-5 Precursor. Both chosen satellites have an inclination change of 98^{o} and support scientific missions. Regardless of the orbit design the mission payload supports is the highest cost impact onto a satellite. The Aura mission was a satellite designed to study the ozone layer, air quality and climate over the duration of its operation. The satellite launched in 2004 with an expected decommissioning in 2023 is still providing scientific data. The Aura mission cost was $785 million with an expected mission duration of 19-years. The Sentinel-5 Precursor satellite is a European scientific mission to monitor air pollution through several different instruments. The satellite was launched in 2017 and is currently still in operational use. The mission cost of the satellite was about $49.5 million with an expected duration of about 7-years. Given the two LEO satellites cost ranges are significantly large

with varying missions at the same inclination. Additionally, the Δv for an inclination is not a dollar cost amount and cannot be directly defined given both satellites launched from a site to provide the desired inclination, those sites being Vandenberg Air Force Base and Plesetsk Cosmodrome Russia respectively. Given the calculation conducted with equation 1.1 an inclination change would have consumed approximately half the Δv of the velocity of their orbit, costing a considerable amount of fuel altering the overall costs.

Comparing deep space missions like Genesis and ISEE-3 to missions that stayed in LEO like the Aura and Sentinel-5 Precursor are used to provide cost differences. For the missions that are considered deep space their costs seem to be near if not over $200 million. In some of the cases traditional LEO satellite missions seem to approximately range from $50 - $800 million. Given the range of cost for each mission fuel usage does not appear to be the largest factor. Each satellite had specific mission objectives that all differ from each other and some were constructed by different entities making a direct comparison for cost impossible. The mission types under comparison are all scientific and are often designed for a level of flight worthiness for environmental conditions. Other cost drivers that could not be directly compared, are if any potential difference exist with payload for radiation protection, or contributions from the launch vehicle to achieve initial orbit or a parking orbit. From an economic cost the use of traditional methods appears no different from an overall perspective compared to a deep space impulse maneuver. With costs not providing a direct result of which type of maneuver is more efficient other factors such as risk, time of flight, and potential usage need to be taken under consideration.

4.4 Environmental and Design Concluding Remarks

An efficient transfer orbit is determined by improving a parameter for a given transfer. Although studies of efficient transfer orbits demonstrate savings in Δv another question to ask is if such maneuvers are also efficient on a global scale for a mission. In evaluating overall efficiency, the harmful effects of radiation are reviewed to understand potential impacts. With radiation, risks can be mitigated by monitoring solar weather and timing of missions, selection of material components for shielding, and designing software to handle error. Additionally, with the hazards of radiation contingency orbits in case of component failure better ensure success of the maneuver. The idea of the contingency maneuvers with the conducted research is based on the mission design created from ISEE-3 in the event a potential issue. Separate from radiation at altitudes of LEO

atmospheric conditions can also impact satellites causing the need for slight orbital corrections because of friction. Once again, like radiation, the atmospheric effects also create the need for careful selection of material for component design. From the previous section in determining cost between the two different maneuvers no difference was determined. Costs for specific components and for various other aspects are not openly shared. In addition to cost determination issues the time spent for mission planning and development is also not shared. Mission information is often provided from the time of launch and onward. With no discernable difference in cost, efficiency of transfer orbits is further reviewed with time of flight and risk. Time of flight is typically extended for low fuel maneuvers and risks with using LPOs can also bring communication issues as objects can come between a satellite the further in space a satellite goes. For cost differences between maneuvers using LPOs to be the same as maneuvers that stay in LEO potentially means one of three outcomes. For no cost savings to be realized between the two different maneuvers the fuel savings is the same as protective measures, cost savings are being utilized in other aspects of the system design, or cost benefits are not being utilized. The Δv efficient transfer orbits are clearly advantageous compared to traditional methods when in need for rescue and salvage, or when such a maneuver directly benefits mission objectives.

5. Conclusion

5.1 Summary of Results

The problem of inclination change maneuvers as described in section 1 is that they are typically avoided due to their cost in Δv. With the research conducted and other associated research different methods have been developed to provide initial cost savings possibilities. The mission scenario created from section 1.3 was used as an example use case for the maneuver created in section 3.5.1. With the overall research being conducted the goal was to seek a more efficient transfer using a vertical and horizontal Lyapunov orbit and compare the results to a Hohmann transfer. When developing a model of the CR3BP different aspects that needed to be taken into consideration included equilibrium points, method of numerical analysis for computing the model data, and the use of linear approximations of different potential desired trajectories. Solutions were created using analytical approximation in the vicinity of the L_2 equilibrium point to provide a strategy for numerical computation of the horizontal Lyapunov family. Additionally, the brief introduction of invariant manifold theory provides a description for a method to use the manifold in the formulated trajectory. The combination of the topics covered provide general foundation on the components behind different trajectories being modeled with the CR3BP.

The first test case successfully recreated the work of by Baines et al. (2018) demonstrates the functionality of the CR3BP within a Python script. After successfully creating the same results further changes to the model were created to expand the model to cover the z-axis and modifications for the change in coordinates. The modifications further allowed for approximate like trajectories for Davis et al. (2011). The second test case successfully provided inclination changes more efficient compared to the traditional Hohmann transfer. Creating a maneuver with the stable manifold to the LPO and the unstable manifold to achieve GEO was vital to creating a maneuver with two LPOs to further increase inclination. The use of a 90^o plane change demonstrates the capability for other orbits of different inclinations to be possible. The combination of Baines et al. (2018) and Davis et al. (2011) provided the ability for the proposed orbit to be created. While testing the Python script and making changes it was noted that velocity has an error of 0.02 km/s. The error is caused by the step size of the system to allow the computer to run the model due to limitations in system memory. The differences in results from Davis et al. (2011) are primarily from not knowing the research's original state vector as input into the system. Given that the results are similar it would prove that their method does indeed meet the claim

mentioned and has the possibility to be extended for wider range of orbital maneuvers. Another issue with the model regarding error is that model is sensitive to the millimeter level of precision. Having a millimeter level of precision is inherently wrong for a system that should only realistically be precise to meters. The reason for the error in precision is due to the incredibly small mass ratio. From section 2 it was noted that the mass ratio of the system must be μ: $0 < \mu \leq 0.5$. However, the closer to zero the model the more numerical values are needed to produce similar like orbits. In the Earth-Moon system an L_2 Lyapunov orbit requires a level of precision in meters which seems to be due the mass ratio $\mu = 0.0121505856$ compared to Sun-Earth/Moon system which is four orders of magnitude differences. This type of error would need further investigation if there is a negative impact of the numerical results. With creating trajectories within the model, a certain level of precision is required to achieve expected results increasing the difficulty in determining the correct values.

A new method was presented that was constructed from a transfer trajectory between orbits of LEO and GEO for an inclination change of 90º. The invariant manifold from the horizontal Lyapunov orbit was used for the L_2 location in the Sun-Earth/Moon system. The trajectory departs the initial orbit on a stable manifold and returns with a direct thrust to GEO. The gravitational effects realized act in such a way that the 90º inclination change creates this efficient maneuver. The transfer cost was compared to a Hohmann transfer performed from LEO to GEO with the same inclination change. The total Δv to transfer from LEO to GEO with the use of a horizontal and vertical Lyapunov orbit was 5.076 km/s. Overall, approximately 48% savings was realized using the method created with a potential for more savings to be realized. This maneuver is specifically constructed for a 90º inclination change which is a greater change of inclination to the use of a single LPO. For small inclination changes of about 8.75º or less the Hohmann transfer will produce the least amount of cost for Δv. For an inclination change greater than 8.75º up to 71.6º a single LPO can save on Δv. The use of two LPOs has shown that a 90º inclination change is achievable to be more efficient for total Δv. As mentioned in the mission scenario and in section 3.5.2 this method has the potential to provide significant fuel and cost savings to missions that would have similar situations. The drawback to these efficient methods using the manifold trajectory and two different LPOs is with an increase in time of flight. With studies that involve saving fuel, time is typically the cost. In the case of this maneuver a total approximate time is close

to 2 years. While constructing the maneuver in section 3.5.1 many different and important continuations have presented themselves, some of which are captured in the next section.

5.2 Recommendation for Future Research

As a preliminary study there are many different possible routes to continue exploring the ideas presented in this document. The research set out to analyze a specific transfer that departs from LEO on a stable manifold trajectory to use two different LPOs and arrive at GEO. The return path to GEO from the vertical Lyapunov orbit is a direct transfer which is inefficient. A natural continuation to this research is to continue the maneuver with the unstable manifold being used on the return trajectory. The use of the stable manifold was the original intent of this research but due to time constraints and complexity of the maneuver that was not achieved. With the use of the unstable manifold for the trajectory return the maneuver created has the potential to have the same level of cost savings as the Davis et al. (2011) research of 40 – 70%. Currently the method developed has a savings of 48% which has potential to increase with further efficiencies and optimization. After using the unstable manifold to further refine this maneuver the techniques mention in section 3.4.1 and 3.4.2 can be introduced to add even further cost savings.

The scope of this research was limited to the use of a horizontal and vertical Lyapunov orbit for a specific 90^o change of inclination at the L_2 point. However, given the use of any two distinct Halo orbits another investigation worth studying is the use of different combinations of Halo orbits to provide a wide range of large inclination changes. In addition to the use of multiple distinct Halo orbits the use of L_1 and L_2 equilibrium points can be explored to see if they yield the same benefits. Given the 48% increase in efficiency with the maneuver created in this research and the work of Davis et al. (2011) for missions that do not have a time constraint this method of transfer could provide several advantages. In section 4 the negative impacts from the use of the described maneuver provide potential differences in the space environment. A full realization of the potential cost savings and mission design cannot be realized as information on mission specifics such as length of time under production is not often common publicly shared. A study of different Halo orbits at both the L_1 and L_2 is valuable in potentially determining a limit for this kind of maneuver with a change of inclination and to the full extent of what inclinations are achievable.

Finally, given the advancements of technology this research was able to be conducted on a personal computer with modeling done in Python. This means that the research conducted in this document can be recreated on most computers. However, one of the difficult aspects of the

research conducted was the calculations outside of Python to determine an approximate solution to then refine the solution within the model to achieve a certain trajectory. Numerically determining solutions followed by correcting for nonlinearities of the model is time consuming and still has a manual process involved. With the use of graphical processing units (GPUs) there exist a potential for a computer to run through a wide range of outcomes given different state vectors. A model that could efficiently take advantage of the GPU ability to compute multiple sets of state vectors would enable the study of the different orbits that could be used for varying mass ratios. Creating a GPU based model of computing different outcomes for different state vectors would rapidly increase calculations and solutions for all the different quasi-periodic, or periodic orbits. Beyond the three ideas of future work mentioned already there are several different ways that this research can continue both mentioned throughout this document and beyond. A greater understanding of the motion about our system would be beneficial beyond the scope of this research as such information could be invaluable to wide range of mission designs.

6. LIST OF REFERENCES

Baines, T., Hew, Y. J., & Toyama, S. (n.d.). The Restricted Three Body Problem Trans-Lunar Injection. Retrieved from http://www.u.arizona.edu/~dpsaltis/Phys305/bainesetal.pdf

Barden, B. T., Howell, K. C., & Lo, M. W. (1996, July). Application of dynamical systems theory to trajectory. Retrieved from https://www.researchgate.net/publication/269044595_Application_of_dynamical_systems_theory_to_trajectory_design_for_a_libration_point_mission

Belbruno, E., & Carrico, J. (2000). Calculation of weak stability boundary ballistic lunar transfer trajectories. *Astrodynamics Specialist Conference*. doi: 10.2514/6.2000-4142

Belbruno, E. (2004). *Capture dynamics and chaotic motions in celestial mechanics with applications to the construction of low energy transfers*. Princeton (N.J.): Princeton University Press.

Boyd, I., & Falk, M. (2001). A review of spacecraft material sputtering by Hall thruster plumes. *37th Joint Propulsion Conference and Exhibit*. doi: 10.2514/6.2001-3353

Breakwell, Brown, & V., J. (1979, March 12). The `Halo' family of 3-dimensional periodic orbits in the Earth-Moon restricted 3-body problem. Retrieved from https://ui.adsabs.harvard.edu/abs/1979CeMec..20..389B/abstract

Campbell, A., Mcdonald, P., & Ray, K. (1992). Single event upset rates in space. *IEEE Transactions on Nuclear Science, 39*(6), 1828–1835. doi: 10.1109/23.211373

Chow, N., Gralla, E., & Kasdin, N. J. (2004). Low earth orbit constellation design using the earth-moon L1 point. Retrieved from https://collaborate.princeton.edu/en/publications/low-earth-orbit-constellation-design-using-the-earth-moon-l1-poin

Curtis, H. D. (2020). *Orbital mechanics for engineering students*. Amsterdam: Elsevier, Butterworth-Heinemann.

Davis, K. E., Anderson, R. L., Scheeres, D. J., & Born, G. H. (2010). The use of invariant manifolds for transfers between unstable periodic orbits of different energies. *Celestial Mechanics and Dynamical Astronomy, 107*(4), 471–485. doi: 10.1007/s10569-010-9285-3

Davis, K. E., Anderson, R. L., & Born, G. H. (2011). Preliminary Study of Geosynchronous Orbit Transfers from LEO using Invariant Manifolds. *The Journal of the Astronautical Sciences, 58*(3), 295–310. doi: 10.1007/bf03321172

Davis, K. E., Anderson, R. L., Scheeres, D. J., & Born, G. H. (2011). Optimal transfers between unstable periodic orbits using invariant manifolds. *Celestial Mechanics and Dynamical Astronomy*, *109*(3), 241–264. doi: 10.1007/s10569-010-9327-x

Davis, K. E., Anderson, R. L., & Born, G. H. (2011). Preliminary Study of Geosynchronous Orbit Transfers from LEO using Invariant Manifolds. *The Journal of the Astronautical Sciences*, *58*(3), 295–310. doi: 10.1007/bf03321172

Dunham, D. W. (1979). CONTINGENCY STUDY FOR THE THIRD INTERNATIONAL SUN-EARTH EXPLORER (ISEE-3) SATELLITE. *Computer Sciences Corporation*.

Farquhar, R. W. (1971, July). THE UTILIZATION OF ORBITS IN ADVANCED LUNAR OPERATIONS. Retrieved from https://ntrs.nasa.gov/archive/nasa/casi.ntrs.nasa.gov/19710005876.pdf

Farquhar, R. W., & Kamel, A. A. (1972, September 13). Quasi-Periodic Orbits about the Translunar Libration Point. Retrieved from https://ui.adsabs.harvard.edu/abs/1973CeMec...7..458F/abstract

Fleetwood, D., & Eisen, H. (2003). Total-dose radiation hardness assurance. *IEEE Transactions on Nuclear Science*, *50*(3), 552–564. doi: 10.1109/tns.2003.813130

Frederickson, A. (1996). Correction to "Upsets Related to Spacecraft Charging" [Correspondence]. *IEEE Transactions on Nuclear Science*, *43*(4), 2454. doi: 10.1109/tns.1996.531795

Gomez, G., & Masdemont, J. (2000, January). (PDF) Some Zero Cost Transfers Between Libration Point Orbits. Retrieved from https://www.researchgate.net/publication/238757196_Some_Zero_Cost_Transfers_Between_Libration_Point_Orbits

Gomez, G., Koon, W. S., Lo, M. W., Marsden, J. E., Masdemont, J., & Ross, S. D. (2001, August 30). Invariant manifolds, the spatial three-body problem and space mission design. Retrieved from https://trs.jpl.nasa.gov/handle/2014/41546

Gómez, G., Koon, W. S., Lo, M. W., Marsden, J. E., Masdemont, J., & Ross, S. D. (2004). Connecting orbits and invariant manifolds in the spatial restricted three-body problem. *Nonlinearity*, *17*(5), 1571–1606. doi: 10.1088/0951-7715/17/5/002

Grebow, D. J. (2006). GENERATING PERIODIC ORBITS IN THE CIRCULAR RESTRICTED THREEBODY PROBLEM WITH APPLICATIONS TO LUNAR SOUTH POLE COVERAGE. *Purdue University*.

Howell, K. (1983, July 8). Three-dimensional, periodic, ?halo? orbits. Retrieved from https://www.academia.edu/23465762/Three-dimensional_periodic_halo_orbits

Hénon, M. (2002, July 8). New Families of Periodic Orbits in Hill's Problem of Three Bodies. Retrieved from https://link.springer.com/article/10.1023/A:1022518422926

Koon, W. S., Lo, M. W., Marsden, J. E., & Ross, S. D. (1999, January 1). Dynamical Systems, the Three-Body Problem and Space Mission Design. Retrieved from https://authors.library.caltech.edu/18885/

Musielak, E., Z., & Quarles. (2015, August 10). The three-body problem. Retrieved from https://arxiv.org/abs/1508.02312v1

Nakamiya, M., Scheeres, D. J., Yamakawa, H., & Yoshikawa, M. (2008). Analysis of Capture Trajectories into Periodic Orbits About Libration Points. *Journal of Guidance, Control, and Dynamics*, *31*(5), 1344–1351. doi: 10.2514/1.33796

No, T.-S., Lee, J.-M., Jeon, G.-E., & Lee, D.-R. (2012). A Study on Earth-Moon Transfer Orbit Design. *International Journal of Aeronautical and Space Sciences*, *13*(1), 106–116. doi: 10.5139/ijass.2012.13.1.106

Ocampo, C. A. (2005). Trajectory Analysis for the Lunar Flyby Rescue of AsiaSat ... Retrieved from https://www.researchgate.net/publication/7268243_Trajectory_Analysis_for_the_Lunar_Flyby_Rescue_of_AsiaSat-3HGS-1

Paffenroth, R. C., Doedel, E. J., & Dichmann, D. J. (2001, September 19). Continuation of periodic orbits around lagrange points and ... Retrieved from https://www.researchgate.net/publication/285946585_Continuation_of_periodic_orbits_around_lagrange_points_and_AUTO2000

Pritchett, R. E. (2016). NUMERICAL METHODS FOR LOW-THRUST TRAJECTORY OPTIMIZATION. *Purdue University*.

Qiao, D., Xu, R., & Shang, H. (2010). Libration Point Orbits and Its Invariant Manifolds Structure. *2010 International Workshop on Chaos-Fractal Theories and Applications*. doi: 10.1109/iwcfta.2010.56

Sellers, J. J., Astore, W. J., Giffen, R. B., & Larson, W. J. (n.d.). *Understanding space: an introduction to astronautics* (3rd ed.). New York: McGraw-Hill.

Sucarrat, E. H., & Soler, J. M. (2009, March 9). Study of LEO to GEO transfers via the L1 Sun-Earth or Earth-Moon libration points. Retrieved from https://upcommons.upc.edu/handle/2099.1/6546

Vallado, D. A., & McClain, W. D. (2001). *Fundamentals of astrodynamics and applications* (2nd ed.). El Segundo, CA: Microcosm Press.

Villac, B. F., & Scheeres, D. J. (2003). New Class of Optimal Plane Change Maneuvers. *Journal of Guidance, Control, and Dynamics*, *26*(5), 750–757. doi: 10.2514/2.5109

Villac, B. F., & Scheeres, D. J. (2009). Third-Body-Driven vs. One-Impulse Plane Changes. *The Journal of the Astronautical Sciences*, *57*(3), 545–559. doi: 10.1007/bf03321516

Williams, K. E. (2002, October 17). Overcoming Genesis mission design challenges. Retrieved from https://www.sciencedirect.com/science/article/pii/S0094576502001674

Appendix A

Appendix A contains the Python code from the (Baines, Hew, & Toyama) research with added alterations to support the research conducted. This script is known to operate with Intel i7 CPU, and 8 GB RAM.

```
import time
import numpy as np
import matplotlib.pyplot as plt
start_time = time.time()

# This script runs our three-body problem using python
def func(ieq, r, theta, dtheta, phi, dphi, mu, dv):
    # This function sets the initial conditions given an object orbiting P2
    v_e = np.sqrt(mu/r)
    v = v_e + dv
    # numerical error fix for each if statement
    if ieq == 1:  # calculate initial x
        if abs(r*np.cos(theta)*np.cos(phi)) < 1e-16:
            return 1 - mu
        else:
            return r*np.cos(theta)*np.cos(phi) + 1 - mu
    if ieq == 2:  # calculate initial y
        if abs(r*np.cos(phi)*np.sin(theta)) < 1e-16:
            return 0.0
        else:
            return r*np.cos(phi)*np.sin(theta)
    if ieq == 5:  # calculates initial z
        if abs(r*np.sin(phi)) < 1e-16:
            return 0.0
        else:
            return r*np.sin(phi)

    if ieq == 3:  # calculates initial vx
        vx_p1 = -v*np.cos(phi)*dtheta*np.sin(theta)
        vx_p2 = v*dphi*np.sin(phi)*np.cos(theta)
        return vx_p1+vx_p2  # - 2eq

    if ieq == 4:  # calculates initial vy
        vy_p1 = v*np.cos(phi)*dtheta*np.cos(theta)
        vy_p2 = v*dphi*np.sin(phi)*np.sin(theta)
        return vy_p1 + vy_p2 + 1 - mu

    if ieq == 6:  # calculates initial vz
        if abs(-1*v*dphi*np.cos(phi)) < 1e-16:
            return 0.0
        else:
            return -1*v*dphi*np.cos(phi)


def RHS(ieq, t, x, y, z, u_x, u_y, u_z, mu):
    """make new parameters to simplify typing inputs"""
    A = (x+mu)
    B = (x-1.0+mu)
    c = 2.0
    C = (1.0-mu)
```

```
    r1 = ((A**2)+(y**2)+(z**2))**(3.0/2.0)
    r2 = ((B**2)+(y**2)+(z**2))**(3.0/2.0)
    """defining equations in order: x , vx, y, vy"""
    if ieq == 1:
        return u_x
    if ieq == 2:
        return (c*u_y)+x-((A*C)/r1)-((B*mu)/r2)
    if ieq == 3:
        return u_y
    if ieq == 4:
        return (-1.0*c*u_x)+(y*(1-(C/r1)-(mu/r2)))
    if ieq == 5:
        return u_z
    if ieq == 6:
        return (-C * (z / r1)) - (mu * (z / r2))


"""Define System Parameters"""
Dv = 0
h = 1000

theta_orb = 0*(np.pi/180)  # covert degrees to radians 226.81
phi_orb = 0*(np.pi/180)   # covert degrees to radians
jacobi_constant = 0
tau = 0.002

m1 = 1.989E30  # mass of sun
m2 = 7.348E22 + 5.972E24  # mass of earth/moon
M = m1 + m2  # total mass of the system
mu_i = m2/M  # order of unity for dimensional form
p1_pos = -mu_i
p2_pos = 1 - mu_i
g_const = 6.674E-20
d = 149.6E6  # distance from Sun to Earth
R_Earth = 6371/d  # radius of Earth
R_Sun = 695510/d
t_char = np.sqrt(d**3 / (g_const * m1))
Dv = Dv*t_char / d
H = h/d  # choose height above radius of primary body
r_orb = R_Earth+H
v_e = np.sqrt(mu_i/r_orb) + Dv

dtheta_orb = v_e/r_orb
dphi_orb = 0
# relationship between dtheta and dphi
# (r*dtheta)^2 = v^2 - (r*sin(theta)*dphi)^2
# (r*sin(theta)*dphi)^2 = v^2 - (r*dtheta)^2

x = func(1, r_orb, theta_orb, dtheta_orb, phi_orb, dphi_orb, mu_i, Dv)
y = func(2, r_orb, theta_orb, dtheta_orb, phi_orb, dphi_orb, mu_i, Dv)
z = func(5, r_orb, theta_orb, dtheta_orb, phi_orb, dphi_orb, mu_i, Dv)

vx = func(3, r_orb, theta_orb, dtheta_orb, phi_orb, dphi_orb, mu_i, Dv) + y
vy = func(4, r_orb, theta_orb, dtheta_orb, phi_orb, dphi_orb, mu_i, Dv) - x
vz = func(6, r_orb, theta_orb, dtheta_orb, phi_orb, dphi_orb, mu_i, Dv)

"""Define list to append values of from RK4"""
```

```
t_list = [0.0]
x_list = [x]
y_list = [y]
z_list = [z]
vx_list = [vx]
vy_list = [vy]
vz_list = [vz]
"""Define initial conditions for RK4 numerical calculation"""
t_i = 0.0
x_i = x
y_i = y
z_i = z
u_xi = vx
u_yi = vy
u_zi = vz
# Note that changing the N size impacts backwards traceability and
# lower numbers will lead to larger integration errors
N = 1000000  # minimal acceptable performance N = 1000000
step = 1/N  # step size
x = np.linspace(-10.0, 10.0, 3000)
y = np.linspace(-10.0, 10.0, 3000)
X, Y = np.meshgrid(x, y)
# This is to save the data generated for further analysis by other scripts
str = r"C:\Users\Desktop\data"
str2 = r"\position.txt"
path = str + str2
text_file = open(path, "a")

"""Run RK4"""
while t_i <= tau:
    # /*Calculate all K1 values: first step*/
    K1_x = step*RHS(1, t_i, x_i, y_i, z_i, u_xi, u_yi, u_zi, mu_i)
    K1_y = step*RHS(3, t_i, x_i, y_i, z_i, u_xi, u_yi, u_zi, mu_i)
    K1_z = step*RHS(5, t_i, x_i, y_i, z_i, u_xi, u_yi, u_zi, mu_i)
    K1_ux = step*RHS(2, t_i, x_i, y_i, z_i, u_xi, u_yi, u_zi, mu_i)
    K1_uy = step*RHS(4, t_i, x_i, y_i, z_i, u_xi, u_yi, u_zi, mu_i)
    K1_uz = step*RHS(6, t_i, x_i, y_i, z_i, u_xi, u_yi, u_zi, mu_i)
    """/*Calculate all K2 values: half step*/"""
    K2_x = step*RHS(1, t_i + step/2, x_i + K1_x/2, y_i + K1_y/2,
                    z_i + K1_z/2, u_xi + K1_ux/2,
                    u_yi + K1_uy/2, u_zi + K1_uz/2, mu_i)
    K2_y = step*RHS(3, t_i + step/2, x_i + K1_x/2, y_i + K1_y/2,
                    z_i + K1_z/2, u_xi + K1_ux/2,
                    u_yi + K1_uy/2, u_zi + K1_uz/2, mu_i)
    K2_z = step*RHS(5, t_i + step/2, x_i + K1_x/2, y_i + K1_y/2,
                    z_i + K1_z/2, u_xi + K1_ux/2,
                    u_yi + K1_uy/2, u_zi + K1_uz/2, mu_i)
    K2_ux = step*RHS(2, t_i + step/2, x_i + K1_x/2, y_i + K1_y/2,
                     z_i + K1_z/2, u_xi + K1_ux/2,
                     u_yi + K1_uy/2, u_zi + K1_uz/2, mu_i)
    K2_uy = step*RHS(4, t_i + step/2, x_i + K1_x/2, y_i + K1_y/2,
                     z_i + K1_z/2, u_xi + K1_ux/2,
                     u_yi + K1_uy/2, u_zi + K1_uz/2, mu_i)
    K2_uz = step*RHS(6, t_i + step/2, x_i + K1_x/2, y_i + K1_y/2,
                     z_i + K1_z/2, u_xi + K1_ux/2,
                     u_yi + K1_uy/2, u_zi + K1_uz/2, mu_i)
    """/*Calculate all K3 values : half steps*/"""
```

```
    K3_x = step*RHS(1, t_i + step/2, x_i + K2_x/2, y_i + K2_y/2,
                    z_i + K2_z/2, u_xi + K2_ux/2,
                    u_yi + K2_uy/2, u_zi + K2_uz/2, mu_i)
    K3_y = step*RHS(3, t_i + step/2, x_i + K2_x/2, y_i + K2_y/2,
                    z_i + K2_z/2, u_xi + K2_ux/2,
                    u_yi + K2_uy/2, u_zi + K2_uz/2, mu_i)
    K3_z = step*RHS(5, t_i + step/2, x_i + K2_x/2, y_i + K2_y/2,
                    z_i + K2_z/2, u_xi + K2_ux/2,
                    u_yi + K2_uy/2, u_zi + K2_uz/2, mu_i)
    K3_ux = step*RHS(2, t_i + step/2, x_i + K2_x/2, y_i + K2_y/2,
                     z_i + K2_z/2, u_xi + K2_ux/2,
                     u_yi + K2_uy/2, u_zi + K2_uz/2, mu_i)
    K3_uy = step*RHS(4, t_i + step/2, x_i + K2_x/2, y_i + K2_y/2,
                     z_i + K2_z/2, u_xi + K2_ux/2,
                     u_yi + K2_uy/2, u_zi + K2_uz/2, mu_i)
    K3_uz = step*RHS(6, t_i + step/2, x_i + K2_x/2, y_i + K2_y/2,
                     z_i + K2_z/2, u_xi + K2_ux/2,
                     u_yi + K2_uy/2, u_zi + K2_uz/2, mu_i)
    """/*Calculate all K4 values: full step*/"""
    K4_x = step*RHS(1, t_i + step, x_i + K3_x, y_i + K3_y,
                    z_i + K3_z, u_xi + K3_ux, u_yi + K3_uy, u_zi + K3_uz,
                    mu_i)
    K4_y = step*RHS(3, t_i + step, x_i + K3_x, y_i + K3_y,
                    z_i + K3_z, u_xi + K3_ux, u_yi + K3_uy, u_zi + K3_uz,
                    mu_i)
    K4_z = step*RHS(5, t_i + step, x_i + K3_x, y_i + K3_y,
                    z_i + K3_z, u_xi + K3_ux, u_yi + K3_uy, u_zi + K3_uz,
                    mu_i)
    K4_ux = step*RHS(2, t_i + step, x_i + K3_x, y_i + K3_y,
                     z_i + K3_z, u_xi + K3_ux, u_yi + K3_uy,
                     u_zi + K3_uz, mu_i)
    K4_uy = step*RHS(4, t_i + step, x_i + K3_x, y_i + K3_y,
                     z_i + K3_z, u_xi + K3_ux, u_yi + K3_uy,
                     u_zi + K3_uz, mu_i)
    K4_uz = step*RHS(6, t_i + step, x_i + K3_x, y_i + K3_y,
                     z_i + K3_z, u_xi + K3_ux, u_yi + K3_uy,
                     u_zi + K3_uz, mu_i)
    """/*Update conditions*/"""
    t_i += step
    x_i += ((K1_x + K4_x)/6) + ((K2_x + K3_x)/3)
    u_xi += ((K1_ux + K4_ux)/6) + ((K2_ux + K3_ux)/3)
    y_i += ((K1_y + K4_y)/6) + ((K2_y + K3_y)/3)
    u_yi += ((K1_uy + K4_uy)/6) + ((K4_uy + K3_uy)/3)
    z_i += ((K1_z + K4_z)/6) + ((K2_z + K3_z)/3)
    u_zi += ((K1_uz + K4_uz)/6) + ((K4_uz + K3_uz)/3)
    """/*Append to values to list*/"""
    t_list.append(t_i)
    x_list.append(x_i)
    y_list.append(y_i)
    z_list.append(z_i)
    vx_list.append(u_xi)
    vy_list.append(u_yi)
    vz_list.append(u_zi)

text_file.write("%s\n" % x_list)
text_file.write("%s\n" % y_list)
text_file.write("%s\n" % z_list)
```

```
"""Convert List into array"""
Time = np.vstack(np.array(t_list))  # time array
x_array = np.vstack(np.array(x_list))
y_array = np.vstack(np.array(y_list))
z_array = np.vstack(np.array(z_list))
vx_array = np.vstack(np.array(vx_list))
vy_array = np.vstack(np.array(vy_list))
vz_array = np.vstack(np.array(vz_list))
XY = np.append(x_array, y_array, axis=1)  # positions array
XYZ = np.append(XY, z_array, axis=1)  # positions array
VXY = np.append(vx_array, vy_array, axis=1)  # velocities array
VXYZ = np.append(VXY, vz_array, axis=1)  # velocities array
Data = np.append(Time, (np.append(XYZ, VXYZ, axis=1)), axis=1)  # data

"""Parameter Coordinates to be plotted"""
t_val = Data[:, 0]  # select all time values
x_val = Data[:, 1]  # select all x values
y_val = Data[:, 2]  # select all y values
z_val = Data[:, 3]  # select all z values
vx_val = Data[:, 4]  # select all velocity-x values
vy_val = Data[:, 5]  # select all velocity-y values
vz_val = Data[:, 6]  # select all velocity-z values

leo = R_Earth + (185/d)
phi = np.linspace(0, 2*np.pi, 100)  # generate values for plot
leo1 = leo*np.cos(phi) + 1 - mu_i
leo2 = leo*np.sin(phi)

geo = R_Earth + ((42164 - 6371)/d)
geo3 = geo*np.cos(phi) + 1 - mu_i
geo4 = geo*np.sin(phi)

sol_r1 = R_Sun*np.cos(phi) - mu_i
sol_r2 = R_Sun*np.sin(phi)

''' Graph: Transfer Maneuver '''

plt.title("Transfer Maneuver")
plt.xlabel("x (non-dimensional)")
plt.ylabel("y (non-dimensional)")
plt.plot(x_val, y_val, 'k--')  # plot x y phase space
plt.plot([p1_pos], [0], marker='o', markersize=3, color='orange')  # Sun
plt.plot([p2_pos], [0], marker='o', markersize=3, color='blue')  # Earth/Moon
plt.plot(0, 0, 'rx')  # center of mass of earth-moon system
plt.plot(leo1, leo2, 'g-')
plt.plot(geo3, geo4, 'y-')
plt.plot(sol_r1, sol_r2, 'r-')
plt.show()

# print time that it takes to run code
print("My program took", time.time() - start_time, "to run")
```

Appendix B

In section 3.4.1 the research of Scheeres, Davis, Anderson, & Born, 2010 bounding sphere is reviewed to provide a method of increased efficiency. Appendix B contains an image from their research to provide a visual aid in understanding bounding spheres. The direct use of their research with the impulse maneuver created is left to future research to be conducted.

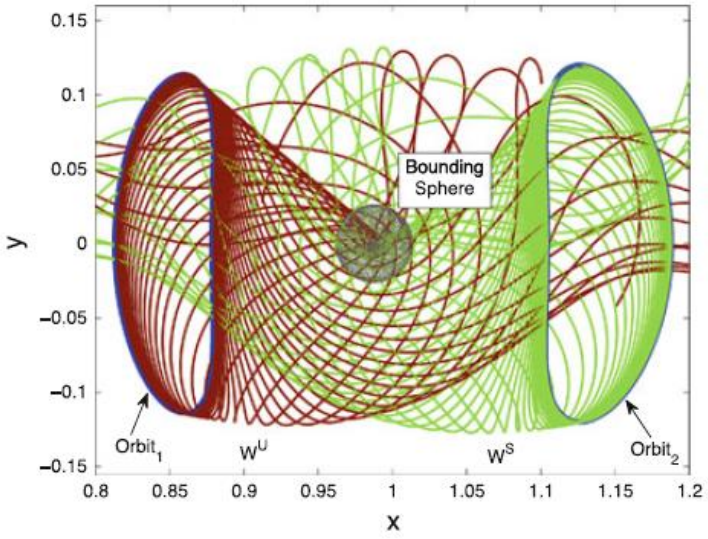

Fig. 3 A bounding sphere of radius *R* is placed around the center of mass of the secondary. The unstable manifold of Orbit 1 and the stable manifold of Orbit 2 are propagated, and the states are stored each time a trajectory pierces the bounding sphere (not sized to scale)

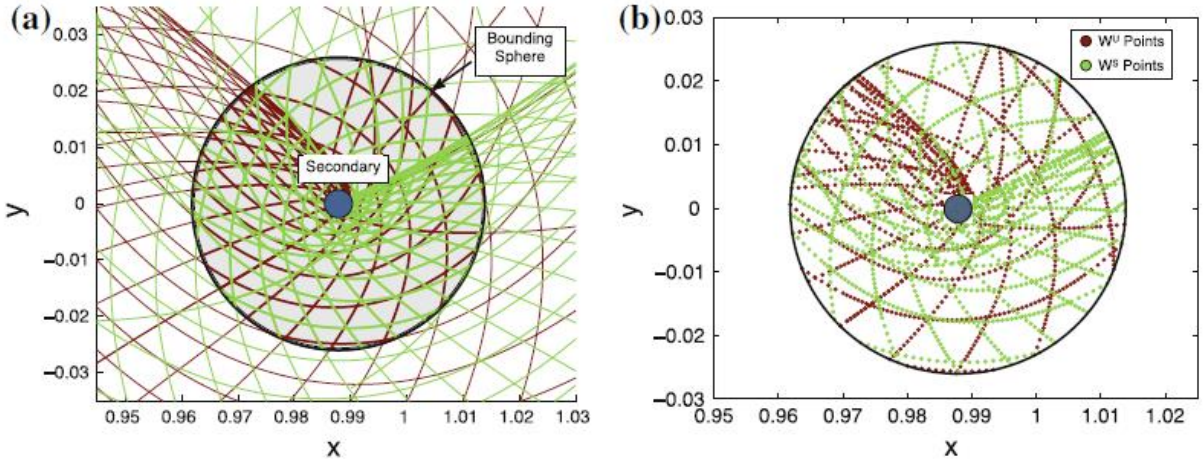

Fig. 4 **a** The manifold trajectories that pass through the sphere are highlighted. **b** Each trajectory is integrated such that successive points are spaced approximately equal in position

Scheeres, D. J., Davis, K. E., Anderson, R. L., & Born, G. H. (2010, June 5). The use of invariant manifolds for transfers between unstable periodic orbits of different energies. Retrieved December 30, 2019, from https://www.academia.edu/22450737/The_use_of_invariant_manifolds_for_transfers_between_unstable_periodic_orbits_of_different_energies.